Cape Peninsula
University of Technology

Orbital configuration and maintenance of nanosatellite constellations through electric propulsion

by

Marthinus Laurentius Joubert

Thesis submitted in fulfilment of the requirements for the degree

Master of Engineering: Electrical Engineering

in the Faculty of Engineering

at the Cape Peninsula University of Technology

Supervisor: Prof. Robert Van Zyl

Bellville Campus
Date submitted: April 2022

CPUT copyright information

The dissertation/thesis may not be published either in part (in scholarly, scientific or technical journals), or as a whole (as a monograph), unless permission has been obtained from the University

.

DECLARATION

I, Marthinus Laurentius Joubert, declare that the contents of this thesis represent my own unaided work, and that the dissertation/thesis has not previously been submitted for academic examination towards any qualification. Furthermore, it represents my own opinions and not necessarily those of the Cape Peninsula University of Technology.

Signed

3 April 2022

Date

ABSTRACT

South Africa is in the process of developing a low Earth orbit (LEO) nanosatellite constellation to monitor activity in its exclusive economic zone (EEZ) within the continental shelf to facilitate marine domain awareness. This project investigates how electric propulsion can be utilised in nanosatellites to form, maintain, alter or change the orbit of a constellation of nanosatellites for a three- to five-year lifespan. The constellation is assumed to be deployed from the International Space Station (ISS) in a cluster that will be spread out to form a constellation. With limited propellant on-board, altitude manoeuvres will be investigated that use atmospheric drag, rather than propellant, to form the initial constellation, and then use the on-board propulsion to maintain the desired constellation configuration. The study also determines whether there will be enough propellant left to de-orbit the constellation at the end of the mission to mitigate orbital debris.

A literature review covered possible constellation configurations and orbital mechanics to determine the most suitable constellation to meet the mission requirements, as well as an in-depth study of electric propulsion technologies. Once the feasibility of a constellation configuration and maintenance was confirmed, the study then determined through a link budget whether communication would be possible between the constellation and the ground segment.

The research was simulation based, and made extensive use of commercially available orbital dynamics simulation packages, such as STK.

The constellation formation and maintenance assume deployment from the International Space Station (ISS) in a 6x2 Walker-delta configuration, deploying a cluster of six satellites per plane. A ΔV budget is a crucial factor in determining whether electric propulsion presents a feasible option to carry out the mission and what the manoeuvre limitations will be for the mission lifespan.

The research shows that through electric propulsion it is possible to form an evenly spaced out constellation in roughly 17.2 days with a total ΔV of 9.97 m/s and at a cost of 8.12 g of propellant (from a total of 100 g propellant assumed).

To maintain this constellation for five years, it will take an estimated ΔV of 8.18 m/s by utilising the on-board propulsion twice, using a total of 6.7 g of propellant. After the constellation formation and five-year maintenance simulations, enough propellant would be available to de-orbit the constellation. De-orbiting will take between three and six months and an estimated ΔV of 50 m/s

with an anti-burn from the propulsion in the opposite direction of flight. This would consume 40.2 g of propellant, which means there would be ample propulsion left for additional manoeuvres during the lifespan of five years.

Communication between the ground and the constellation would be possible on the VHF uplink, S-Band downlink and UHF up- and downlink bandwidth, each having an acceptable link margin for communication.

ACKNOWLEDGEMENTS

I wish to thank the following persons for the assistance and guidance to help me complete this paper:

- Professor Robert Van Zyl, my supervisor;
- Professor Norman-Fitz Coy;
- Professor Graeme Oliver; and
- Dr Jonathan Lunn.

I wish to thank the French South African Institute of Technology (F'SATI) and the National Research Foundation (NRF) for financial assistance. The NRF has contributed a substantial amount of money towards this research and that is hereby acknowledged.

TABLE OF CONTENTS

LIST OF FIGURES

LIST OF TABLES

ACRONYMS

ADCS	- Altitude determination and control subsystem
AIAA	- American Institute of Aeronautics and Astronautics
AIP	- American Institute of Physics
AIS	- Automated information service
BER	- Bit error rate
BPSK	- Binary phase-shift keying
CMG	- Control moment gyro
CPUT	- Cape Peninsula University of Technology
DAS	- Debris assessment software
DC	- Direct current
EEZ	- Exclusive economic zone
EIRP	- Effective isotropic radiated power
EP	- Electric propulsion
ESA	- European Space Agency
EUV	- Extreme ultraviolet
F'SATI	- French South African Institute of Technology
FEEP	- Field emission electric propulsion
GEO	- Geosynchronous equatorial orbit
IEEE	- Institute of Electrical and Electronics Engineers
IOP	- Institute of Physics
Isp	- Specific impulse
ISS	- International Space Station
ISS	- International Space Station
LEO	- Low earth orbit
LLA	- Latitude, longitude, and altitude
LMFI	- Liquid metal field ion
M2M	- Machine to machine
MCS	- Mission control sequence
MDA	- Marine domain awareness
MDASat	- Maritime Domain Awareness Satellite constellation
Meniscus	- Curved shape
NASA	- National Aeronautics and Space Administration
PPU	- Power processing unit

RAAN - Right ascension of the ascending node
SNR - Signal-to-noise ratio
SPT - Stationary plasma thruster
STELA - Semi-analytic tool for end-of-life analysis
STK - Systems Tool Kit
TAL - Thruster with anode layer
TLE - Two-line element
UHF - Ultra-high frequency
VDES - VHF data exchange service
VHF - Very high frequency
ΔV (Δv) - Available change in vehicle velocity

Keywords

- Electric propulsion
- Nanosatellites
- Space
- Constellation
- Orbit

CHAPTER 1: RESEARCH OVERVIEW

This chapter will cover the research problems, objectives, questions and significance of the research, as well as an outline of the work to be done in this research.

1.1 INTRODUCTION

Since the 1960s, electric propulsion has been used effectively for many types of satellites. A wide range of thruster applications has been developed, from Sun pointing and attitude control to orbit-raising applications. Originally, electrical thrusters were developed as a secondary propulsion system to provide altitude control and station keeping, mainly for geostationary satellites. To accomplish missions with high precision requirements, propulsion systems such as field emission electric propulsion are of interest, due to its high specific impulse and high efficiency (Fernando, 1970).

1.2 RESEARCH CONTEXT

The Cape Peninsula University of Technology (CPUT) in the Western Cape, South Africa, is a leader in the field of space technology with its satellite programme that has produced over 70 postgraduate students in supporting the space industry. The Satellite Programme is hosted by the French South African Institute of Technology (F'SATI), and offers postgraduate programmes in satellite engineering. CPUT has already developed and successfully launched five nanosatellites, namely ZACube-1, ZACube-2 and MDASat-1a, -b and -c. The programme is funded by the South African government.

1.2.1 Operation Phakisa (translated "Hurry Up")

The South African government needs a cost-effective, space-based solution to monitor shipping activity within its exclusive economic zone to facilitate marine domain awareness (MDA).

CPUT and its strategic technology partner, Stone Three Communications, are developing such a constellation of nanosatellites, namely the MDASat constellation, which will provide South Africa with a flexible communications platform to improve and extend maritime data associated with sovereign security and control of its current automated identification service (AIS) and VHF data

exchange system services (Operation Phakisa, 2019). In addition, the MDA constellation will also enable other satellite-based services for South Africa and the greater continent, e.g. narrow-band machine-to-machine communication services.

CPUT has just developed and launched three CubeSats for the MDASat-1 mission. This was the first South African mini constellation. The constellation will augment the AIS data of ZACube-2 in relaying ship beacon locations and short messages through to the CPUT ground station in Bellville.

CPUT is also planning to develop, with funding from the South African government, two more nanosatellites, namely M2MSat, that will be equipped with state-of-the-art VHF data exchange system (VDES) software-defined radios for machine-to-machine (M2M) communication (https://www.cput.ac.za/newsroom/news/article/4201/maritime-domain-awareness-satellite-mission-launch-imminent). VDES is an emerging M2M communications platform in the maritime industry (Bradbury, 2019:1).

For future missions like MDASat-1, electric propulsion could play an important role in maintaining an optimal constellation formation and ensuring timely deorbiting at end of life.

1.2.2 Background to research problem

The potential of CubeSats lies in the ability to be part of a constellation of relatively inexpensive satellites to achieve observations with relatively long mission times, optimised coverage over specific areas and improved global revisit times (Cahoy & Marinan, 2013:3). In case such a satellite should fail in a constellation, there would still be other satellites in orbit to continue the mission. CubeSats operate in LEO, between 400 km and 650 km above the surface of the Earth, where residual atmosphere is still present. Depending on mission requirements, the altitude can cause the orbital lifespan of a satellite to be either too long after the operational mission end-of-life and cause space debris, or deviate from orbit due to aerodynamic forces (Rawashdeh & Samir, 2015:1).

With electric propulsion, not only can an orbit be maintained, but electric propulsion can also be used to overcome atmospheric drag and enable lower orbital operations. Atmospheric drag causes a shift in the constellation configuration. Electric propulsion should be able to correct and

realign the constellation. Electric propulsion could also allow for the replacement of a satellite by de-orbiting it and manoeuvring a replacement back into the constellation.

1.2.3 Research justification

The primary way to launch CubeSats is as secondary payloads, or being launched from the International Space Station (ISS). This means that the orbit and plane are seldom as desired, which requires an active propulsion solution. Satellites in LEO also experience perturbations where atmospheric drag is the most dominating force that acts against the velocity vector of the satellites, causing decaying in altitude and drifting (Sin, Arcak & Packard, 2017). Although this force is small over the typical mission lifespan of five years, such as for MDASat, it can have a significant impact on the formation of the constellation. Electric propulsion is a possible solution for orbital management and constellation formation, as it is a highly efficient form of space propulsion (Oleson, 1993:1).

1.3 STATEMENT OF THE RESEARCH PROBLEM

Nanosatellites, also known as CubeSats, have very limited manoeuvring capabilities due to their size and power constraints, which limit mission capabilities. The international standard for these CubeSats specify dimensions of 10 x 10 x 10 cm with a mass of up to 1.3 kg that is also referred to as a 1U (1 unit) CubeSat. These units can be stacked together to form between 1U to 6U CubeSats depending on mission requirements (Cahoy & Marinan, 2013:4). Integrating a propulsion system with the CubeSat platform is crucial in increasing mission capabilities of future CubeSats, including plane and orbit change and orbit raising, formation flying in a constellation, proximity operations, fine altitude control, drag compensation, and de-orbiting.

1.4 RESEARCH OBJECTIVES

The focus point for this project was the MDASat mini-constellation of nanosatellites, which are to provide maritime domain awareness services in support of Operation Phakisa.

The baseline for the project was a nanosatellite constellation based on a Walker-delta configuration that was designed by Mtshemla (2017), specifically for coverage of the South Africa exclusive economic zone (EEZ). Mtshemla found that a total of 12 CubeSats that are evenly

distributed in two orbital planes at an inclination of 39° and right ascension of ascending node (RAAN) at 45° for the first plane and 225° for the second (Mtshemla, 2017:76), yield an average daily revisit time of about five minutes and average daily access time of more than 16 hours.

The research attempted to show through theoretical analyses and simulation, whether electric propulsion, specifically FEEP thrusters, is able to configure and maintain an ideal orbital configuration for the MDASat constellation, and for the required orbital lifetime of three to five years. With limited propellant on board, a feasibility study was done to determine whether plane-change manoeuvres will be possible and will depend on simulation results and the ΔV budget. Additionally, other mechanisms were investigated to form the initial constellation, such as altitude control, and drag manoeuvres to make in-plane changes to the orbits, without the use of the on-board propulsion system.

Finally, a communications link performance and coverage characteristics between the constellation and the ground station were investigated. The aim was to achieve revisit times of approximately 45 minutes over the South African EEZ. This was based on a case study done by Mtshemla on the MDASat mission.

1.5 RESEARCH QUESTIONS

In order to achieve the research objectives described in section 1.4, the following research questions have been defined:

- How long does it take to set up the constellation of satellites launched from the ISS?
- Is propulsion needed or will altitude control using atmospheric drag be able to form and maintain the constellation?
- What is the ΔV budget for a five-year mission and is plane-change feasible within the capabilities of existing electrical propulsion systems?
- What is the impact of lower orbits compared to higher orbits still in LEO on constellation performance and can electric propulsion enable improved utility of such lower orbits?
- How long will it take for a satellite to de-orbit with and without propulsion?
- Does the constellation configuration support a feasible MDA case study in the South African EEZ?

1.6 SIGNIFICANCE AND CONTRIBUTION OF THE RESEARCH

The research is significant for the future of the MDASat constellation of nanosatellites that will provide MDA services in South Africa in support of Operation Phakisa. Integrating electric propulsion into the satellites in the constellation will allow for the optimal placement of satellites within the mini-constellation, which is even more important in small constellations, rather than larger ones. Furthermore, electric propulsion will ensure that South Africa meets its commitments to international treaties for the sustainable use of outer space through active deorbiting utility.

1.7 RESEARCH DELINEATION

The research boundaries are as follows.

- The research did not deal with developing a thruster, but assumed that existing off-the-shelf thruster technology is available.
- The propulsion systems were not tested in practice. Research was limited to a theoretical analysis, supported by simulation of the constellation.
- Only 2U CubeSats were investigated, similar to the MDASat conceptual design.
- The thrusters did not support attitude control maneuverers. Attitude control would be done by the attitude determination and control system of CubeSat and was not a focus of this work.
- After the initial formation of the constellation, only the propellant cost, total mission ΔV and time were covered.

When forming a constellation from a single deployment, each satellite needs a different ΔV thrust to be able to phase away from one another to spread evenly out in the orbit. When the desired phasing of the constellation has been reached, each satellite will have a different velocity, altitude and elliptical orbit. To lock the constellation in place, each satellite will need to initiate a precise thrust at the correct time to circularise and synchronise the constellation (Birkeland & Skanke, 2018:5).

1.8 RESEARCH DESIGN AND METHODOLOGY

This section investigates the methods, approaches and the processes to achieve the end results of this work.

1.8.1 Research investigations

- The method of investigation was mathematical modelling and simulation of classical orbital mechanics. Laboratory and in-orbit operational results from the manufacturer of the thruster were used as the basis for the data for the thruster calculations. With all the ever-changing parameters of space conditions in LEO, experimental and numerical methods were used to determine and compare approximate results.
- A case study was done to validate whether a drag coefficient of 2.2 for typical spacecraft is reasonable (Oltrogge & Leveque, 2011). This was done with two-line element (TLE) data from an actual CubeSat mission in a similar orbit to that of MDASat and which had already completed its mission and had de-orbited. As the atmospheric conditions in LEO vary with time, position, and the solar cycle, the results will be estimated through numerical calculations over 11 months.
- For the optimal constellation, an adapted case study from the work done by Mtshemla (2018) was done to determine whether the constellation would produce the required performance at the ISS inclination of 51.43 degrees, compared to the 39 degrees assumed by Mtshemla (2018). From this, a link budget was simulated in STK to calculate whether the communication system would meet the mission requirements.
- The optimal orbit configuration requires plane changing, so the necessary calculations needed to be made to determine whether the propulsion system would be able to achieve this.
- For the formation of the constellation from a cluster of satellites deployed from the ISS, two approaches were undertaken to phase satellites evenly throughout the orbital plane. This was done in the simulation software STK and using the Astrogator propagator within STK. The first approach looked at body orientation to manipulate the drag effect on the satellite, and to separate and configure the satellites from one another to form the constellation. The primary objective of this approach was to save on propulsion for the initial configuration. The second approach incorporated the on-board propulsion system to achieve the same constellation configuration. The results of the separation with propulsion would be vital in a final ΔV budget calculation, as propulsion is limited and could make this approach invalid if it uses too much propulsion.
- Orbital maintenance was the cornerstone of this research, so an accurate case study was needed. STK Astrogator is a powerful part of STK that specialises in interactive orbit

manoeuvres and spacecraft trajectory design. Astrogator is highly customisable with customised engine models, propagators, atmospheric models, central bodies, force models and other elements of a space mission analysis scenario. This allowed for a highly specialised mission design capability, which is vital in determining accurately mission behaviour over five years.

- De-orbit capability was determined by assessing if there was sufficient propellant left after the initial orbit configuration, and five years of orbit maintenance.

1.9 THESIS OUTLINE

Chapter 1 presents a research overview of the project, the research problem, research questions, objectives and delineation, as well as methodology.

Chapter 2 covers the literature review of electric propulsion, orbital mechanics and dynamics, satellite communication, software and optimal constellations.

Chapter 3 offers a case study on estimating the drag coefficient of space craft in LEO; then builds upon a previous case study to determine the optimal constellation for the South African EEZ. The final section in Chapter 3 is the corner stone of the thesis, covering the formation forming and maintenance of a constellation through electric propulsion. Chapter 3 ends by determining if de-orbiting will be possible after a five-year mission.

Chapter 4 covers the communications system design, specifically the link budget for VHF, UHF and S-Band communications.

Finally, Chapter 5 submits conclusions of the completed work and proposals for future work.

The last sections include references and appendices.

CHAPTER 2: LITERATURE REVIEW

This chapter looks at the literature available on electric propulsion technology, different constellation configurations, orbital mechanics, space mission design software and communications systems.

2.1 ELECTRIC PROPULSION

This section looks at the different electric prolusion technologies that are available for nanosatellites, as well as off-the-shelf options that are currently on the market.

2.1.1 Introduction

Electric propulsion is a kind of technology that can achieve thrust with high exhaust velocities by using electricity to increase the propellant exhaust velocity. It was first successfully used in the 1990s in the Deep Space 1 mission of NASA, after the theory was developed in 1906 by Robert Goddard and by Konstantin Tsiolkovsky in 1911 (Botha, 2014:23).

2.1.2 Specific impulse (Isp)

Specific impulse, or more accurately "mass specific impulse", is the change in momentum per unit mass for the thruster and is directly related to the efficiency of the thruster, which is a determination of how much thrust accumulates as the propellant is being emitted (scienceabc, 2019). In simpler terms, the specific impulse of the thruster propellant is a rough measure of the rate that the propellant is being emitted out of the thruster exhaust, and in return can be used to give an estimated time for when the thruster will run out of propellant. This is a crucial parameter in thruster selection and mission design when propulsion is utilised (aprende, 2019).

A thruster with high specific impulse consumes much less propellant than a thruster with low specific impulse. Therefore, the higher the specific impulse, the longer the thruster can operate with a limited amount of propellant on board. There is a trade-off, however, as it is difficult for a thruster to have a high specific impulse as well as high thrust capabilities, where thrust is a measure of power and specific impulse is a measure of the amount of thrust a given amount of propellant can supply.

With the limited available space on a CubeSat, a high specific impulse thruster that requires little propellant (and volume) is the most suitable option.

2.1.3 Types of electric propulsion thrusters

The three main types of electric propulsion thrusters are described below.

2.1.3.1 Electrothermal propulsion

Electrothermal propulsion generates high exhaust velocities, based on the principle of thermal expansion by heating the propellant using a tungsten heating element within a heat exchange chamber. An example of this kind of thruster is the Resistojet thruster shown in Figure 1.

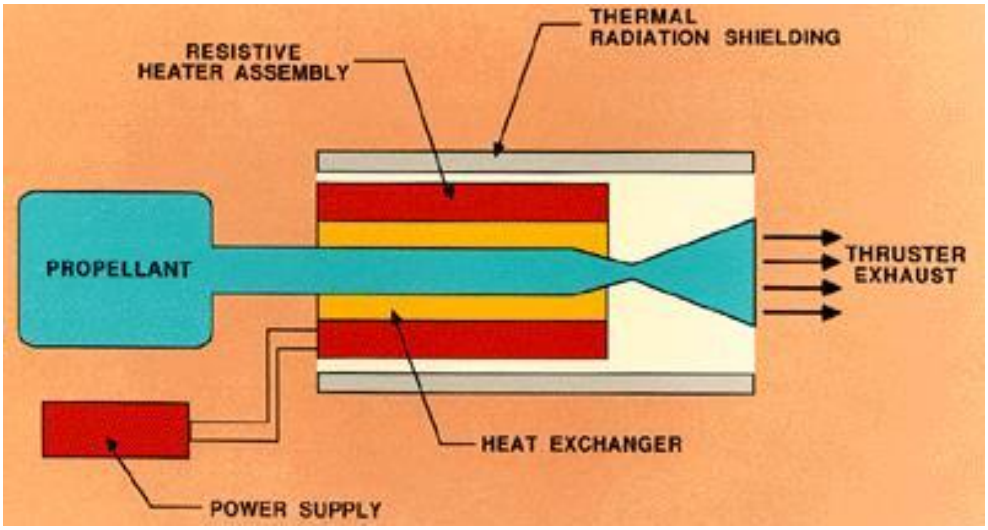

Figure 1: The working principle of the Resistojet thruster (Jordan, 2000:14)

2.1.3.2 Electrostatic propulsion

Electrostatic electric propulsion generates thrust by accelerating positively charged ions through a large direct current electrical field, as seen in Figure 2. The type of ion thruster is of interest, as it is a field emission electric propulsion (FEEP) thruster, and as it provides a high specific impulse.

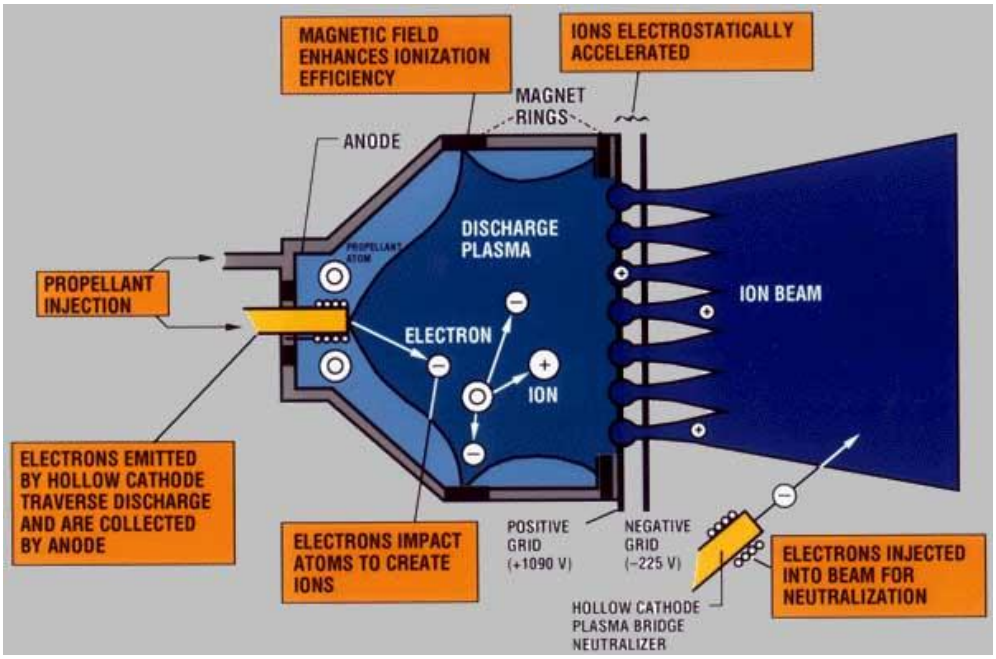

Figure 2: The principle of electrostatic electric propulsion (Jordan, 2000:14)

Field emission electric propulsion is based on the field emission effect, where electrons are extracted from a metal (which acts as the propellant) by an electric field, ionising the metal by creating positively charged ions that can be directed by an electric field to create thrust. This is made possible by capillary forces and the Taylor cone or electrospinning effect (Doshi & Reneker, 1995:152). The propellant investigated for this thesis was gallium, as it has a low melting point (30 °C) and a high boiling point, which means less power is required to liquidise and ionise the propellant (Bock, 2018:423–424).

The solid propellant is melted in the heater assembly to a liquid, and then the needle is wetted through capillary forces. By applying several kilovolt of electric potential between the sharp needle and circular extractor electrode, a Taylor cone is formed, as seen in Figure 3. When the applied total voltage between the needle and extractor electrode is in excess of a critical electrical field value of 10^{10} V/m, which is called the onset electrical field (Mitterauer, 1987:593), the metal propellant is evaporated, ionised and accelerated, generating the thrust. As the emitting ions exit the thruster, a neutraliser is needed to discharge the ions to prevent them from returning and charging the thruster as well as the entire satellite.

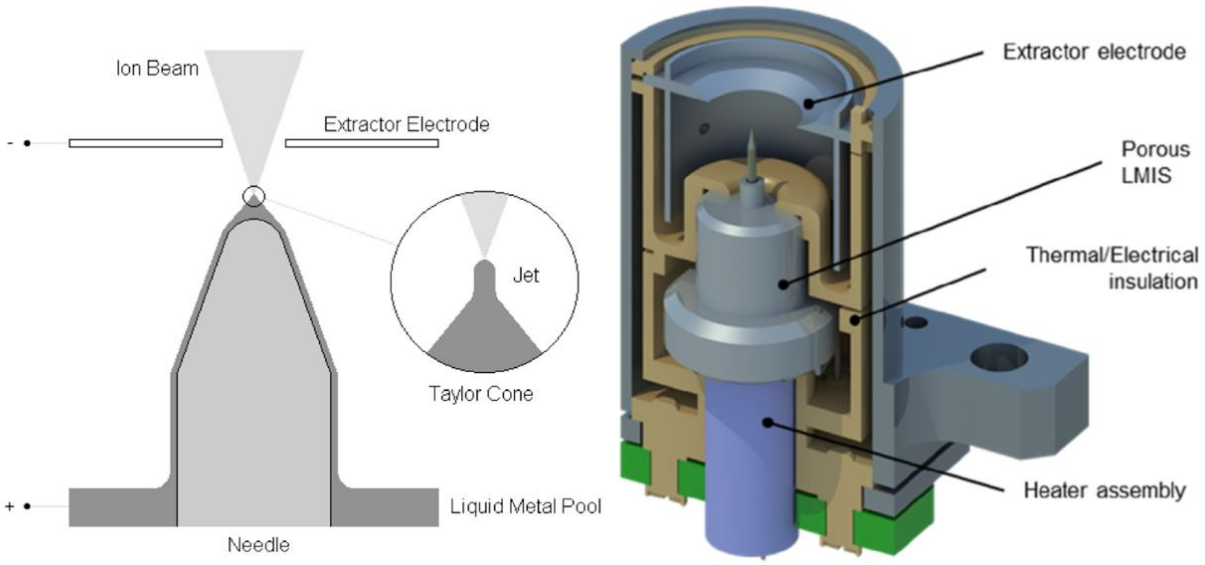

Figure 3: A cut-away view of the FEEP working principle (Bock, 2018:423)

The thrust and specific impulse of a FEEP thruster can be approximated by the following equations (Jelem & David, 2018:2):

$$F = I \cdot \sqrt{2 \cdot V_e \cdot \frac{m}{qe}} \cdot f \tag{2.1}$$

$$Isp = \frac{1}{g0} \cdot \sqrt{2 \cdot V_e \cdot \frac{qe}{m}} \cdot \eta \cdot f \tag{2.2}$$

Where:

- F - Thrust $[N]$
- Isp - Specific impulse $[s]$
- I - Net emitted current $[A]$
- V_e - Emitter potential $[V]$
- $\frac{qe}{m}$ - Charge-to-mass ratio of a singly ionised indium ion
- $g0$ - Standard acceleration due to gravity $[m/s^2]$
- f - Factor accounting for the beam spreading and associated radial component of the particle velocity that does not contribute to thrust
- η - Mass efficiency of the emitter

IFM Nano FEEP thruster in LEO demonstration

On 12 January 2018, a 3U CubeSat integrated with a single IFM Nano Thruster was launched from India on the PSLV-C40 rocket into a nominal 500 km LEO. During the commissioning phase, before thrust was applied, all subsections of the thruster were successfully tested and verified (Jelem, 2018:1–4).

Within the LEO demonstration, two tests with 15 min and 30 min burn times, respectively, were executed to determine the performance of the thruster. GPS data was collected before and after the thrust manoeuvres to precisely determine the change in orbit. For the calculated telemetry from the thruster, a pointing inaccuracy during thrust operation was estimated to be within 10°. GPS data was processed using a 50x50 gravity model. The 50x50 gravity model is one of many Earth gravity field models used to validate in-orbit assessments (Papanikolaou & Tsoulis, 2018:2). Based on the thruster telemetry and CubeSat properties, a calculated and measured comparison was made, as summarised in Table 1 (Jelem & David, 2018:6–10).

Table 1: LEO demonstration results of the IFM Nano FEEP thruster (Jelem & David, 2018:6–10)

Manoeuvre parameters			**Average change in semi-major axis**	
			Calculated from thruster telemetry	**GPS measurements**
Test	Emission current	Burn duration		
Test 1	2 mA	15 min	72 m	70 m ± 5 m
Test 2	2 mA	30 min	115 m	116 m ± 5 m

From the results of the two tests and comparing GPS data before and after the firing of the thruster, it can be seen from Table 1 that a significant change in the semi-major axis was verified. This demonstrates that this kind of thruster is potentially sufficient for this project.

2.1.3.3 Electromagnetic propulsion

Electromagnetic thrusters apply electromagnetic forces in a plasma discharge chamber to accelerate a charged propellant to generate thrust. The Hall thruster in Figure 4 is an example of such a thruster (Jordan, 2000:12).

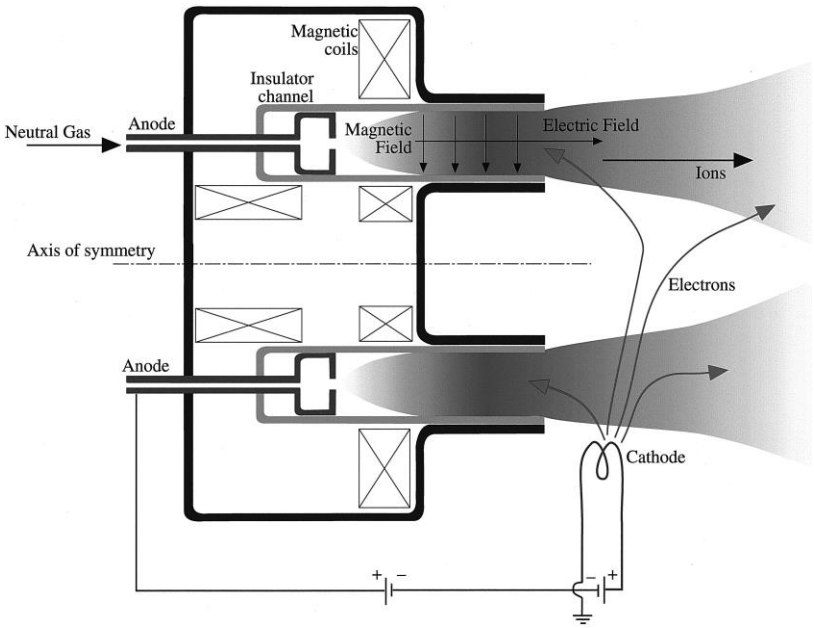

Figure 4: The principle of an electromagnetic Hall thruster (Jahn & Choueiri, 2003)

It can be seen from Table 2 (Jordan, 2000:18) that ion thrusters are the most efficient thrusters by means of their high specific impulse, which is why a thruster using field emission electric propulsion, which is based on ion propulsion, is the thruster of interest.

Table 2: Expected performance parameters for different types of electric propulsion

Propulsion type	**Specific impulse (s)**	**Specific power (kW/kg)**	**Electric power or thrust (kW/N)**	**Energy conversion efficiency**	**Thrust level (mN)**
Electrothermal propulsion: Resistojet	150–700	$10^{-3} - 10^{-1}$	1–3	35% to 90%	5–5,000
Electrostatic propulsion: (FEEP)	4,000–6,000		60	80% to 98%	0.001 to 1000
Electromagnetic propulsion: Hall-effect	1,500–2,500	0.2	17 to 25	40% to 60%	< 220

2.1.4 Commercial off-the-shelf products

2.1.4.1 IFM nano thruster for CubeSats

The IFM Nano Thruster in Figure 5 (Cubesatshop, 2019) is based on FEEP technology and has been developed and extensively tested at FOTEC in cooperation with the European Space Agency (ESA) (Reissner & Alexander, 2016:3). The thruster is currently commercially marketed by Enpulsion and comes as a complete package featuring the heritage ion emitter, propellant reservoir, neutraliser and power processing unit, taking up 0.8U of space with dimensions of 10 cm x 10 cm x 8.2 cm, as seen in Figure 5.

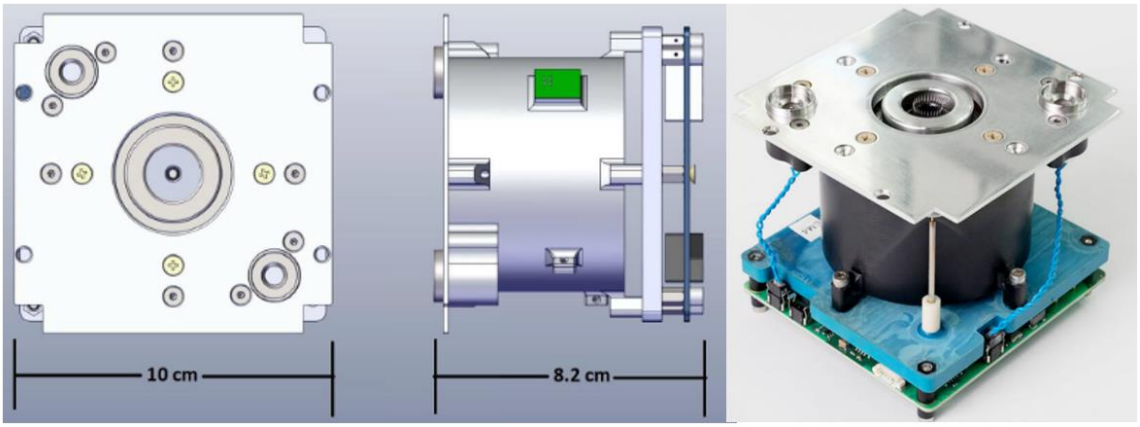

Figure 5: The IFM Nano Thruster (Reissner & Buldrini, 2016)

The thruster has been proven to be reliable, with more than 15 years of testing and results demonstrating more than 17 000 hours of firing more than 100 emitters, without degradation of performance. The thrust is variable and can be controlled between a specific impulse of 2000 s and 6000 s by varying the electrode voltages. The properties and performance of the thruster, based on a 12 V-power supply setup, are summarised in Table 3.

Table 3: IFM Nano thruster properties (Enpulsion, 2019)

Parameter	**Value**
Dynamic thrust range	10 µN to 0.4 mN
Nominal thrust	350 µN
Specific impulse	2000 to 6000 s
Propellant mass	230 g
Total impulse	more than 5000 Ns
Power at nominal thrust	40 W incl. neutraliser
Outside dimensions	100.0 x 100.0 x 82.5 mm
Mass (dry/wet)	670/900 g
Total system power	8–40 W
Hot standby power	3.5 W
Command interface	RS422/RS485
Temperature envelope (non-operational)	-40 to 105 °C
Temperature envelope(operational)	-20 to 40 °C
Supply voltage	12 V, 28 V, other

2.1.4.2 Hypernova plasma thruster

Hypernova Space Technologies offers electric propulsion solutions for CubeSats based on more than 10 years of research and development. They offer a plasma thruster running on pre-loaded solid-state unpressurised and non-toxic fuel. This reduces complexity, cost and risk for integrating propulsion into a CubeSat (hypernovaspace, 2020). The thruster is built for station-keeping, constellation phasing, collision avoidance, and other critical in-orbit manoeuvres therefor this thruster will be used for this thesis.

Figure 6: Hypernova plasma thruster (NanoThruster A - XS | satsearch, 2021)

Hypernova also supports a mission calculator based on their thruster for predicting and estimating mission parameters and data that would be helpful for simulation predictions and comparisons. Relevant product data of the thruster appears in Table 4 (NanoThruster A - XS | satsearch, 2021).

Table 4: Hypernova plasma thruster specifications

Propulsion system performance	**Value**	**Unit**
Specific impulse, Isp	500	s
Thrust-power ratio	8	μN/W
Mass	0.8	kg
Total impulse	200	N s
Power consumption	1 to 20	W
Volume	0.5	U

2.2 ADVANTAGES AND WEAKNESSES OF ELECTRIC PROPULSION

Electric propulsion offers a high specific impulse that makes it efficient on propellant consumption. This means that not only can the thruster operate for years from a single propellant source, but it also reduces the overall mass, compared with other conventional propulsion systems such as chemical propulsion (Frisbee, 2003). Electric propulsion systems can be compact and a feasible solution for nanosatellites (Maria, 2015:2).

However, electric propulsion systems produce little thrust, from μN to tens of Newtons of force, and have high power demands that require additional electricity-generating apparatus on board (Vanderwyst & Sivaram, 2006:31–36). Electric propulsion systems also generate high-energy ions that can charge the spacecraft and thruster, and can affect the on-board electronics and payloads negatively if the in-flight management is not done properly (Hine & Davis, 2016:2).

2.3 ORBITAL MECHANICS

This section looks at the optimal constellation for this mission, as well as the mechanics and calculations regarding orbits.

2.3.1 Introduction

Orbital mechanics is the cornerstone for orbit calculations and simulations to produce results and determining constellation behaviour. Figure 7 illustrates how to describe the orientation of an orbit in three dimensions using Euler angles (Curtis, 2013:196–197). To define an orbit fully, six classical orbital elements are needed as defined in Figure 7, namely:

- *h*: specific angular momentum;
- *i*: inclination;
- Ω: right ascension of the ascending node (RAAN);
- *e*: eccentricity;
- *ω*: argument of perigee; and
- *θ*: true anomaly.

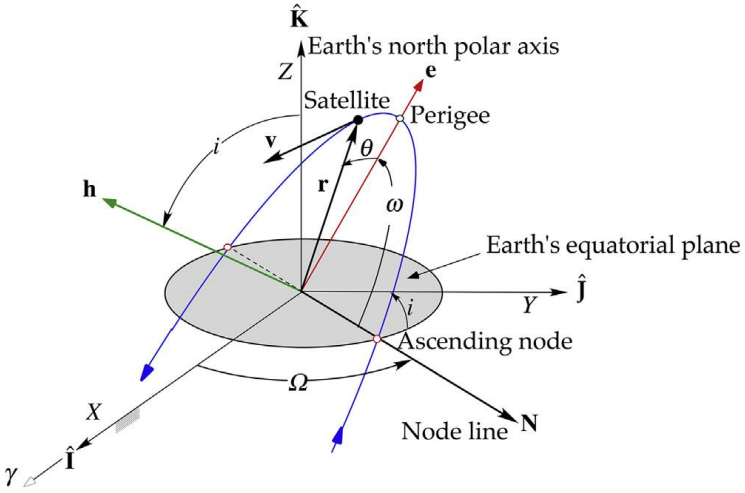

Figure 7: Geocentric equatorial frame and the orbital elements (Curtis, 2013:197)

2.3.2 Two-line element (TLE)

The most accessible real-world orbital data for satellites in orbit is in the form of TLEs, often referred to as Keplerian elements, and is available online at https://www.space-track.org/. Data from TLEs is based on optical observations and radar. TLE data sets contain data easily accessible over long periods of time (Vallado & Cefola, 2012). TLEs come in the form of grouped number sets producing the Keplerian orbital elements of a spacecraft, as seen in Figure 8.

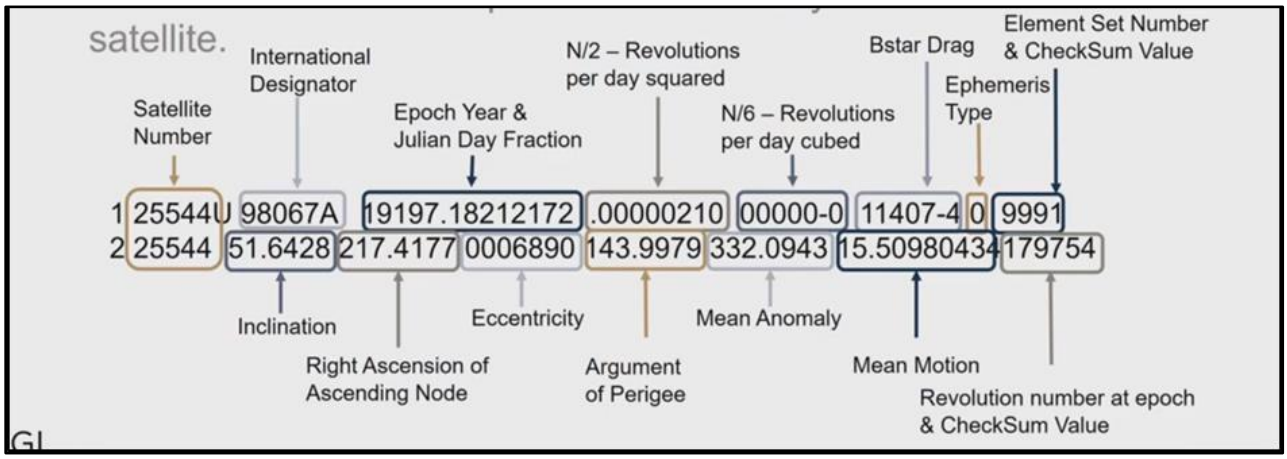

Figure 8: Two-line element format (space-track, 2020)

2.3.3 Constellation configurations

A satellite constellation is a coordinated orbital framework to optimise coverage over specific areas or to improve geographic revisit times, as well as higher reliability under individual satellite failure to ensure mission continuation and success (Savitri, Kim, Jo & Bang, 2017). Several constellation types exist to optimise temporal (revisit and access times) performance and geographic coverage (Marinan & Cahoy, 2013:4). The most common constellation types are the following.

- Geosynchronous - Three to five satellites in GEO can provide worldwide coverage in orbital altitudes of 35,780 km to 42,160 km in the equatorial plane (Larson & Wertz, 2005). The period of a geosynchronous satellite is 1436 minutes or 24 hours, matching the rotational motion of the Earth. This means that the satellite will remain in the same position over the Earth at all times (Birur & Siebes, 2001:1).

- Ellipsoid - Several elliptical orbits that are used to optimise coverage over a specific region or for a specific time of day.
- Walker-delta/Rosette – These types of satellites have identical altitudes and inclinations and they are in individual rotationally symmetric orbital planes, as seen in Figure 9.
- String of Pearls (A-Train) - Multiple satellites that are in the same orbital plane.
- Streets of Coverage - Polar orbits with RAAN spread evenly across one hemisphere.

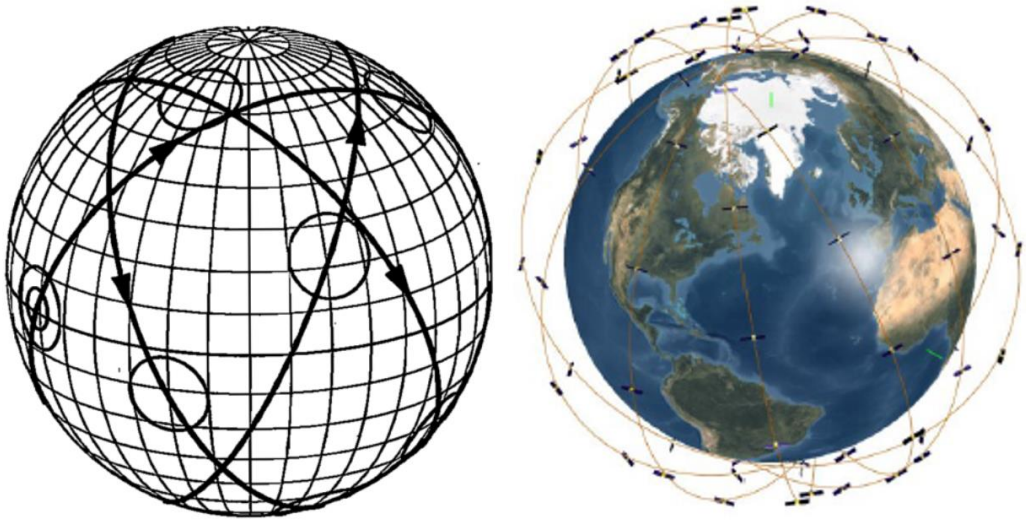

Figure 9: Walker-delta constellation (Larson & Wertz, 2005:195)

2.3.4 Optimal constellation for South African maritime domain awareness applications

Mtshmela (2017) reported extensively on an optimal constellation of nanosatellites to provide near real-time connectivity with ground-based sensors distributed across the African continent, but with specific relevance to coverage of the South African EEZ. The aim of the research was to design and validate the performance of a constellation for revisit times of approximately 45 minutes of the South African EEZ, while utilising a minimum number of satellites.

Mtshmela found that a LEO constellation at 500 km altitude in a Walker-delta configuration consisting of two planes with six evenly distributed satellites per plane at an inclination of between 39° and 45° will provide a solution with an average daily revisit time of about five minutes (Mtshemla, 2017:2). This was the baseline for this project. Chapter 3 will look at how this configuration can be utilised when a constellation is deployed from the ISS at an altitude of 400 km and inclination of 51.6^0.

2.3.5 Delta-V (ΔV) budget

When designing orbits and constellations, there is an energy cost or change in velocity required for each scenario. The ΔV budget is used to account for the total velocity change that a spacecraft will undergo through its mission life-span (Larson & Wertz, 2005:178). It requires energy from the on-board propulsion system to alter and change orbits, and since there is a limited amount of propellant mass on board, the total sum of velocity change will be required to determine whether the propellant will be sufficient for the mission life-span (Ashenberg, 1999:619–627).

To calculate the ΔV budget, all the parameters that need to be considered, are:

- The initial conditions of the launch vehicle;
- Mission orbits;
- Mission duration;
- Required orbit manoeuvres or maintenance; and
- Mechanism for spacecraft disposal.

Each item is then transformed into an equivalent ΔV requirement, using the appropriate formulas.

2.3.5.1 Determining ΔV from rocket theory

The ΔV cost for a mission can be determined from rocket theory with the rocket equation in equation 2.3 (Taylor, McDowell and Elvis, 2018). From rocket theory, the ΔV formula can be written as:

$$\Delta V = I_{sp} g_0 \ln(1 + \frac{M_p}{M_f}) \qquad (2.3)$$

Where:

- I_{sp}= specific impulse (thrust or rate of fuel consumption) [s]
- M_f= spacecraft final mass [kg]
- M_p= propellant mass used [kg]
- g_0= 9.81 [m/s^2]

2.3.5.2 ΔV design budgets

This thesis will be designing a ΔV budget for a nanosatellite constellation deployed from the ISS, manoeuvring into a desired mission orbit, maintaining that orbit for five years, and then de-orbiting. Looking at typical operations from a FireSat satellite with a 1.7 m^3 volume and having a dry mass of 140 kg in Table 5, a propellant budget can be derived by estimating propellant requirements for orbit maintenance and correction (Wertz, 2005:686). The possibility and ΔV cost for de-orbiting will be determined after a five-year mission simulation in Chapter 3.

Table 5: Typical functions and requirements for space propulsion

Spacecraft manoeuvre	**ΔV cost**
Orbit correction ΔV	15 to 75 m/s per year
East-west station keeping ΔV	3 to 6 m/s per year
North-south station keeping ΔV	45 to 55 m/s per year
Survivability or evasive manoeuvres ΔV	150 to 4 600 m/s
LEO to higher orbit raising ΔV	60 to 1 500 m/s
Drag-makeup ΔV	60 to 500 m/s
Controlled-re-entry ΔV	120 to 150 m/s

2.3.6 Orbital manoeuvers

This section looks at the calculations for the ΔV cost for orbit plane change, as well as orbit maintenance and orbit transfer calculations.

2.3.6.1 Orbit maintenance

Due to the perturbations in space, e.g. atmospheric drag, the orbital elements change and need correction (maintenance). The most dominant element that changes is the orbital altitude that decreases as the atmospheric drag causes the satellite slowly to fall back to Earth.

To correct or maintain this orbital altitude, a ΔV from the propulsion along the velocity vector can be applied. In general, to change the velocity vector from one orbit to another, the $\Delta V = V_A - V_B$

where V_A and V_B are the corresponding orbital velocities of orbits A and B, and can be found from the corresponding orbital elements.

Coplanar orbit transfers

To change an orbit in the same plane from a lower altitude to a higher altitude, a manoeuvre must be executed to change the energy and size of the initial orbit. For circular orbits, the final and initial orbits will not intersect and the most cost-efficient method of transferring to the final orbit, is through a Hohmann transfer, as seen in Figure 10 (Larson, 2005:149).

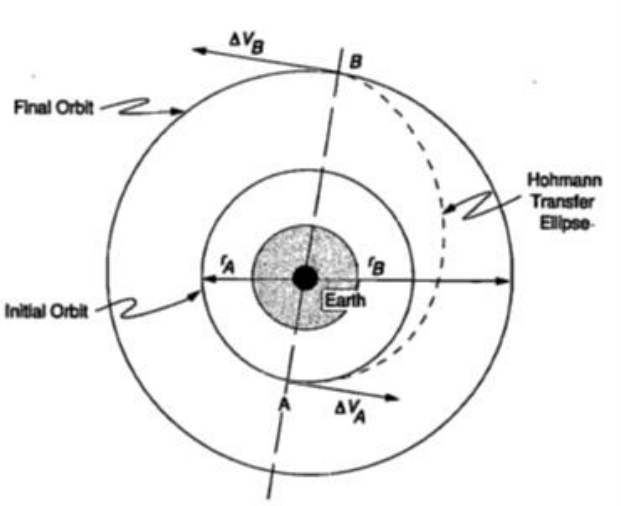

Figure 10: Hohmann orbit transfer (Larson, 2005:149).

Two ΔV manoeuvres are required and the total ΔV can be calculated with the following formula (Larson & Wertz, 2005):

$$\Delta V_T = \sqrt{\mu}\left[\left|\left(\frac{2}{rA}-\frac{1}{aic}\right)^{\frac{1}{2}}-\left(\frac{1}{rA}\right)^{\frac{1}{2}}\right|+\left|\left(\frac{2}{rB}-\frac{1}{aic}\right)^{\frac{1}{2}}-\left(\frac{1}{rB}\right)^{\frac{1}{2}}\right] \quad (2.4)$$

Where:

- $\sqrt{(\mu)} = 631.3481$ = Earth gravitational parameter of the central body $[km^3/s^2]$
- rA = Initial orbit height from the centre of the Earth $[km]$
- rB = Final orbit height from the centre of the Earth $[km]$
- $aic = \frac{rA+rB}{2}$ = semi-major axis of the ellipse $[km]$

2.3.6.2 Orbit plane changes

To change the orbit or inclination of a satellite, the direction of the velocity vector needs to be changed and requires a manoeuvre that has two different methods, as seen in Figure 11 and Figure 12 (Larson, 2005:150-151).

- Simple plane change

The size of the orbit remains constant, so the ΔV can be calculated from equation 2.5.

$$\Delta V = 2.V_t.\sin(\frac{\theta}{2}) \quad (2.5)$$

Where:

- V_t = Velocity before and after the burn $[m/s]$
- θ = angle change required [°]

Table 6 shows an example for the ΔV required to change from an inclination of 28° to an equatorial plane of 0°. From the ΔV equation for simple plane change, it can be seen that if the angular change is equal to 60°, the ΔV required is equal to the current velocity. This implies that plane change is expensive and should be done at lower velocities, e.g. at apogee when in an elliptical orbit.

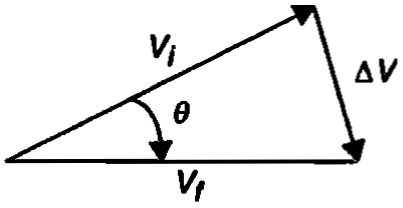

Figure 11: A simple plane change

- Combined plane change

Normally, orbital transfers require a combined plane and size change. This is done in two steps, starting with a Hohmann transfer, as seen in Figure 10 (Larson, 2005:147) to change the size of the orbit, and then a simple plane change. Using the law of cosines the following formula is used:

$$\Delta V = (Vi^2 - Vf^2 - 2Vi.Vf.cos\,\theta)^{\frac{1}{2}} \quad (2.6)$$

Where:

- V_i = Initial velocity $[m/s]$
- V_f = Final velocity $[m/s]$

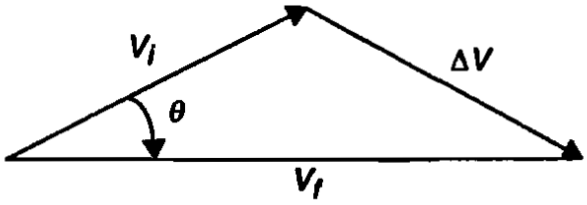

Figure 12: Combined plane change

2.3.6.3 Propellant usage

Propellant usage is proportional to ΔV and the propellant mass used can be found through the rocket equation 2.3 (Gaylor & David, 2000:5):

$$m_p = m_o[1 - e^{-\frac{\Delta V}{g_{o.I_{sp}}}}] \quad (2.7)$$

Where:

- m_p =Propellant mass used $[kg]$
- m_o =Initial satellite mass $[kg]$
- $g_{o.}$ = Gravitational acceleration of the Earth $[m/s^2]$
- I_{sp} =Specific impulse $[s]$

2.3.6.4 ΔV estimates

Table 6 shows typical ΔV estimates for a mission using a standard 3U CubeSat (Kramer, 2019).

Table 6: ΔV estimates for different orbital manoeuvres

Manoeuvre @ 400km altitude	**Formula**	**Approximate ΔV cost (ΔV)**	**Propellant usage (m_p)**	**Notes**
Coplanar orbit transfers	$\Delta V = ViA - VjB$	0.57 m/s	0.116 g	ΔV required for a 1 km altitude change (rB – rA = 1 km)
Orbit plane change simple	$\Delta V = 2000.Vcirc.\sin(0.5\text{deg})$	133.84 (m/s)/deg	27.193 g/deg	Using Vcirc @ 400 km = 7669 m/s

Conclusion

With a limit of 100 g of propellant on board, it can be seen from Table 6 that coplanar orbit transfers use little propulsion. Plane-changing can be seen as a costly manoeuvre with a high energy cost to change just one degree. Lowering the velocity of the satellites will decrease the cost to do plane-changing, but will require manoeuvres and time. Further studies will need to be conducted to establish whether this will be a feasible manoeuvre.

2.4 SIMULATION SOFTWARE

This section investigates the different simulation software available that will be needed to complete this work.

2.4.1 STK (Systems Tool Kit)

STK is a physics-based software package to solve problems through simulations and calculations involving Earth-orbiting satellites (Systems Tool Kit (STK), 2020). STK is the primary software to use, as it is one of the best software programs available for accurate mission design and a crucial tool in reaching the research objectives.

The software features include:

- 3D viewing capabilities;
- Orbit analysis;
- Access calculations;
- Orbit collision avoidance;
- Real-time visualisation;
- Powerful propagators; and
- Specialised modules.

STK features a specialised module namely Astrogator, which is the cornerstone for complex simulations.

STK Astrogator

STK Astrogator models spacecraft trajectories and reveals mission critical insights to develop, validate and refine solutions. Astrogator features a versatile and modular architecture that provides a framework for addressing most spaceflight trajectory problems (AGI, 2020).

STK Astrogator Mission Control Sequence (MCS) is the interface in Astrogator for designing custom and specialised missions. The MCS is the core of the space mission scenario that functions as a graphical programming language. Missions are designed in segments that dictate

how Astrogator calculates the trajectory of the spacecraft with respect to the initial settings that have been specified for the MCS itself.

2.4.2 STELA

STELA stands for ‘semi-analytic tool for end-of-life analysis’ and was developed by the French Space Agency to allow for semi-analytical models and assessment of protected LEO and GEO orbits. STELA produces a summarised report file of the spacecraft characteristics, criteria status, initial and final orbits, and computation parameters (Águeda, 2013).

2.4.3 DAS

Debris assessment software, or DAS, is used for the assessment of debris risk from satellite programmes for mission planning, to comply with the NASA standards (Johnson, N.L., 2001). The aim is to deliver adequate results and research to establish that it will be viable to use electric propulsion on CubeSats to reach the objectives stated in this thesis.

2.4.4 Open Cosmos

Open Cosmos is a cloud-based online platform for space mission design and incorporates modular hardware and standardised interfaces to optimise the performance of every mission. The platform consists of two tools: *beeKit*, that interfaces with the hardware, and the *beeApp* online software, that offers three sections for designing the mission (Baudet, 2020).

2.4.4.1 beeInnovative

beeInnovative makes it easy to plan and design missions by using mission and constellation analysis and includes:

- Mission simulation;
- Mission analysis summary; and
- Mission optimiser.

2.4.4.2 beeReady

beeReady prepares you to use the beeApp for flying a mission and offers access to a variety of tools, such as:

- Full payload development;
- Mission and system design (MSD); and
- Hardware-in-the-loop (HIL) applications.

2.4.4.3 beeOrbital

beeOribital compiles all your plans with flight preparation, launch and orbital exploration.

2.5 COMMUNICATIONS SYSTEM DESIGN

This section covers the theory and calculations for a communication design between a satellite and the ground through a link budget that will be implemented in Chapter 4.

2.5.1 Link budget

The link budget refers to the communication link via signal transmission between a transmitter and a receiver module. Generally, for CubeSats, these are amateur radio frequency bands. Satellites use uplink and downlink communication channels to transmit and receive data to and from a ground station. The word uplink refers to the ground station transmitting data up to the next available receiver on a satellite as illustrated in Figure 13.

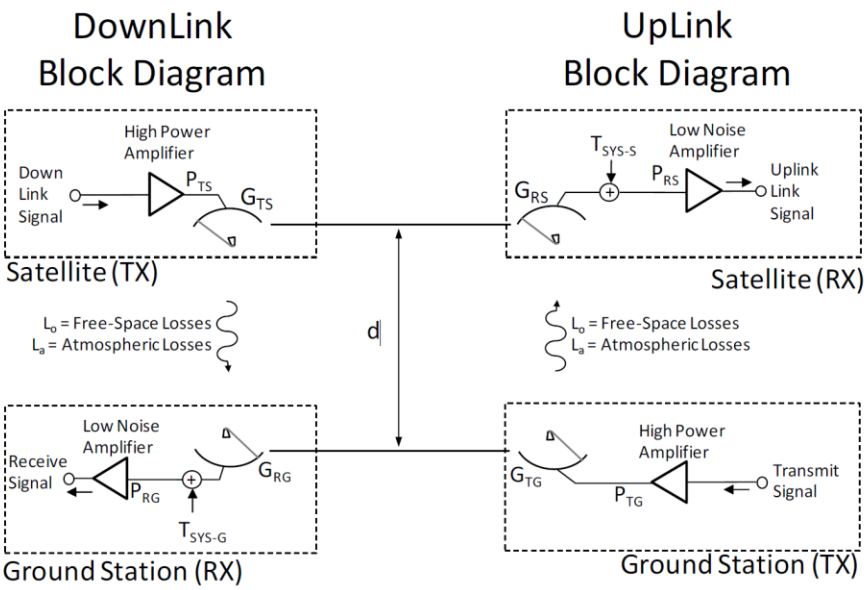

Figure 13: Satellite uplink and downlink block diagram (Sturdivant & Chong, 2016).

The term link budget refers to the signal strength and system noise of the communications link and how to account for the noise, while link margin determines the performance of the link. The following section will cover the basic concepts and components of a link budget, as well as the calculations.

Antenna gain

Antennas transmit power either omni-directionally, i.e. in all directions, or in a directive manner, with the antenna gain being a measure of how much power is being transmitted in that certain direction. The gain of aperture antennas can be calculated with equation 2.8 (Pozar, 2005:639–641).

$$G = \eta \left(\frac{\pi D}{\lambda}\right)^2 \tag{2.8}$$

Where:

- D = Antenna diameter
- η = Efficiency of the antenna
- $\lambda = c/f$ is the wavelength of the RF signal with frequency *f*

A directive antenna will have an antenna gain of $G > 0\, dBi$, as the power radiates more in a certain direction, while an omni-directional antenna radiates in all directions and therefore has a

$G = 0\,dBi$. At UHF and VHF frequencies, aperture antennas require a large cross-sectional area, which makes them impractical for use in CubeSats (Balanis, 2005:183). Wire antennas (monopoles and dipoles) are used instead.

Antenna beam-width and antenna gain are inversely proportional to each other, resulting in a high gain antenna having a small beam-width. This makes this antenna sensitive to an accurate pointing direction.

Effective isotropic radiated power ($EIRP$)

The effective isotropic radiated power ($EIRP$) is the ideal power that a transmitter can transmit to a receiver to have the same amount of power at the receiver than the transmitter has transmitted (Pozar, 2005:648). $EIRP$ is calculated as:

$$EIRP = P_{tx} + G_{tx} \ [dB] \tag{2.9}$$

Where:

- P_{tx} = Transmitter power [dBW]
- G_{tx} = Gain of transmit antenna [dBi]

Antenna noise temperature

The noise temperature in communication systems can be defined as the equivalent temperature of a body (a resistor) that would create similar amounts of noise over the relevant range of frequencies.

Thermal effects are the main source of natural noise. Therefore, the antenna on a satellite pointing towards Earth would pick up significant noise from thermal and man-made sources, while a ground station antenna pointing into cold space will pick up less noise.

From Balanis (2005:106), the brightness temperature that different sources emit, is intercepted by antennas at their terminals as “antenna noise temperature”. The antenna noise temperature is the combined temperature produced by the brightness emitted from external sources captured at the antenna and the thermal noise generated by the antenna and can be calculated by equation 2.10 (Pozar, 2005:644).

$$T_A = \eta_{rad} T_b + (1 - \eta_{rad}) T_b \quad (2.10)$$

Where:

- T_A = Receiver antenna noise temperature [K]
- η_{rad} = Radiation efficiency of the antenna
- T_b = Equivalent brightness temperature of the background seen by the antenna beam [K]

System noise

The overall system noise temperature, T_{sys}, from the perspective of the radio receiver is a combination of the noise temperature of the antenna plus the noise temperature of the cascaded transmission line connecting the antenna with the receiver, and the receiver itself. This noise temperature of both the transmission line and receiver is defined at the antenna terminals as the overall system noise temperature, T_{sys} (Pozar, 2005:653):

$$T_{sys} = T_A + (L_T - 1) T_p + L_T T_{REC} \; [K] \quad (2.11)$$

Where:

- T_p = Physical temperature of the antenna [K]
- L_T = Losses in the transmission line connecting the antenna to receiver, converted to linear units
- T_{REC} = Equivalent noise temperature of the receiver [K]

The noise temperature of the system is dependent on where the antenna is pointing, as well as the noise contribution of the receiver electronics.

Received noise power equation

Figure 14 illustrates the equivalent noise temperature of a noisy and noiseless amplifier, where the received noise power N_{RX} can be calculated with equation 2.12.

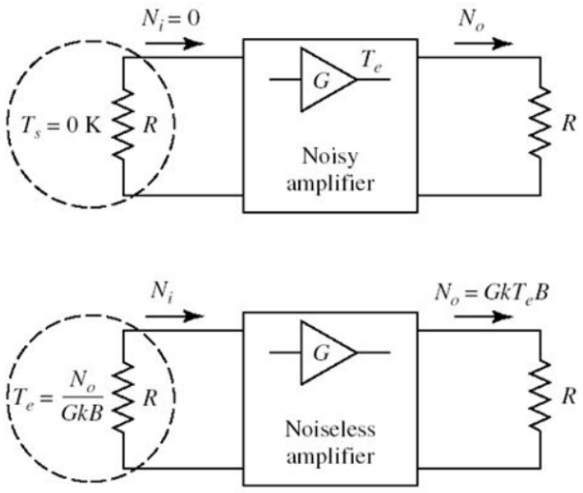

Figure 14: Noisy and noiseless amplifier (Pozar, 2005:491)

$$N_{RX} = kT_{sys}B\ G_{RX} \tag{2.12}$$

$$T_{RX} = (F-1)T_o \tag{2.13}$$

Where:

- N_{RX} = Received noise power $[dBm]$
- T_A = Receiver antenna noise temperature $[K]$
- T_{RX} = Transmitting temperature $[K]$
- B = Bandwidth $[Hz]$
- G_{RX} = Receiver antenna gain $[dBi]$
- F = Noise figure or factor of receiver
- T_o = Room temperature $[K]$
- k = Boltzmann's constant = $1.3803 \times 10^{-23}\ J/K$

Figure of merit

The figure of merit, $\frac{G}{T}$, of the receiver is the ratio of the antenna gain to the equivalent noise temperature of the station at the receiving frequency (Orfanidis, 2008:9):

$$\frac{G}{T} = G_{RX} - T_s\ [dB] \tag{2.14}$$

Where:

- G_{RX} = Gain of the receive antenna $[dBi]$
- T_s = System noise temperature $[dBK]$

Signal losses

Several mechanisms contribute to the total signal loss, *L*, in the link budget, for instance (Cowley & Glover, 2008:3):

$$L = FSL + AAL + TFL + AML + PL + IL\,[dB] \quad (2.15)$$

Where, in units of $[dB]$:

- FSL = Free space loss
- AAL = Atmospheric absorption loss
- TFL, RFL = Transmitter (or receiver) feeder loss
- AML = Antenna alignment (pointing) loss
- PL = Polarisation loss
- IL = Insertion loss

The free space lost is determined by distance and frequency:

$$FSL = 32.45 + 20log\,(R) + 20log(f) \quad (2.16)$$

Where:

- FSL = Free space lost $[dB]$
- R = Link distance $[km]$
- f = Frequency $[MHz]$

The free space loss is proportional to the square of both the frequency and link distance.

Receiver antenna received power

The power received at the antenna from the satellite can be calculated using the *Friis radio link formula* in equation 2.17.

$$P_r = \frac{G_t G_r \lambda^2}{(4\pi R)^2} P_t\,[W] \quad (2.17)$$

Where

- P_r = Received power $[W]$
- G_r = Receive antenna gain

- G_t = Transmit antenna gain
- $\lambda = c/f$ is the wavelength of the RF signal with frequency f $[m]$
- P_t = Transmit power $[W]$
- R = Link line of sight path distance $[m]$

Longest path distance (D_p) equation

The longest path distance that the signal travels between the ground station and the satellite is measured from a certain angle from when a satellite crosses the horizon plane and has line-of-sight to the ground station. This is called the slant range or path distance and can be seen in Figure 15. A typical worst-case horizon elevation angle is at 5° for LEO satellites (Cakaj, 2011).

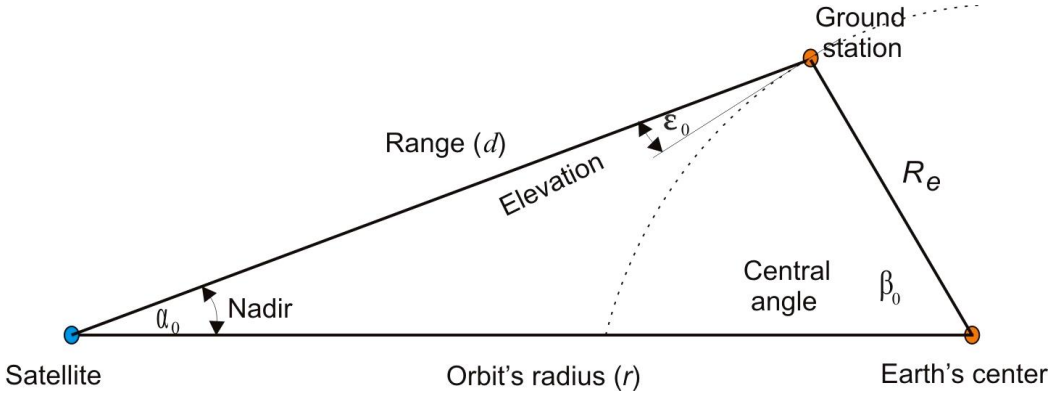

Figure 15: Satellite slant range (Cakaj, 2011)

Through the cosines law for a triangle, equation 2.18 gives the slant range in terms of the elevation angle:

$$D_p = R_e \left[\sqrt{\left(\frac{H+R_e}{R_e}\right)^2 - \cos^2(e_5)} - \sin(e_5) \right] \quad (2.18)$$

Where:

- D_p = Slant range $[m]$
- R_e = Earth radius $[m]$
- H = Orbit height $[m]$
- e_5 = Elevation angle at 5°

Link budget equation

To design a satellite communications system, all the above quantities are critical and the relationships between them are referred to as the link budget, which relates to all communication links. The link equation is given by (Cowley & Glover, 2008:4):

$$P_{rx} = P_{tx} + G_{tx} + G_{rx} - L \tag{2.19}$$

Where:

- P_{tx} = Power transmitted [dB]
- G_{tx} = Gain of the transmit antenna [dBi]
- G_{rx} = Gain of the receive antenna [dBi]
- L = Total link losses

Signal-to-noise ratio

The signal-to-noise ratio is dependent on the signal power, as it is the ratio of the necessary signal power to unwanted noise, as seen in equation 4.20 (Pozar, 2005:654):

$$\frac{S_o}{N_o} = \frac{S_i}{kT_{sys}B}\,[dB] \tag{4.20}$$

For digital signals, the energy received per bit equates to the energy received per second, divided by the number of bits per second. For a digital system with a bit rate of r_b bps:

$$E_b = P_{rx}/r_b \tag{4.21}$$

The energy per bit (E_b) was used because it allows for the comparison between different digital modulation schemes.

The link performance can be determined by taking the ratio of the received energy per bit to the system noise spectral density, $\frac{E_b}{N_o}$, where (Yuen, 2013:9):

$$\frac{E_b}{N_o} = P_{tx}(dBW) + G_{tx}(dBi) + G_{rx}(dBi) - L(dB) - 10logr_b - 10\log k - 10logT_s \tag{2.22}$$

Where:

- N_o = System noise spectral density [W/Hz]
- k = Boltzmann's constant
- T_s = System noise temperature [K]
- S_i = Input signal power [dBm]
- r_b = system bit rate [bps]

Combining all relevant quantities results in (Cowley & Glover, 2008:4):

$$\frac{E_b}{N_o} = EIRP(dBW) + \frac{G}{T}(dB) - L(dB) - 10logr_b - 10\log K \quad (4.23)$$

The received energy per bit to system noise spectral density can also be written as (Babu & Rao, 2011):

$$E_b/N_o = SNR/\eta \quad (4.24)$$

Where:

- SNR = Signal to noise ratio
- η = "gross" link spectral efficiency [$bit/s/Hz$]

For a digital communications system, the $\frac{E_b}{N_o}$ may be regarded as a signal-to-noise ratio. The bit error rate (BER) of a communications link that is based on a certain modulation scheme is related to the $\frac{E_b}{N_o}$, as shown in Figure 16 and Figure 17.

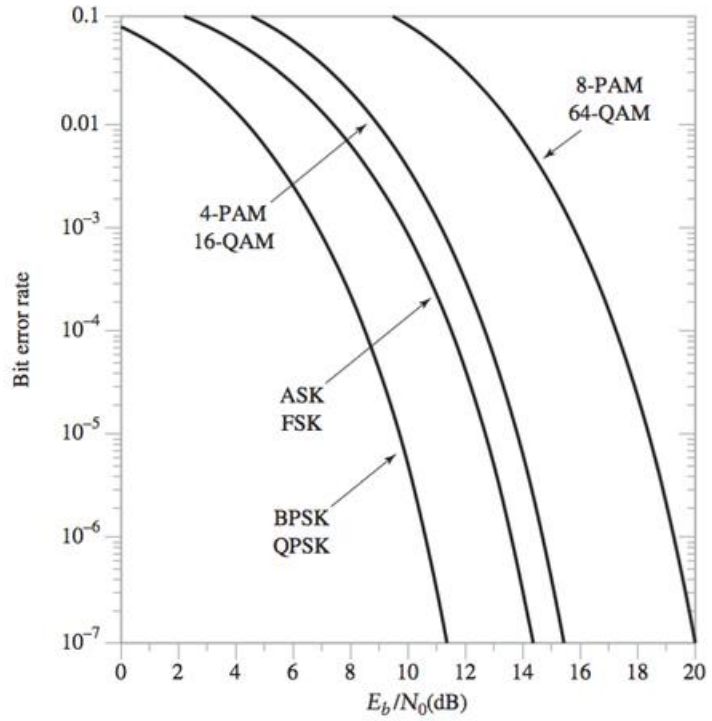

Figure 16: Bit error rate vs $\frac{E_b}{N_o}$ for different modulation schemes (Sklar, 2001:218)

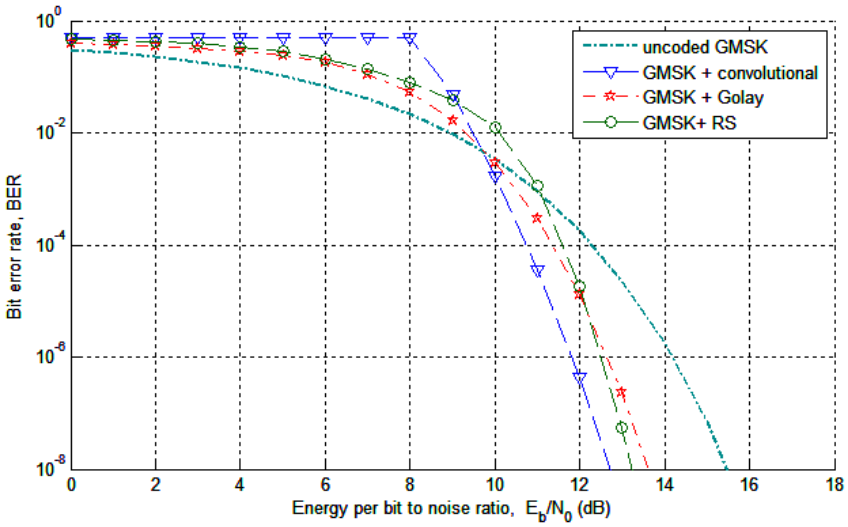

Figure 17: Coded and non-coded bit error rate vs $\frac{E_b}{N_o}$ for GMSK modulation schemes (Anane, Raoof & Bouallegue, 2015)

When comparing the BER performance of different modulation schemes, the $\frac{E_b}{N_o}$ ratio determines the best signal performance (Pisacane, 2005).

Link margin

The link margin is the final validation to determine the integrity of the communication link. It is the difference between $\frac{E_b}{N_o}$ required and $\frac{E_b}{N_o}$ actual (in dB), and can be calculated with equation 4.25:

$$Link\ margin\ = \frac{E_b}{N_o}\ actual - \frac{E_b}{N_o} required\ [db] \quad (4.25)$$

The $\frac{E_b}{N_o}$ required is determined from a graph such as in Figure 16 with different theoretical BER vs $\frac{E_b}{N_o}$ curves to determine the best performance that a digital link will deliver (Pisacane, 2005).

From Mtshemla (2017), a communication design for low bitrate sensor networks operating in the amateur frequency bands, specifically for the South African region, was conducted. The link calculations are done using a VHF/UHF receiver, VHF/UHF transmitter and S-band transmitter that have been developed at CPUT (Clyde Space, n.d.). Typical performance specifications are listed in Table 7, Table 8 and Table 9 below.

Table 7: VHF/UHF receiver specifications

DC power	< 220 mW
Sensitivity	140–150 MHz / 420–450 MHz, -117 dBm for 12 dB SINAD
Noise figure	< 1.5 dB
Channel spacing	12.5 kHz
Spurious response	<-65 dBc
Dynamic range	-117 dBm to -70 dBm
Frequency stability	± 2.5 ppm
Modulation (1200 baud)	AFSK
Modulation (9600 baud)	GMSK

Table 8: VHF/UHF transmitter specifications

DC power	3 – 7 W (27 – 33 dBm)
Frequency	140–150 MHz / 400–420 MHz (CMCC) 430 – 440 MHz (CMC)
RF power	27 – 33 dBm (3 dBm steps)
Channel spacing	25 kHz
Spurious response	<-65 dBc
Frequency deviation	3 kHz (FM)
Frequency stability	± 50 ppm
Modulation (1200 baud)	AFSK
Modulation (9600 baud)	GMSK
Protocol	AX.25

Table 9: S-band transmitter characteristics

DC power	< 5 W (30 dBm)
Frequency	2.4 - 2.483 GHz
RF power	24 – 30 dBm
Channel spacing	500 kHz
Transmission data rate	Up to 1 Mbps
Spurious response	<-60 dBc
SNR	> 20 dB
Frequency stability	± 2.5 ppm
Output return loss	7 dB
Modulation	QPSK

Sensor data uplink communication

The link budget was calculated with the satellite considered at 5° above the horizon (the lowest elevation to satisfy the link budget) to ensure that communication is obtainable. The VHF ground sensor antenna system (assumed to be AIS transponders on ships) was assumed to be dipole antennas, as they do not include tracking capabilities.

2.6 SUMMARY

This chapter looked at the literature on electric propulsion, as well as available off-the-shelf options that can be integrated into CubeSats. Different satellite constellation configurations were investigated, as well as the most suitable configuration for the EEZ of South-Africa, namely a Walker-delta constellation.

The deployment of the constellation for the South African EEZ was determined to be from the ISS at an altitude of 400 km. The literature on basic plane change, as well as coplanar orbit raising transfers, was looked at as well as general ΔV costs for different orbit manoeuvres.

Different space simulation software packages were looked at as this research is based on simulations.

Finally, the underlying communication theory was covered, focussing on the link budget which will be the final part of the thesis, to be able to determine whether sufficient communication will be possible between the constellation and the ground station.

The following chapter will look at how perturbations affect a satellite in LEO and will include a case study on the drag coefficient that is part of the drag force equation.

CHAPTER 3: ORBITAL CONFIGURATION AND MAINTENANCE

This chapter is the cornerstone of this work and includes two case studies and orbital simulations. The first section covers a case study on the drag coefficient used for small satellites with specific shapes. The second case study looks at the orbital performance of a constellation to determine what configuration would be the most suitable for the South African EEZ, and whether the constellation would yield sufficient coverage. The final part of the chapter covers simulations on the formation of the constellation from a single deployment of a cluster of CubeSats from the ISS for MDA applications in the South African EEZ.

3.1 INTRODUCTION

The chapter starts with determining and examining atmospheric drag on a satellite, focussing on the drag coefficient parameter. With the complexity and inconsistency of the atmosphere in LEO, it is nearly impossible to determine exact values for all the components of the atmosphere. To determine and estimate the average values for the drag components, a case study on observational data was the chosen approach. The case study looks at whether the industry-recommended drag coefficient of 2.2 would be realistic for the mission specified in this work. Next, a case study on the orbital performance of the constellation was done from an existing case study to determine which configuration would be the most suitable for the EEZ of South Africa, and whether the constellation would yield sufficient coverage.

The final part is simulation of the formation of the constellation from a single deployment of a cluster of CubeSats from the ISS, the maintenance of the constellation on a five-year mission and determining whether de-orbiting would be possible in terms of the remaining fuel after the five-year mission.

3.2 DRAG COEFFICIENT CASE STUDY

This section defines and investigates the drag force and drag coefficient acting on a satellite by means of real-world satellite TLE data.

3.2.1 Introduction

A spacecraft in LEO below 1000 km experiences perturbations that influence its orbit, causing it to lose energy and slowly decay back to Earth (Bedingfield, 1996:7). To maintain these orbits, it is important to understand and determine these forces to be able to overcome them. The biggest perturbation force affecting a spacecraft in LEO is atmospheric drag, and as stated in the literature (Sin, Arcak & Packard, 2017), this force is difficult to calculate due to the fluctuations in the atmosphere due to the solar cycle and unpredictable space weather conditions. A case study on the atmospheric effects and determining the drag coefficient of an actual LEO satellite that is similar to the maritime domain awareness satellites considered in this work, will provide a good basis for simulation input and real-world data to compare to simulation results.

As the main goal of this thesis is to overcome these perturbations to maintain an orbit, this case study will prove to be valuable in determining whether electric propulsion will be sufficient and a viable option for a five-year mission. In addition to overcoming the perturbations, these forces may be utilised in the initial formation of the constellation by using the drag force as a form of velocity control to phase out the constellation. This will be looked at later in this chapter.

3.2.2 Atmospheric drag force

The most dominant perturbation and the most difficult perturbation to determine, is atmospheric drag acting on the satellite in LEO (Mostaza-Prieto, Graziano & Roberts, 2014:1). Determining this force and its components accurately was vital for the evaluation of the feasibility of electrical propulsion for orbital maintenance, ΔV budget calculations and orbital dynamic simulations presented in this work. With the complexity of determining this drag force, the next section will look at different approaches to estimate this force.

3.2.3 Basic approach

The simplified method in finding the atmospheric drag can be found through equation 3.1 (Mostaza Prieto, Graziano & Roberts, 2014:2):

$$a_{drag} = \frac{1}{2}\rho V^2 C_d \frac{A}{m} \tag{3.1}$$

Where:

- a_{drag} = atmospheric drag force (N)
- ρ = atmospheric density (kg/m^3)
- V = relative velocity of the spacecraft with respect to the atmosphere (m/s)
- C_d = drag coefficient (dimensionless)
- A = projected surface area of the spacecraft (m^2)
- m = mass of the spacecraft (kg)

The difficulty in determining the drag force lies with the following three variables.

- Atmospheric density (ρ)

The density of the atmosphere is part of a moving mass of air that varies with altitude, time and geographical location. The largest factor that influences these changes is the Sun as it undergoes a complex 11-year solar cycle. Throughout this cycle, the Sun heats up the atmosphere through extreme ultra-violet radiation (EUV), which causes the upper layers of the atmosphere to rise periodically, influencing the density of the air. EUV radiation cannot be measured directly on Earth, so the radiation of the Sun at a 10.7 cm wavelength was used as a basis. This value is defined as the F10.7 value and also varies with the solar cycle of the Sun (Mance, 2010).

- Relative velocity (V)

The atmosphere rotates with the Earth, so the presence of wind needs to be considered. In-track winds make the problem more uncertain as it influences the drag force, depending on the direction in which the wind is blowing (Gaposchkin and Coster, 1988:209).

- Drag coefficient (C_d)

The drag coefficient is used to balance the drag acceleration and atmospheric density (Mostaza Prieto, Graziano & Roberts, 2014:3). It is a unitless number that is mainly a function of the atmospheric and spacecraft surface temperature, gas composition, relative velocity and the loss of energy of incoming molecules as they collide with the surface of the spacecraft (Pilinski & Palo, 2009:4). To determine this value for most applications is extremely difficult and challenging. Therefore, to make the process easier, the drag coefficient is sometimes combined with the projected area (*A*) and mass (*m*) to form the ballistic coefficient (C_b), as in equation 3.2 (Mance, 2010:iv):

$$C_b = (C_d A)/m \tag{3.2}$$

3.2.4 Atmospheric drag force through observation

A more accurate method of determining the atmospheric drag force is needed since atmospheric density has been observed to oscillate by up to 800% during geomagnetic events (Li & Lei, 2021:11). A method of observation can be used by looking at the semi-major axis of the satellites at different points in time and then use this information to deduce the drag acceleration and force. Another approach would be to use space-borne accelerometers to model the influences of non-atmospheric perturbations on the satellite and then subtract it from the measured acceleration. The formula is presented in equation 3.3. (Pilinski & Palo, 2009:1):

$$\vec{a}_{drag} = \frac{(A_{sc}\rho C_d(\overrightarrow{V_w}-\overrightarrow{V_{sc}})^2}{M_{sc}}\ (-\widehat{V_T}) \tag{3.3}$$

Where:

- $-\widehat{V_T} = (\overrightarrow{V_w} - \overrightarrow{V_{sc}})$
- $\vec{a}_{drag}$ = Drag acceleration vector (m/s^2)
- A_{sc} = Projected area of the object (m^2)
- C_d = Drag coefficient
- $\overrightarrow{V_w}$ = Atmospheric wind vector (m/s)
- $\overrightarrow{V_{sc}}$ = Spacecraft velocity vector (m/s)
- M_{sc} = Spacecraft mass (kg)

The new formula takes into account the atmospheric winds in the upper atmosphere. These winds can exceed speeds of 1000 m/s and can have a 10% to 14% impact on the density component when calculating the atmospheric drag, so it is important to have these winds taken into account (Pilinski & Palo, 2009:11).

3.2.5 Experimental approach

Predicting and determining the atmospheric drag force on a satellite with a varying atmospheric density acting on it is a difficult task and the results could be questioned. For more convincing results, a case study through experiment was performed to be able to observe the impact that a fluctuating atmospheric density has on a satellite in LEO.

As the CubeSat constellation for this thesis is being deployed from the ISS and each satellite has a 2U form factor, the satellite of choice for this case study will be the 2U CubeSat nSight-1, a nanosatellite designed and built by SCS Space. Apart from having the same deployment altitude and orbit, this work focussed on nSight1 particularly as the flying orientation was also stabilised in a forward-facing position along the velocity vector within 10 degrees, using its attitude determination and control subsystem (ADCS) (nSight-1 - eoPortal Directory - Satellite Missions, 2020).

It is important to have this constant forward-facing flying orientation to maintain a constant drag force surface for the most accurate results in determining the drag force through observational results.

nSight-1 was deployed from the ISS into an approximate 400 km LEO on 25 May 2017 and de-orbited on 24 April 2020. The full lifetime of the satellite will provide ample data on the orbit to be collected. To be able to do this, CubeSat data in the form of two-line element (TLE) data and an accurate atmospheric model will be needed.

A TLE can be directly imported into STK and modelled to produce a satellite in that given orbit. With some knowledge or a diagram, TLEs can be interpreted as in Figure 8, but it does not include latitude, longitude and altitude (LLA) data, which is needed to find specific atmospheric density data. STK is able to model a satellite from a TLE file and is able to generate the LLA from it, as seen in Figure 18. This is vital in finding the specific densities for the experiment.

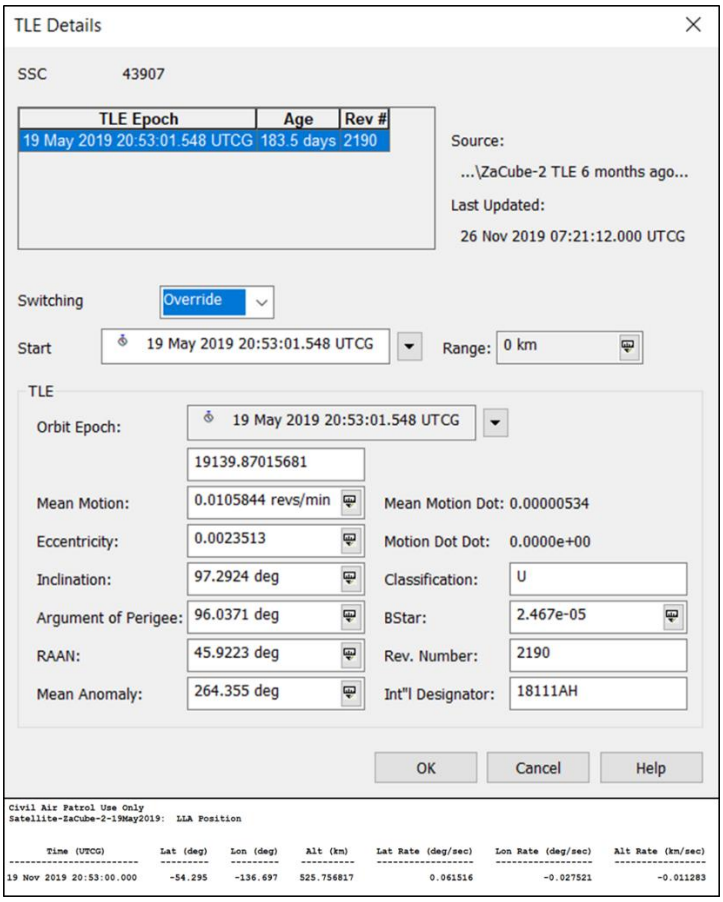

Figure 18: STK TLE and LLA

3.2.5.1 Atmospheric density model NRLMSISE-00

Calculating the drag force relies on using an accurate density model of atmosphere of the Earth. The location of the satellite in the atmosphere is of extreme importance, as the density and conditions are different for each location. Multiple atmospheric models exist, so using the correct model is important for accurate results. The atmospheric density model NRLMSISE-2000 will be the most suitable for this project, as it has become the standard for international space research in predicting satellite decay due to atmospheric drag (Smith, 2017). The model includes shuttle flight data and incoherent radar scattering data that is used to produce temperature and total density information on a longitude- and latitude-specific basis (Fortescue, Stark & Swinerd, 2011). Atmospheric conditions at specific locations in the atmosphere require specific inputs to be able to estimate an accurate density at that point for the instantaneous drag coefficient calculations. The parameters required for the model are the longitude, latitude, altitude and time stamp of the satellite to be able to produce the atmospheric density composition at that specific time and place.

TLE data contains all the necessary inputs for the model at the desired position. The next section will use the general drag force formula from equation 3.1 to derive a new formula for the drag coefficient to be used with the experimental data from the TLEs and atmospheric model.

3.2.5.2 Drag coefficient equation derivation

With observational TLE data, a formula was derived that is based on the rocket theory in equation 2.3 to find an approximate value for the drag coefficient. Two-line element (TLE) data from nSight-1 was used in conjunction with STK to estimate an approximate drag coefficient for the satellite.

As the atmospheric conditions fluctuate in LEO, approximate data over time was used and implemented from the atmospheric drag equation 3.1. As stated previously, there are atmospheric winds in the upper atmosphere, but as this is already accounted for in the TLE data, the approximate velocity from the TLEs can be used without compensating for those winds.

- General rocket equation from the basic approach

Equation 3.4 presents the basic rocket (equation 3.1) with the drag force broken down as the subject of Newton's second law of motion, $F = ma$:

$$F_d = m.a = \frac{1}{2}.\rho.V^2.A.C_d \tag{3.4}$$

Where:

- a = Acceleration (m/s^2)
- ρ = Atmospheric density (kg/m^3)
- V = Relative velocity of the spacecraft with respect to the atmosphere (m/s)
- C_d = Drag coefficient (dimensionless)
- A = Projected surface area of the spacecraft (m^2)
- m = Mass of the spacecraft (kg)

- Approximate acceleration and average velocity

$$\bar{a} = \frac{-(V_f - V_i)}{t_{f-t_i}} \tag{3.5}$$

$$\bar{v} = \frac{V_f + V_i}{2} \quad (3.6)$$

Where:

- $\bar{a}$ = Approximate acceleration (m/s^2)
- $\bar{v}$ = Approximate average speed (m/s)
- V_i= Initial velocity at 0 seconds (m/s)
- V_f= Final velocity after x number of days, months or years, converted to seconds (m/s)
- t_i = Initial or starting time (s)
- t_f = Final or ending time (s)

- Approximate drag coefficient ($\boldsymbol{Cd}$) from equation 3.4

By making the drag coefficient ($\boldsymbol{Cd}$) in equation 3.4 the subject of the formula and substituting equations 3.5 and 3.6 into equation 3.4 to replace the acceleration and velocity with their averages, an approximate drag coefficient vector is found in equation 3.7.

$$\overline{Cd} = \frac{2.m.\bar{a}}{\rho.A.\bar{v}^2} \quad (3.7)$$

By using start and end TLE data from specific time periods, the approximate drag coefficient over that period of time can be found using equation 3.7.

- Approximate drag force

Now that the uncertain elements in the general rocket equation have been found, the approximate drag coefficient in equation 3.7 can be substituted into the original rocket equation 3.1 to form an approximate drag force equation in equation 3.8:

$$F_d = \frac{1}{2}.\rho.V^2.A.\left(\frac{2.m.\bar{a}}{\rho.A.\bar{v}^2}\right) \quad (3.8)$$

Where:

- F_d = Drag force (N)
- m= Mass of the spacecraft (kg)
- A = Projected surface area of the spacecraft (m^2)
- ρ = Atmospheric density (kg/m^3)
- $\bar{a}$ = Approximate acceleration (m/s^2)
- $\bar{v}$ = Approximate average speed (m/s)

With the approximate equations derived, TLE data sets can now be used that are available online for almost all CubeSats in orbit, as well as CubeSats that have already de-orbited. With the TLE data being raw numbers, the software package STK was used to process the data.

The experimental approach in this section uses multiple TLE data sets from nSight-1 over a period of 11 months of being in orbit. The data of the first month will be skipped for the stabilising phase where the CubeSat is orientated from a tumbling position to a stable nadir flying orientation. All the data and equations were sorted in tables and then transferred to Matlab to generate graphs.

In order to determine the approximate drag coefficient from equation 3.7, the approximate velocity and acceleration from equations 3.5 and 3.6 were compiled in tables.

The next part of this thesis will work towards solving equations 3.7 and 3.8 by solving each of the variables in the following order.

(a) Find the approximate velocity by inputting the TLEs from all the desired times into STK to generate the mean motion in revolutions per minute (RPM) and the altitude for each instance with equation 3.9 (angular velocity to linear velocity formula).

$$V = r.\omega = r\,x\,\frac{2\pi}{60}.N \quad (3.9)$$

$$r = Radius\ of\ the\ earth + Altitude \quad (3.10)$$

Where:

- V = Instantaneous linear velocity (m/s)
- ω = Angular velocity (Rad/s)
- r = Distance to satellite from the centre of the Earth (m)
- N = Mean motion or revolutions per minute of the satellite around the Earth (rpm)

Table 10 breaks down equation 3.9 into a table in order to sort out and calculate the approximate velocity for each instance in time and position. The Earth volumetric mean radius is taken as 6371000 m.

Table 10: Approximate velocity calculations

Month	**Date and instantaneous time (UTCG)**	**Surface altitude (km) [From TLE]**	**Altitude from the centre of the Earth (km)**	**Mean motion around Earth (RPM)**	**Approximate velocity (m/s)**
1 (Start date)	25 Jun 2017 @ 22:58:50.847	398,510	6371398,5	0,010799	**7205,081**
2	25 Jul 2017 @ 21:38.59	402,808	6371402,8	0,010801	**7206,554**
3	25 Aug 2017 @ 23:53.42	404,531	6371404,51	0,010805	**7208,891**
4	25 Sep 2017 @ 08:52.00	394,530	6371394,50	0,010809	**7212,283**
5	25 Oct 2017 @ 22:05.00	395,895	6371395,89	0,010815	**7216,021**
6	25 Nov 2017 @ 21:43.00	397,464	6371397,46	0,010821	**7219,625**
7	25 Dec 2017 @ 21:57.49	390,151	6371390,15	0,010824	**7222,019**
11 (End date)	31 May 2018 @ 20:45.00	388,515	6371388,51	0,011000	**7234,094**

(b) Determine instantaneous atmospheric densities for each TLE from the online website “amentum.com.au/atmosphere” by using the LLA positions generated from the TLEs in STK.

Table 11: Instantaneous atmospheric densities

Date and instantaneous time (UTCG)	**NRLMSISE00 Atmospheric density**	**Altitude (km) [From TLE]**	**Latitude (deg)**	**Longitude (deg)**	**Exospheric temp neutral, K**
25 Jun 2017 @ 22:58:50,847	**2,318E-12**	398,510	-2,604	93,607	862,4
25 Jul 2017 @ 21:38,59	**4,997E-12**	402,808	-3,022	-65,745	1207,1
25 Aug 2017 @ 23:53,42	**2,044E-12**	404,531	-2,189	75,18	869,5
25 Sep 2017 @ 08:52,00	**5,840E-12**	394,530	-0,801	119,694	1221,3
25 Oct 2017 @ 22:05,00	**2,423E-12**	395,895	-1,835	97,561	868,8
25 Nov 2017 @ 21:43,00	**5,932E-12**	397,464	-0,998	-82,132	1210,3
25 Dec 2017 @ 21:57,49	**2,762E-12**	390,151	0	94,795	880,7
31 May 2018 @ 20:45,00	**6,730E-12**	388,515	-2,775	-113,17	1 145,0

(c) Determine the approximate acceleration and $(velocity)^2$ component of equation 3.7.

The following equations were used in solving Table 12:

- Approximate average drag coefficient

$$\overline{Cd} = \frac{2.m.\bar{a}}{\rho.A.\bar{v}^2} \quad (3.7)$$

- Approximate average acceleration

$$\bar{a} = \frac{-(V_f - V_i)}{t_{f-t_i}} \quad (3.5)$$

- Approximate average velocity

$$\bar{v} = \frac{V_f + V_i}{2} \quad (3.6)$$

Table 12: Approximate drag coefficient data

Date and instantaneous time (UTCG)	**Acceleration (m/s^2)**	**$(Velocity)^2$ (m/s)**	**Initial velocity (V_i) (m/s)**	**Final velocity (V_f) (m/s)**	**Time difference between V_i & V_f (s)**	**Notes on time**
25 Jun 2017 @ 22:58:50.847	0.0000006	51923808.2	7205.08	7206.55	2587209	Time to 25 Jul 2017 (s)
25 Jul 2017 @ 21:38.59	0.0000009	51951265.4	7206.55	7208.89	2686483	Time to 25 Aug 2017 (s)
25 Aug 2017 @ 23:53.42	0.0000013	51992564.1	7208.89	7212.2	2624298	Time to 25 Sep 2017 (s)
25 Sep 2017 @ 08:52.00	0.0000014	52043983.8	7212.28	7216.0	2639580	Time to 25 Oct 2017 (s)
25 Oct 2017 @ 22:05.00	0.0000013	52096968.3	7216.02	7219.62	2677080	Time to 25 Nov 2017 (s)
25 Nov 2017 @ 21:43.00	0.0000009	52140272.6	7219.62	7222.01	2592889	Time to 25 Dec 2017 (s)
25 Dec 2017 @ 21:57.49	0.0000011	52035305.7	7205.08	7222.01	15807539	Time from 25 Jun 2017 (s)
31 May 2018 @ 20:45.00	0.0000009	52244798.1	7222.01	7234.09	13560431	Time from 25

						Dec 2017 (s)
31 May 2018 @ 20:45.00	0.0000010	52122443.2	7205.08	7234.09	29367970	Time from 25 Jun 2017 (s)

(d) Determine approximate drag coefficients with equation 3.7 from Table 10, Table 11 and Table 12 to calculate the approximate drag coefficient using month-to-month TLE data and over an 11-month time period.

Table 13: Approximate drag coefficient

Date and instantaneous time (UTCG)	**Drag coefficient**	**Acceleration (m/s²)**	$(Velocity)^2$ **(m/s)**	**Mass (kg)**	**Cross section area (m²)**	**Average density (kg/m^3)**	**Notes on density from Table 9**
	$\overline{Cd} = \frac{2.m.\overline{a}}{\rho.A.\overline{v}^2}$	$\overline{a} = \frac{-(V_f - V_i}{t_{f-t_i}}$	$\overline{v} = \frac{V_f + V_i}{2}$				
25 Jun 2017 @ 22:58:50.847	1,4987171	0,0000006	51923808,15	2,5	0,01	3,66E-12	Average density between June 2017 and July 2017
25 Jul 2017 @ 21:38.59	2,3782519	0,0000009	51951265,35	2,5	0,01	3,52E-12	Average density between July 2017 and

							August 2017
25 Aug 2017 @ 23:53.42	3,1527167	0,0000013	51992564,07	2,5	0,01	3,94E-12	Average density between August 2017 and September 2017
25 Sep 2017 @ 08:52.00	3,2931522	0,0000014	52043983,84	2,5	0,01	4,13E-12	Average density between September 2017 and October 2017
25 Oct 2017 @ 22:05.00	3,0936730	0,0000013	52096968,27	2,5	0,01	4,18E-12	Average density between October 2017 and November 2017
25 Nov 2017 @ 21:43.00	2,0364933	0,0000009	52140272,57	2,5	0,01	4,35E-12	Average density between November 2017 and

							December 2017
25 Dec 2017 @ 21:57.49	4,0534712	0,0000011	52035305,66	2,5	0,01	2,54E-12	Average density between December 2017 and June 2017 (start date)
31 May 2018 @ 20:45.00	1,7955226	0,0000009	52244798,09	2,5	0,01	4,75E-12	Average density between December 2017 and May 2018
31 May 2018 @ 20:45.00	**2,0948355**	**0,0000010**	**52122443,22**	**2,5**	**0,01**	**4,52381E-12**	**Average density between May 2018 and June 2017**

It can be seen from Table 13 that the approximate drag coefficient over a month-to-month time period yielded oscillating results due to the varying atmospheric density at different locations and times within LEO. From the literature in the Research Design and Methodology section, it was found that a drag coefficient of 2.2 for a typical spacecraft, such as a CubeSat, was a reasonable value. Table 13 shows how the drag coefficient oscillates from month to month and illustrates the variations in atmospheric density over time, position and altitude. A study done by Vallado (2005)

shows that atmospheric propagation results could fluctuate from 50–100 km purely by how the space weather parameters are treated within a programme (Vallado & Kelso, 2005). This shows how small parameter changes have significant effects on results, so using the correct value for the drag coefficient is crucial.

By using a longer time period of 11 months, an approximate drag coefficient of 2.1 was found and by comparing that result to the recommended value of 2.2, it is safe to assume that the recommended drag coefficient value of 2.2 is accurate for this specific CubeSat in this altitude range. This value is critical for the STK simulation software to be able to produce accurate results.

(e) Approximate ΔV calculations

From Table 13 the ΔV over the 11 months can be calculated with equation 3.11 by subtracting the initial velocity from month 1 from the final velocity in month 11. The values are given in Table 12.

- Approximate ΔV

$$\Delta V_{approximate} = V_{need} - V_{current} \quad (3.11)$$
$$\Delta V_{approximate} = 7234.1 - 7205.1$$
$$\boldsymbol{\Delta V_{approximate} = 29.01\ m/s}$$

The ΔV loss over 11 months was found to be approximately 29.01 m/s.

The propellant needed to get the satellite back to the initial altitude after 11 months of altitude drop due to drag was calculated with equation 3.12, which was derived from the rocket equation 2.3 in Chapter 2:

$$m_p = m_o[1 - e^{-\frac{\Delta V}{g_{o.}I_{sp}}}] \quad (3.12)$$

Where:

- $\mathrm{m_p} = \text{Propellant mass used } (kg)$
- $\mathrm{m_o} = \text{Initial satellite mass} = 2.5\ kg$
- $\mathrm{g_{o.}} = \text{ Gravitational constant of Earth} = 9.80665\ m/s^2$
- $\mathrm{I_{sp}} = \text{Specific impulse} = 500\text{s}$

- $\Delta V_{approximate} = 29.01\ m/s$

Calculations:

$$m_p = m_o[1 - e^{-\frac{\Delta V}{g_o.I_{sp}}}]$$

$$m_p = 2.5[1 - e^{-\frac{29.01}{500x9.81}}]$$

$$m_p = 0.014743\ kg$$

$$m_p = 14.73\ g$$

It would take approximately 14.73 g of propulsion at 500 s I_{sp} to raise the orbit back to the initial altitude after 11 months with the TLE data from nSight-1.

3.2.6 Summary

This section looked at how the drag coefficient can be estimated using an experimental approach through the use of TLE data from the CubeSat nSight-1 that has completed its mission from deployment to de-orbit. nSight-1 has very similar parameters and orbit characteristics to the mission planned in this work, so it is an ideal candidate for comparison. As stated in the research, determining exact values is almost impossible with all the uncertainties and unpredictable meteorology. An estimated drag coefficient of 2.1 was found over an average of 11 months. Even with all the uncertainties, this result is very close to the recommended drag coefficient of 2.2 for spacecraft that include small satellites, such as CubeSats. With the findings of this chapter, the recommended drag coefficient of 2.2 will be used for all simulations throughout the rest of this thesis. The results of this case study will also form a good baseline for comparison and predictions for simulations and calculations in this thesis.

3.3 MDASAT CONSTELLATION ORBITAL PERFORMANCE CASE STUDY

The following sections look at the performance of the constellation when deployed from the ISS and determine whether this deployment would be feasible in terms of its mission requirements and orbital configuration and maintenance using electric propulsion.

3.3.1 Introduction

The constellation will be deployed from the ISS as a cluster of satellites so that the constellation will be in the orbit of the ISS with a 51.43 degrees inclination. From Mtshemla (2017), the optimal solution for coverage for the South African EEZ area is a Walker-delta constellation. From Mtshemla's work, revisit times of between 5 and 12 minutes are possible with 12 satellites in 6x2 or 4x3 constellation configurations at 39 degree and 45 degree inclinations, respectively. The 6x2 constellation is the favourable configuration as two planes have fewer complexities than three planes (orbital plane change is costly in terms of ΔV budgets, so fewer planes imply fewer launches required).

At this point it will be assumed that plane change is not possible, so the optimal constellation of 6x2 will be at an inclination of 51.43 degrees compared to the optimal 39 degree inclination. This chapter will do a case study on a 6x2 Walker-delta constellation at a 51.43 degree inclination to determine whether deploying from the ISS will meet the mission requirements. All simulations will assume the satellites are in a stable nadir flying position from the start with no tumbling.

3.3.2 ISS deployed Walker delta 6x2 constellation at 51.43 degrees

A visual representation of the constellation can be seen in Figure 19 with the EEZ zone boundary marked around the coast of South Africa where the focus point of the simulations will be.

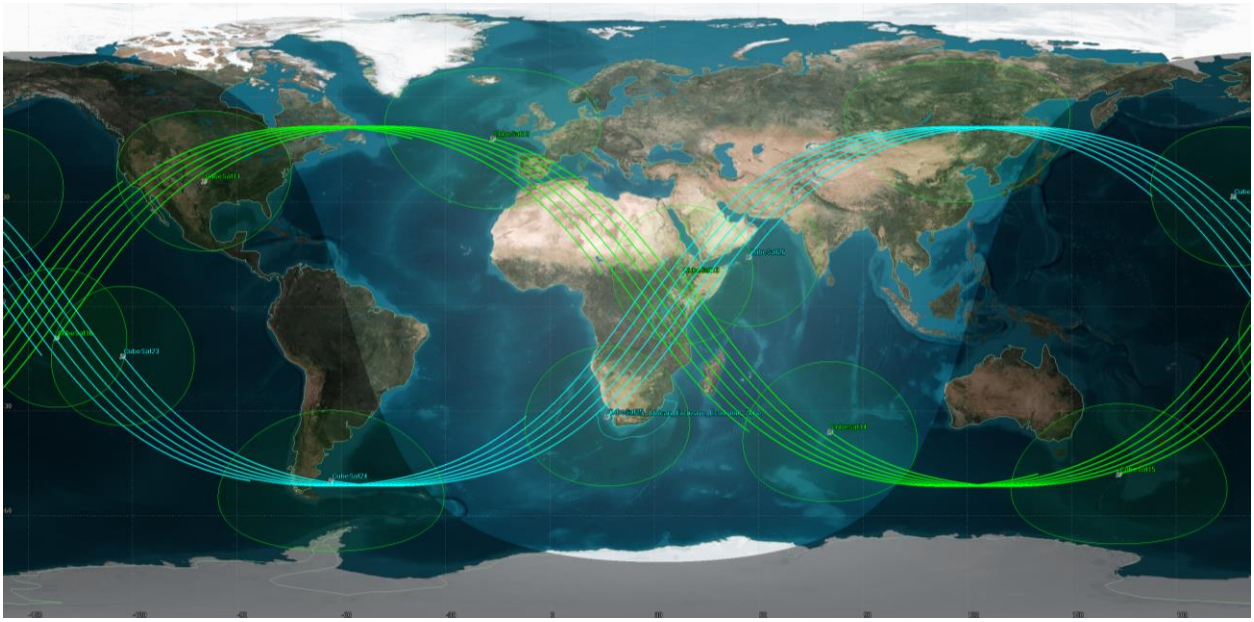

Figure 19: ISS deployed 6x2 constellation

The orbital elements for the 6x2 Walker-delta constellation is shown in Table 14 with the STK simulation results in Figure 20 for the average daily access and revisit times over the EEZ zone in South Africa.

Table 14: Satellite orbital elements for ISS constellation

Orbital planes	**Plane 1**	**Plane 2**
Altitude (km) Inclination (°) RAAN (°) True anomaly (°)	405 51.43 328.987 Satellites 1-6: 0, 60, 120, 180, 240, 300	405 51.43 148.987 Satellites 7-12: 30, 90, 150, 210, 270, 330

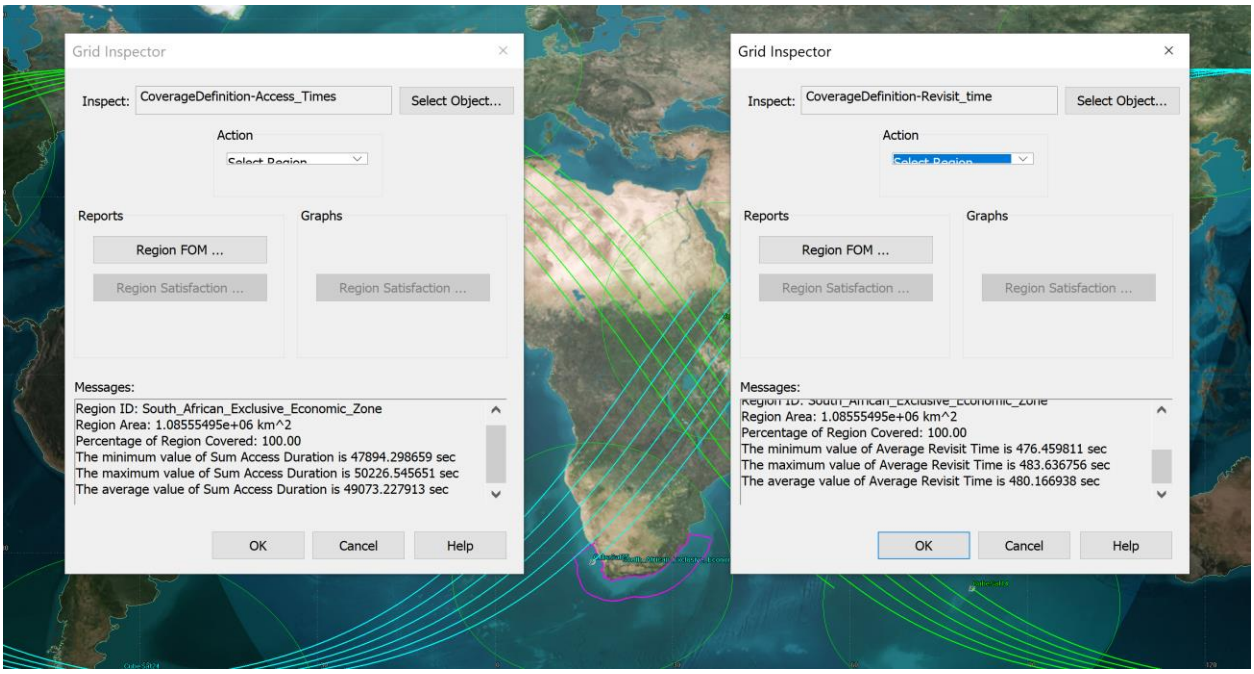

Figure 20: ISS 6x2 Walker-delta constellation EEZ region simulation results

From Figure 20 on the left the average daily access time was found to be 49073.23 seconds or 13.6 hours, and on the right daily revisit time of 480.17 seconds or 8 minutes. The comparison of results between Mtshemla's work (2017) in a 39 degree constellation, and the ISS deployed constellation, can be seen in Table 15.

Table 15: Comparison of constellations

Constellation inclination	**Constellation configuration**	**Daily average revisit times**	**Daily average access times**
51.43 degrees	6x2	8 minutes	13.6 hours
39 degrees	6x2	5 minutes	16.4 hours

From the results in Table 15, it can be seen that the ISS constellation did not perform as well as the constellation on 39 degrees, but still performed well within in the range specified in the objectives of the research and this indicates that deployment from the ISS would perform sufficiently well for the mission.

3.3.3 Summary

This section looked at the optimal constellation for coverage of the South African EEZ. Mtshemla (2018) found the optimal constellation to be a 6x2 Walker-delta configuration at a 39 degree inclination. The mission specifications for this work state that the constellation will be deployed from the ISS, which orbits at an inclination of 51.43 degrees compared to 39 degrees. As assumed so far, plane change might not be possible. With the optimal constellation requiring two planes, plane change will be needed when deploying all 12 CubeSats at the same time from a single deployment, or alternatively, two deployments need to be made into the two desired planes.

With the ISS constellation performing similarly to the optimal constellation on 39 degrees, the next section will look at the configuration and maintenance of the constellation.

3.4 ORBITAL CONFIGURATION AND MAINTENANCE SIMULATIONS

This section starts with the mission details, setting up of STK and calculating whether plane change will be possible within the capabilities of the electric propulsion. STK simulations will then be done on orbital configuration and the phasing out of the constellation, a 5-year mission and finally, whether de-orbiting is a possibility.

3.4.1 Introduction

This section looks at the configuration and maintenance of the constellation deployed as a single cluster of CubeSats from the ISS. It was determined that for optimal coverage a Walker-delta configuration of 12 satellites evenly spread out over two planes meets the coverage requirements for the South African EEZ. From the mission requirements, the constellation will be deployed as a single cluster and then spread out with on-board capabilities. This means that for the considered mission configuration, a plane change will be needed in addition to phasing out the satellites from a single position throughout the orbit.

This chapter will consider all the perturbations acting on a satellite. Therefore, to validate that STK is properly set up, a simulation was run and compared with the TLE results from the case study at the start of this chapter. A plane change will then be calculated, followed by the phasing out of the cluster of satellites into an evenly spread-out constellation. Once the phasing out has been

completed, a five-year mission will be designed and simulated in STK. Finally, de-orbiting will be investigated for the end of the five-year mission. The five-year mission simulations will also be used to validate whether the commercial off-the-shelf propulsion solution from Hypernova Space Technologies, used in this work, are feasible to support a five-year mission from the initial phasing to the end-of-life de-orbiting.

3.4.2 Mission details

The CubeSat for this mission was originally stated as a 2U CubeSat, but with the propulsion system using up 0.5U of space, it will be a 3U CubeSat with a weight of 4 kg, including the propulsion system. The thruster of choice for the mission will be the Hypernova plasma thruster, as it has local support and availability and was designed for CubeSats. The thruster data from Chapter 2 in Figure 6 was used for the propulsion calculations.

3.4.3 STK validation

For the most accurate results, a proper setup of the propagator within Astrogator needed to be set up. The NRLMSISE-2000 atmospheric model was selected with the latest space weather data from http://celestrak.com/SpaceData/, as seen in Figure 21.

The space weather data file contains daily observed solar flux and geomagnetic indices, approximately 10 years of predicted data and will be propagated daily within the simulations.

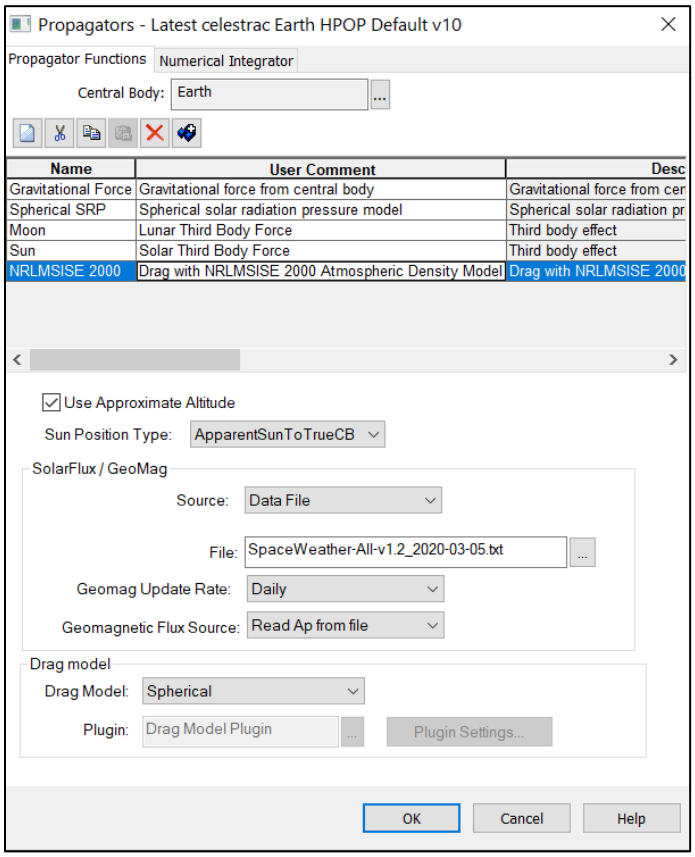

Figure 21: STK Propagator setup

STK validation simulation and results

To validate that STK is properly set up for the specific mission conditions, the real world TLE observation results from nSight-1 will be simulated and compared using the observation data from nSight-1 as the inputs to STK.

The 11-month mission from nSight-1 earlier in this chapter was exactly recreated in STK from 25 Jun 2017 22:58:50.847 until 31 May 2018 20:45. TLE data from Chapter 3 indicated that the altitude dropped from 398.51 km to 388.52 km. This will be compared to the STK results next.

Results

The orbit became more elliptical compared to the original orbit, so the point of perigee will be the altitude of interest to use as it is the lowest point to Earth in the orbit. The left side of Figure 22

below displays the initial starting conditions (as per TLE data) and setup of nSignt-1, and the right side displays the results of the simulated 11-month period in orbit.

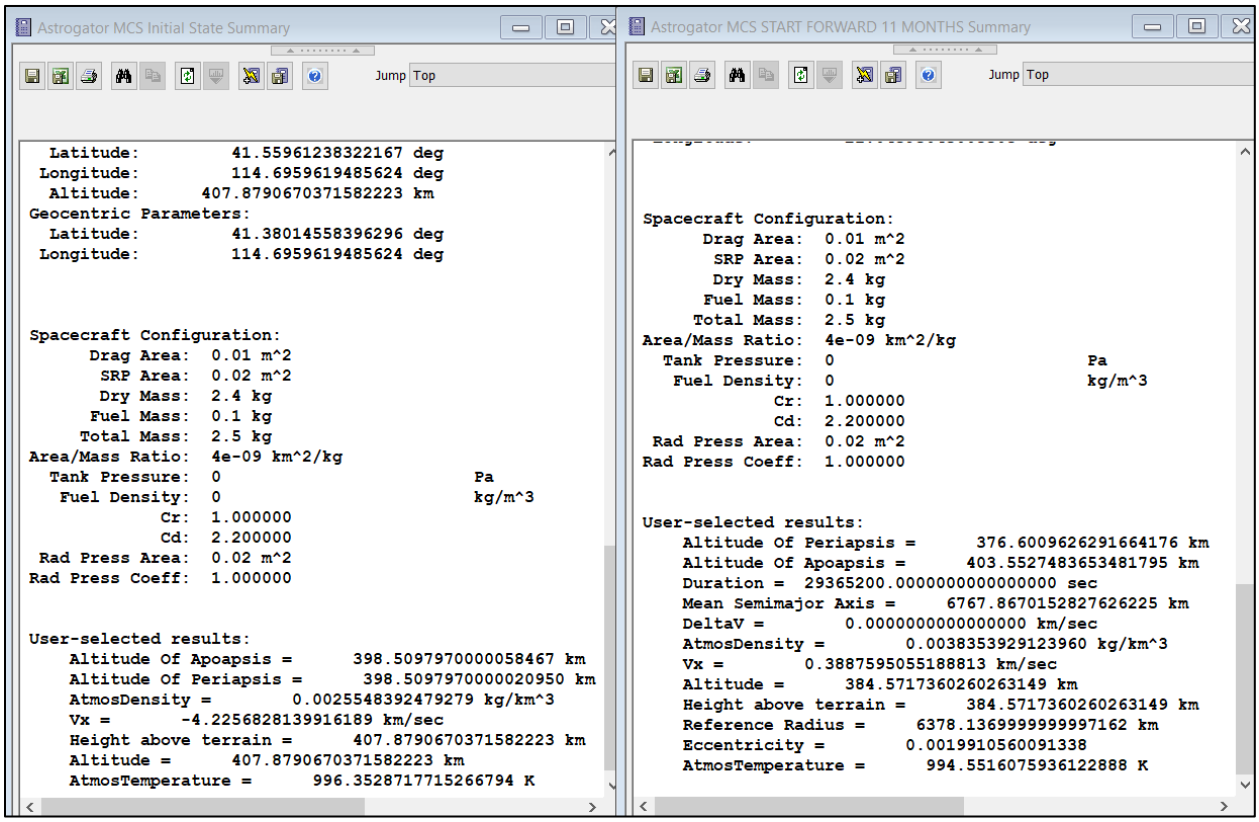

Figure 22: The 11-month orbital decay STK results

Looking at the altitude of 384.57 km on the right in Figure 22 of the 11-month simulated results it was found that the altitude difference between the actual TLE position data of 388.52 km and the simulated data differ roughly 4 km from each other. From Vallado and David (2013), it was found that atmospheric propagation results can differ by up to 50–100 km, purely by how the propagator treats the space weather parameters. Therefore, setting up the simulation with the correct parameters is crucial for accurate results. An altitude difference of 4 km between real life data and simulated data is, therefore, a good indication that STK has been properly set up. The next section will look at plane change.

3.4.4 Plane change

Two different plane change manoeuvres will be looked at, namely:

- Inclination (*i*) plane change; and
- RAAN (Ω) plane change.

Although it was confirmed previously that inclination change will not be necessary, the cost in ΔV to plane change from the 51.43 degrees of the ISS to the optimal 39 degrees will still be explored. For a Walker-delta configuration with two planes, the right ascension of the ascending node (RAAN) is phased out by 180 degrees, while maintaining a set inclination and altitude (Gagliano, 2018).

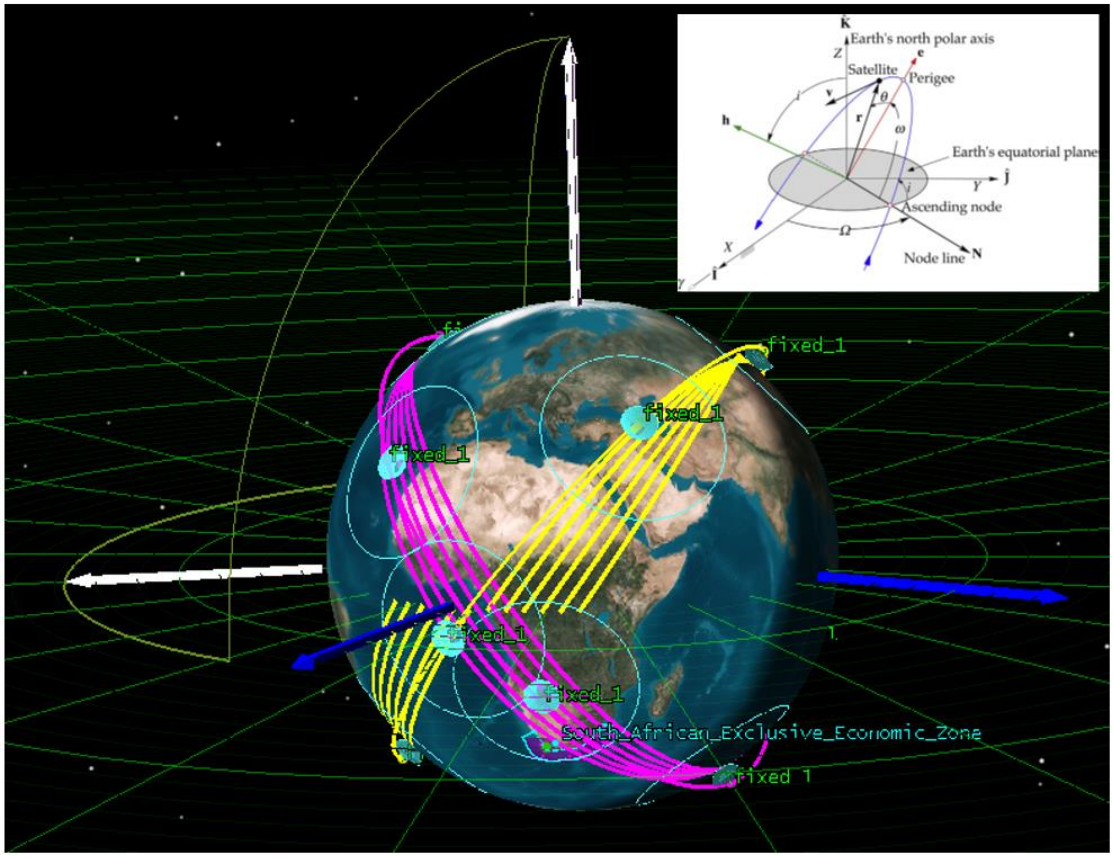

Figure 23: 51.43 degree, 6x2 Walker-delta constellation

The simple plane change formula from equation 2.4 in Chapter 2 will be used to determine whether plane change will be possible.

3.4.4.1 Plane change

Inclination plane change calculations

Angle change required (θ):

- θ = 51.43 – 39 degrees

  θ = 12.43 degrees

Velocity before and after the burn:

The velocity at 405 km at an inclination of 51.43 degrees was found in STK to be:

- $Vt = 7665\, m/s$

From equation 2.5, the plane change calculation for 12.43 degrees yields a ∆V of

- $\Delta V = 2.Vt.\sin(\frac{\theta}{2})$
- $\Delta V = (2)(7665)(\sin(\frac{12.43}{2}))$
- $\Delta V = 15330\sin(6.215)$
- $\boldsymbol{\Delta V = 1659.62\, m/s}$

RAAN plane change calculations

From the satellite orbital elements for the ISS constellation in Table 14, we have:

Angle change required (θ):

- θ = 328.987– 148.987

  θ = 180 degrees

Velocity before and after the burn:

The altitude and velocity remain the same. The velocity at 405 km at an inclination of 51.43 degrees was found in STK to be:

- $Vt = 7665\, m/s$

180 degree plane change calculation:

- $\Delta V = 2.Vt.\sin(\frac{\theta}{2})$

- $\Delta V = (2)(7665)(\sin(\frac{180}{2}))$
- $\Delta V = 15330\sin(90)$
- $\boldsymbol{\Delta V = 15330\, m/s}$

Hypernova total ΔV calculations

The maximum ΔV that the Hypernova thruster can achieve with the $100\ g$ of on-board propellant can be calculated with the rocket equation in equation 2.3 from chapter 2.

Recalling equation 2.3:

$$\Delta V = I_{sp} g_0 \ln(1 + \frac{M_p}{M_f}) \quad (2.3)$$

Hypernova thruster data:

- I_{sp} = $500s$
- M_p = $0.1\ kg$
- M_f = $3.9\ kg$

Hypernova maximum total ΔV:

- $\Delta V = I_{sp} g_0 \ln(1 + \frac{M_p}{M_f})$
- $\Delta V = (500\text{x}9.81)\ln(1 + \frac{0.1}{3.9})$
- $\boldsymbol{\Delta V = 124.184\, m/s}$

Plane change conclusion

As was expected, plane change is a costly manoeuvre to perform and beyond the capabilities of the thruster system. The ΔV cost for moving from the ISS inclination 12.43 degrees was found to be $1659.62\, m/s$ while the Hypernova thruster can only achieve a maximum total ΔV of $124.184\, m/s$. To achieve two planes is even more costly. This indicates that to form a 2-plane Walker-delta constellation, each plane of CubeSats has to be deployed into their desired orbits as a cluster. The following section covers the configuration of the constellation.

3.4.5 Orbital configuration and phasing simulations

This section will use STK to phase out six CubeSats deployed in a cluster from the ISS. As the Walker-delta configuration in this work was based on two identical constellations on different orbital planes, one constellation in a single orbit will be simulated and assumed it is the same for the second plane. Two possible approaches will be looked at to phase out and configure the constellation from a single cluster.

3.4.5.1 Phasing by atmospheric drag

By changing the attitude of the flying orientation from one CubeSat to the next, the area on which the aerodynamic drag force acts, will be different and cause a drift between the two bodies. This change in drag area will be looked at to determine whether this will be a viable option to form the constellation in an attempt to save on propulsion for the initial formation and configuration of the constellation. The two flight orientations will be forward facing and sideways facing, to change the surface area on which the atmospheric drag will act.

The flight orientations can be seen in Figure 24 with cross-sectional areas of $0.01\ m^2$ and $0.03\ m^2$, respectively.

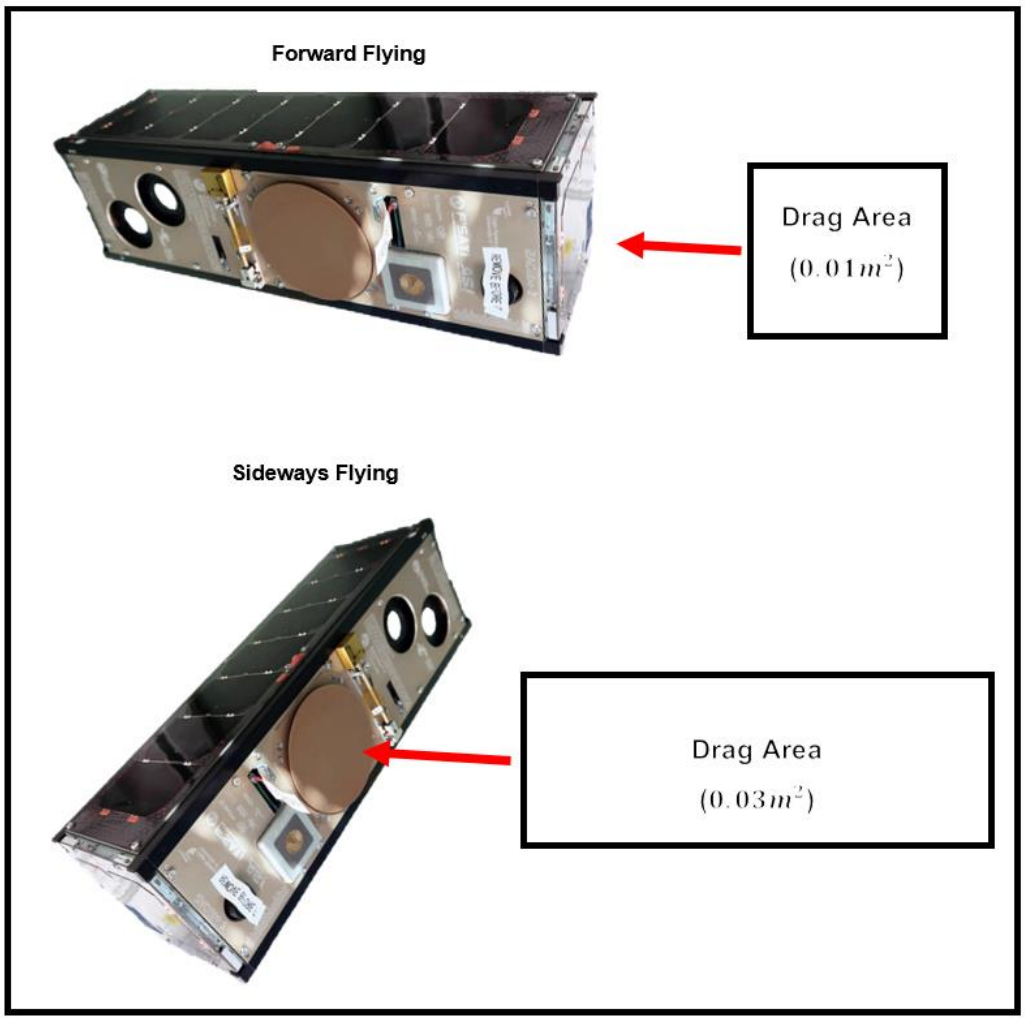

Figure 24: CubeSat flight orientations

3.4.5.2 Phasing by propulsion

The Hypernova plasma thruster will be modelled in STK in Figure 27 and integrated in each CubeSat for the simulations. The thruster will be located at the rear along the long axis of the CubeSat in the forward flying orientation as seen in Figure 25.

Figure 25: Thruster location

3.4.6 Phasing simulations

This section simulates the phasing of a cluster of six satellites evenly spread over an orbit. As mentioned in the previous section, two methods of phasing will be looked at, namely one using only drag and the other using the on-board electric propulsion.

The aim is to phase out the CubeSats evenly into their desired positions as fast as possible. To do this, the simulations will take place in two phases. Firstly, the maximum simulated time will be determined by phasing out two satellites by 180 degrees at full thrust with propulsion. This will determine the minimum time required to phase out two satellites at opposite ends of the orbit. The other satellites will take less time to phase out, as their phasing angles from a reference point will be less than 180 degrees. After the simulated time has been determined, the full phasing of the six-satellite cluster can begin.

To simplify matters and for visual comparison, the drag and propulsion phasing will be simulated simultaneously with three CubeSats starting at the same location with different setups (as described below). The simulation will look at the time duration to achieve a phase angle of 180 degrees from the same starting position between the different setups. It will be assumed they are all in the same location in the correct orientation at the start, although in a real-life situation there will be a small separation between them, as it will take some time for the satellites to orientate themselves, and the satellites will have different drag areas while orientating. In addition to the differential drag areas while orientating, the NanoRacks CubeSat deployer on the ISS gives an initial ΔV of between 0.5 m/s and 1.5 m/s to the satellites of the deployed cluster (NanoRacks, LLC. December 2013.)

The following CubeSat setups will be used to determine the best and fastest way to achieve the 180 degrees phase angle. The forward-facing CubeSat will be the reference satellite and the propulsion CubeSat will be the stopping condition for when a phase angle of 180 degrees has been achieved between the two satellites. The sideways CubeSat will be an additional CubeSat to observe the difference between the forward- and sideways-facing flying positions to determine whether that would be enough to form a constellation to save on propulsion for the initial formation forming from a starting cluster. It is assumed that this will take a long time, hence, the stopping condition will be between the other two satellites.

3.4.7 Initial CubeSat setups

All three CubeSats have identical initial conditions with the exception of the sideways-facing satellite, which has a drag area of 0.03 m^2 instead of the forward-facing drag area of 0.01 m^2. All three of the satellites are equipped with a propulsion system, hence, the masses of all three are also identical at the beginning. The initial start time for the simulations will be 6 Aug 2019 10:00:00. Figure 26 shows the initial setups with the forward-flight reference satellite left, propulsion forward in the centre and sideways flying on the right. The top frame shows the orbital elements and the bottom shows the parameters used to model perturbations.

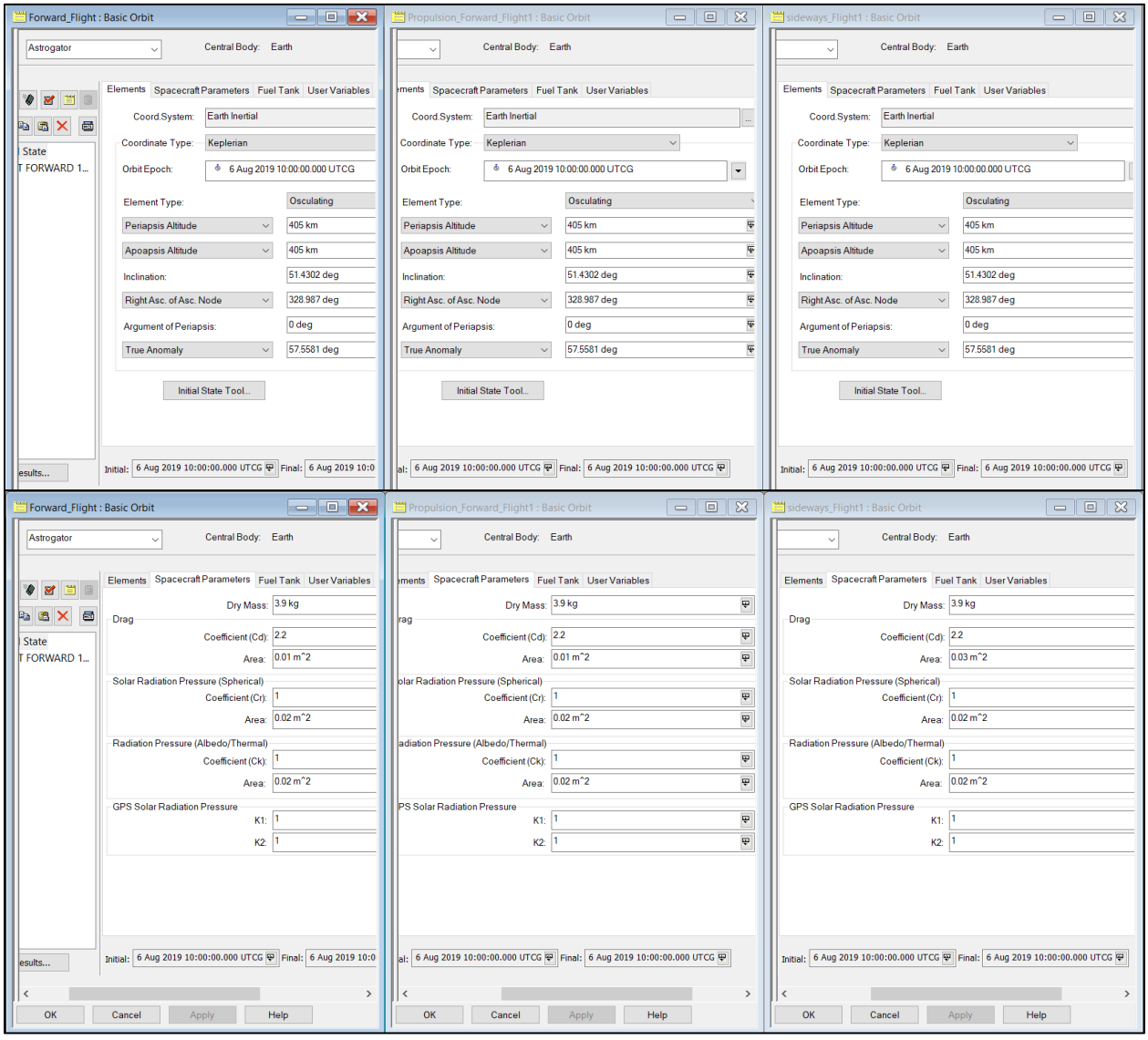

Figure 26: The initial setup of all three CubeSats

Custom Hypernova plasma thruster STK

The thruster data from Hypernova can be found in Table 16.

Table 16: Hypernova thruster data

Propulsion system		
Continous power available for propulsion system	5	W
Specific impulse, Isp	500	s
Thrust-power ratio	8	μN/W
Thrust generated (based on available power)	40	μN
Mass flow rate	8.15E-09	kg/s

The data from Table 16 was modelled in STK in Figure 27 for a custom plasma engine to be used in the propulsion simulations.

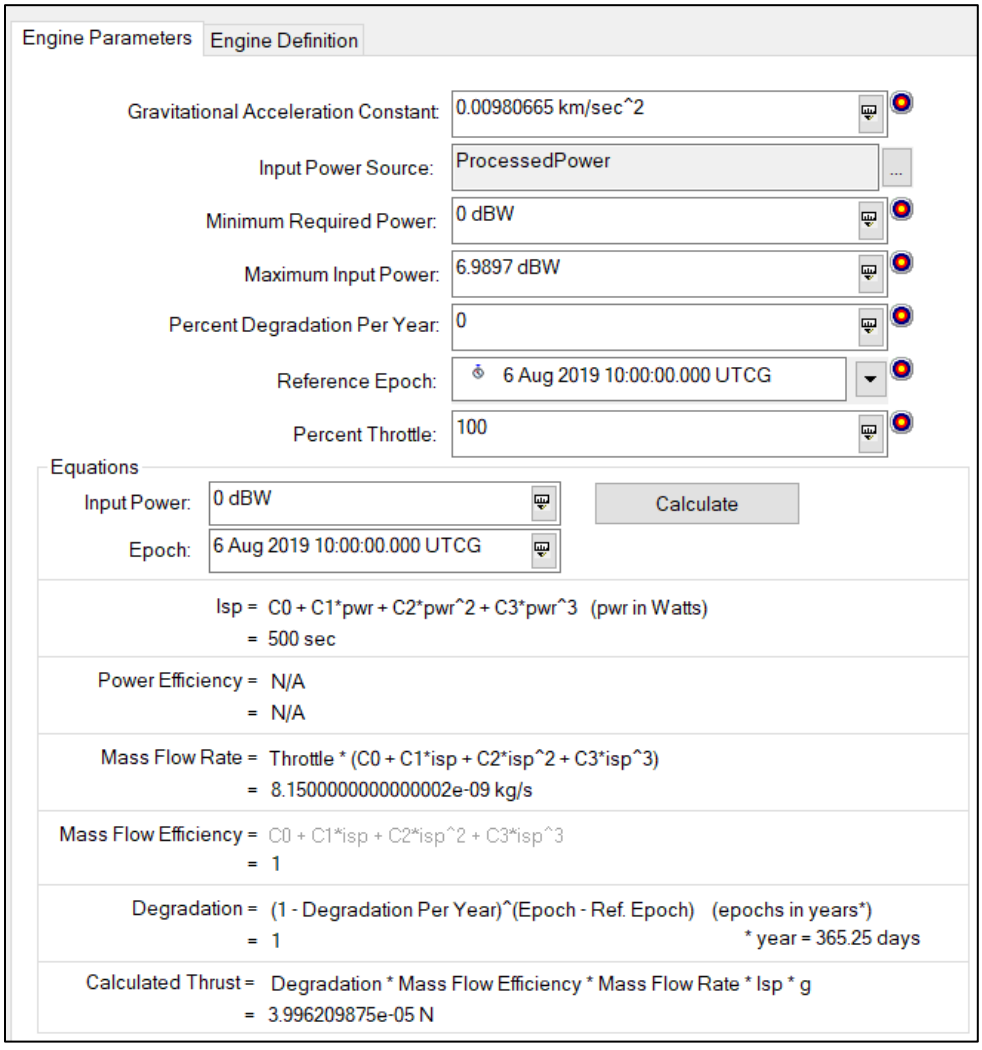

Figure 27: The Hypernova thruster model in STK

With all the initial starting parameters set in STK, the visual orientations can be seen in Figure 28.

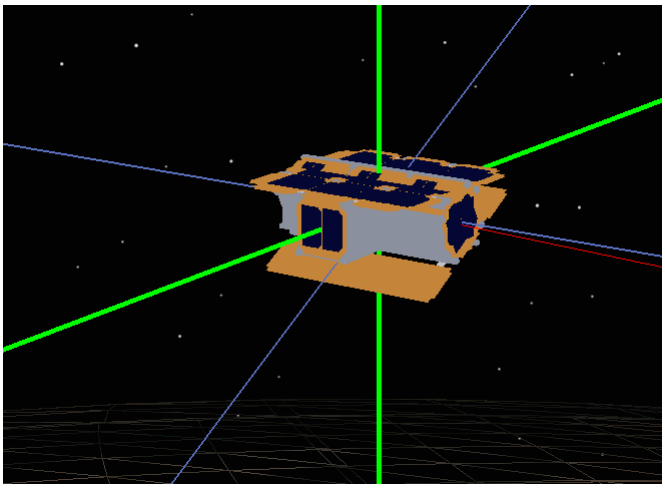

Figure 28: Initial starting cluster in STK

- Forward-facing flight path

The CubeSat is in a forward-facing flight path (with the propulsion OFF) with the smallest side pointing into the flight path and has a drag coefficient of 2.2 and a drag area of $0.01\ m^2$.

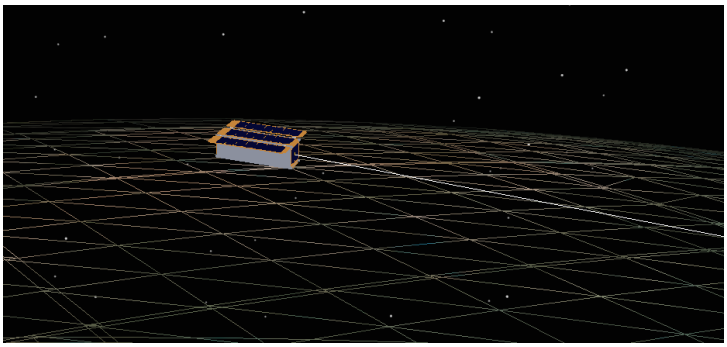

Figure 29: Forward-facing flight path (propulsion OFF) in STK

- Propulsion forward-facing flight path

The CubeSat is in a forward-facing flight angle, again with the smallest side pointing along the flight path, but the propulsion system will be ON and will burn constantly for the entire duration of flight. The drag coefficient of 2.2 and a drag area of $0.01\ m^2$ will remain the same as seen in

Figure 30. Note that the orientation is only visual and has no effect on the simulations. The flipped model is to distinguish between the propulsion ON and propulsion OFF CubeSats.

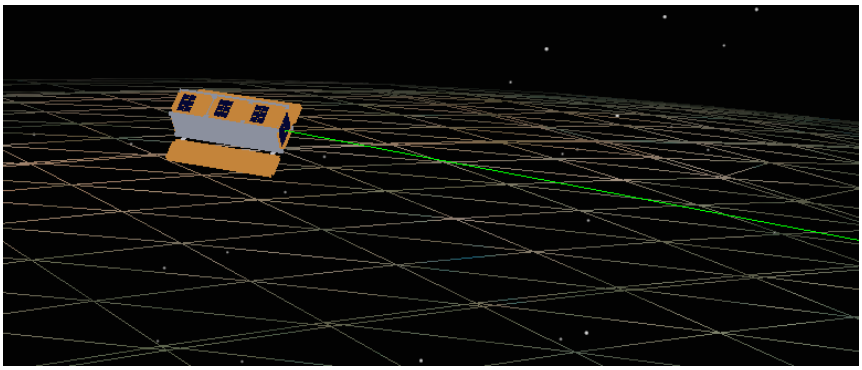

Figure 30: Propulsion forward facing flight path in STK

- Sideways facing flight path (drag satellite)

The CubeSat will be rotated 90 degrees from the forward-facing position to produce the most drag possible to determine whether this would be sufficient and possible to form the constellation without the use of propulsion.

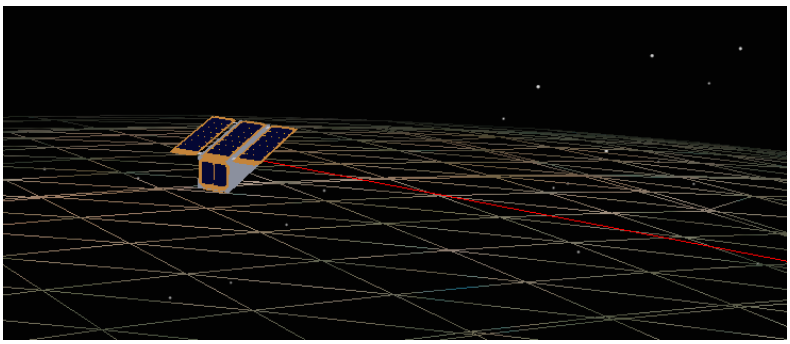

Figure 31: Sideways-facing flight path (drag satellite) in STK

3.4.8 Simulation phasing results

The phasing was started with all the CubeSats at the same location within the same orbit. As time progressed, the separation was observed until a phase angle of approximate 180 degrees between the reference forward-facing satellite and the propulsion forward-facing satellite was

observed. A yellow line shows the angle and distance to the propulsion satellite, and a blue line shows the angle and distance to the drag satellite from the reference satellite in Figure 34.

Phasing time frame

After 10 minutes there was already a large increase in distance to the propulsion satellite while the drag satellite had very little movement from the reference satellite.

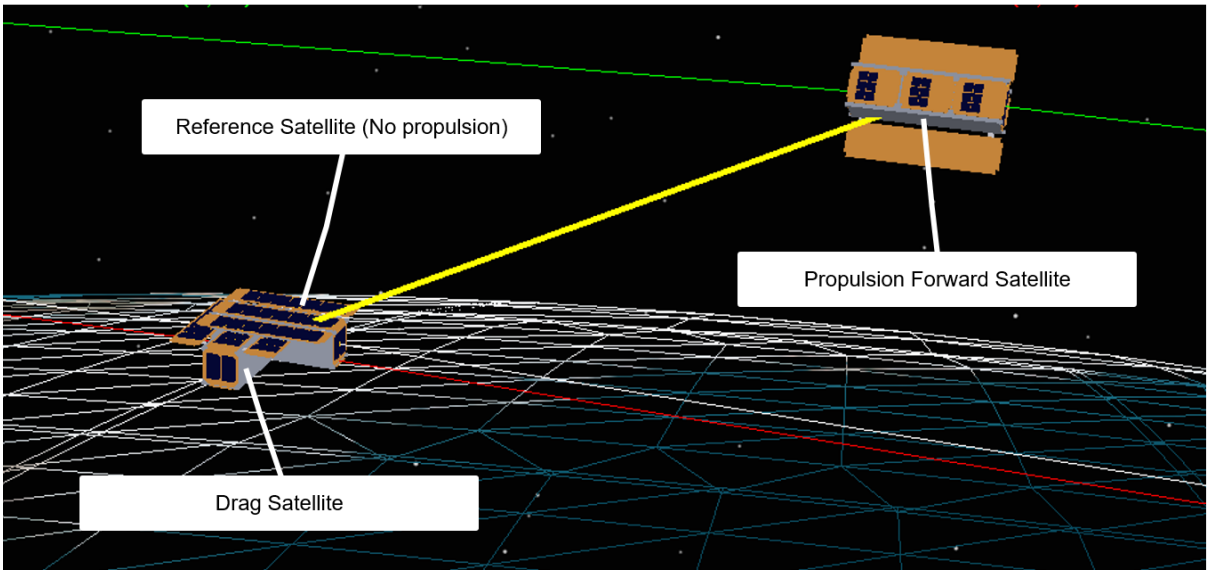

Figure 32: Satellite cluster separation after 10 minutes of flight time

After an hour a significant phase angle can be observed, as seen in Figure 33. Compared to the propulsion satellite, the drag satellite showed very little separation.

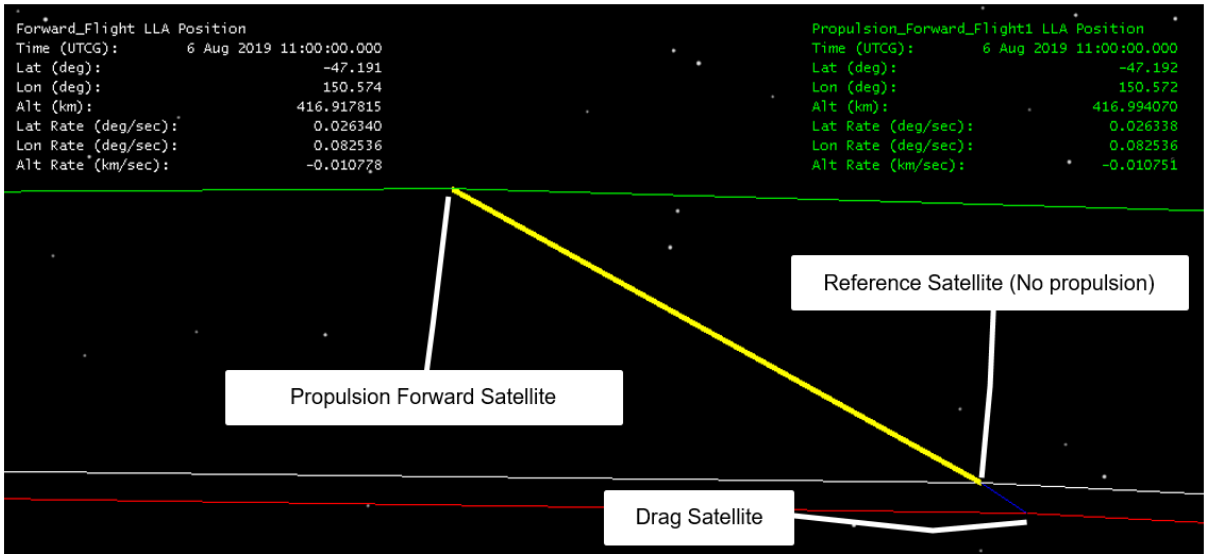

Figure 33: Satellite cluster separation after one hour of flight time

The simulation was run until the desired 180 degrees phase angle was achieved after 413 hours or 17.2 days. The results can be seen in Figure 34.

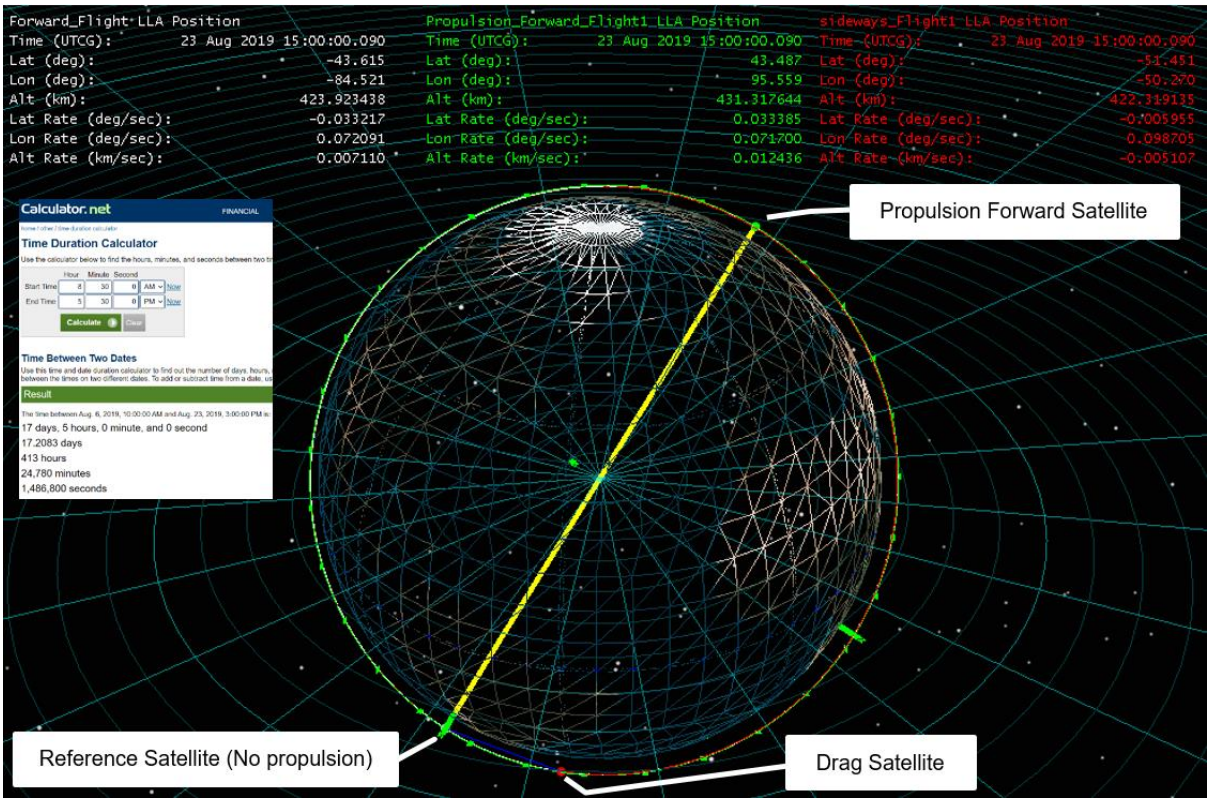

Figure 34: Satellite cluster separation showing a 180-degree phase angle after 413 hours

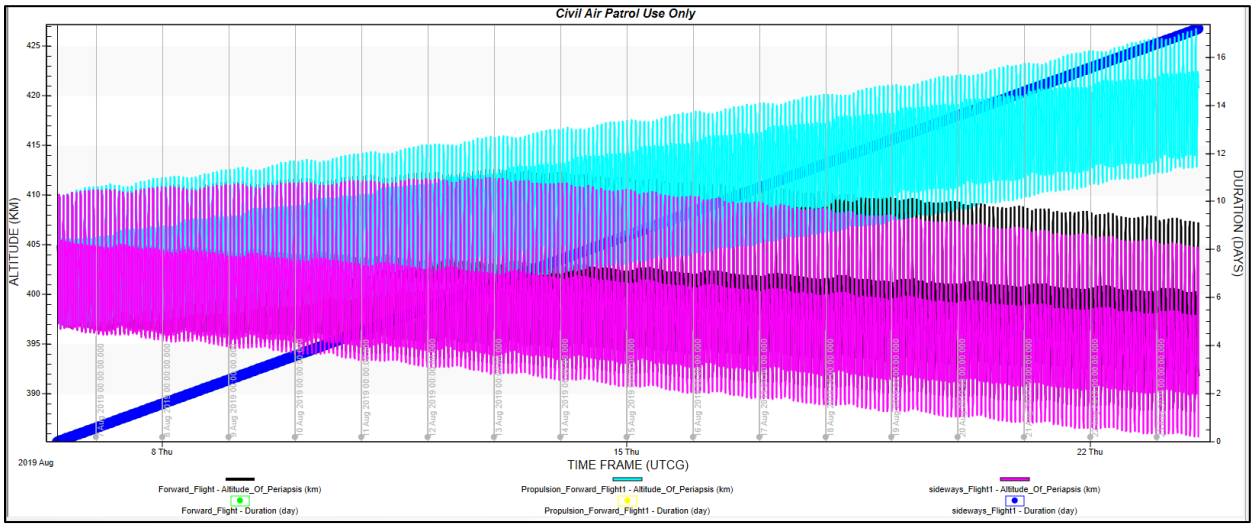

Figure 35: Plotting altitude vs time

The graph in Figure 35 shows the expected results with the propulsion satellite (blue curve) raising the orbit slightly while the other two under the influence of drag and other perturbations slowly loses altitude over the 17 days. This shows the thrust of the propulsion system is not only capable of maintaining an orbit, but also raising the orbit when using full thrust. As expected, the purple graph of the sideways satellite shows a more decayed orbit due to the increased drag area.

3.4.9 Drag satellite results

The results for the sideways-drag satellite showed only a 24 degrees phase angle, compared to 180 degrees with using propulsion. This is also the maximum drag separation possible, so using this method to separate the desired six satellites will not be feasible; propulsion will be needed to form the constellation.

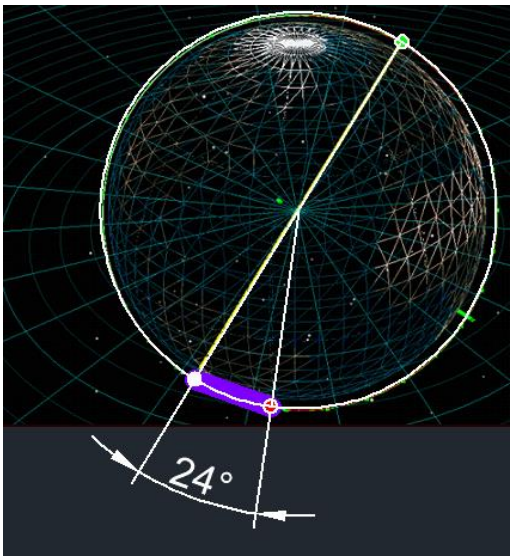

Figure 36: Drag satellite phase angle

The detailed simulated orbital elements results can be seen below in Table 17.

Table 17: Orbital elements results

Flight orientation	**Eccentricity**	**Inclination (deg)**	**Mean motion (deg/sec)**	**Orbit Period (min)**	**Semi-major Axis (km)**	**Fuel used (g)**	**Δ V (m/sec)**	**Duration) (day)**	**Drag area (m^2)**
Forward flight	0.001698	51.384	0.064776	92.627	6781.40302	0	0	17.208	0.01
Propulsion Forward flight	0.000031	51.385	0.064522	92.991	6799.15788	8.12	9.968421	17.208	0.01
Sideways flight	0.001877	51.375	0.064847	92.526	6776.44732	0	0	17.208	0.03

Conclusion

The phasing of two satellites to separate by 180 degrees was successfully simulated within a reasonable time frame. The work done by Skanke and Birkeland (May, 2018) found that with a two CubeSat phasing setup that is deployed from the ISS, a 180 degrees phase angle can be

achieved in less than a week at the cost of a ΔV of $40\ m/s$ for one of them by using a much more powerful thruster than this thesis was using. With a ΔV of only $10\ m/s$ and using only $8.12\ g$ of propellant, the time to reach a phase angle of 180 degrees, appears to be reasonable. With the minimum time of 17.2 days at full thrust to achieve 180 degrees of phasing between the two satellites, the time frame for the full phasing of six satellites is set for the next section.

3.4.10 Full constellation simulations

With a minimum simulatied time of 17.2 days at full throttle to phase two satellites 180 degrees, the other four satellites can now use throttle and direction control to phase out the constellation of satellites evenly throughout the plane. From the reference satellite, apart from the full throttle satellite, two satellites will use precise forward thrust and the other two will use precise reverse thrust for separation. Through *multiple* trial and error simulations, the percentage throttle and direction needed for each satellite to phase out in the 17.2-day time frame was found. The CubeSat legend for the STK simulation can be seen in Table 18.

Table 18: CubeSat STK legend

Cubesat_subscript_0 [REF]	The reference satellite where the other 5 will be phased out from. This satellite will use no propulsion.
Cubesat_subscript_180	180 degrees phased from Reference CubeSat with forward velocity thrusting
Cubesat_subscript_60	60 degrees phased from Reference CubeSat with forward velocity thrusting
Cubesat_subscript_-120	-120 degrees phased from Reference CubeSat with anti-velocity thrusting
Cubesat_subscript_-60	-60 degrees phased from Reference CubeSat with anti-velocity thrusting
Cubesat_subscript_120	120 degrees phased from Reference CubeSat with forward velocity thrusting

The phasing results can be found in Table19 and the orbital elements after phasing in Table 20. The constellation after 17.2 days can be seen in Figure 37.

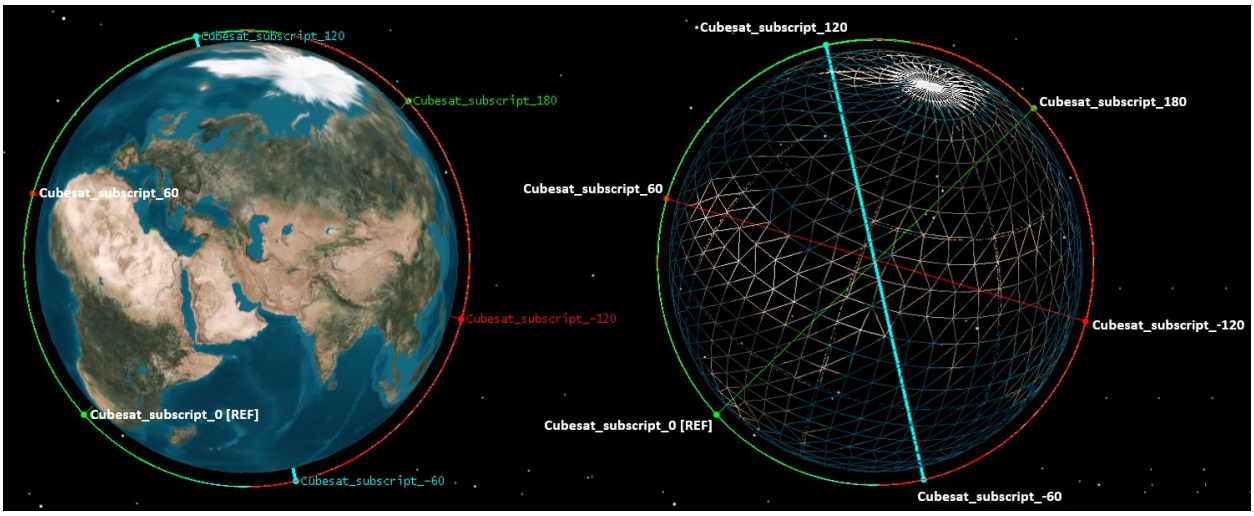

Figure 37: STK orbital phasing results

Table19: Phase results after 17.2 days

180 degree phased pairs	**CubeSat**	**% Throttle**	**ΔV (m/sec)**	**Fuel used (g)**
	Cubesat_subscript_0 [REF]	0	0	0
	Cubesat_subscript_180	100	9.968421	8.12
	Cubesat_subscript_60	33.2	3.297029	2.69
	Cubesat_subscript_-120	67.2	6.660259	5.43
	Cubesat_subscript_-60	33.0	3.272057	2.67
	Cubesat_subscript_120	66.8	6.644267	5.42

From Table19 it is evident that it took precise throttle control to achieve the 60 degree phasing between each pair of satellites, while using little fuel. On the most costly burn of 180 degrees, only $8.12\ g$ of fuel was used. While the fuel consumption is minimal, the five-year maintenance simulation in the next section will determine whether this consumption can be afforded.

Table 20: Constellation post phasing orbital elements

CubeSat	**Perigee altitude (km)**	**Inclination (deg)**	**Eccentricity**	**Duration (days)**
Cubesat_subscript_0 [REF]	391.753	51.384	0.001698	17.208
Cubesat_subscript_180	420.809	51.385	0.000031	
Cubesat_subscript_60	414.247	51.415	0.000598	
Cubesat_subscript_-120	382.014	51.415	0.002731	
Cubesat_subscript_-60	387.606	51.385	0.001514	
Cubesat_subscript_120	409.145	51.386	0.00095	

From Table19 it can be seen that the phasing was successful, but from Table 20 the orbital elements, specifically the altitude, was different for each satellite. This means that the constellation will go out of phase again if the constellation is not locked in place and the orbital elements evened out to be the same for each satellite. This will require a study on its own and is outside of the scope of this work.

Next, a five-year mission for a single satellite will be designed in STK.

3.4.11 A five-year MDASat mission designed within STK

A five-year mission has been designed using the Astrogator propagator within STK, as it specialises in spacecraft trajectory design with highly customisable functions for specific mission conditions. The same 3U CubeSat in a forward flying orientation as in Figure 26 will be modelled in STK Astrogator Mission Control Sequence (MCS). As the phasing used $0.8\,g$ of fuel for the most costly phase manoeuvre, the initial setup will take the mass reduction into account for the most accurate approach. The five-year mission has been designed in the MCS, one segment at a time, starting with an orbital decay followed by a thrust manoeuvre to raise the orbit back to the initial altitude. This sequence was repeated until the five-year time frame was reached followed by the final anti-burn sequence to deorbit

MISSION CONTROL SEQUENCE (MCS)

Each segment of the MCS was run until a desired stopping condition was met before moving on to the next segment. After each segment has been simulated, a number of user results from that segment were used to determine the adjustments needed in order to reach the desired outcome. For this five-year scenario, the mission consists of four types of segments, namely:

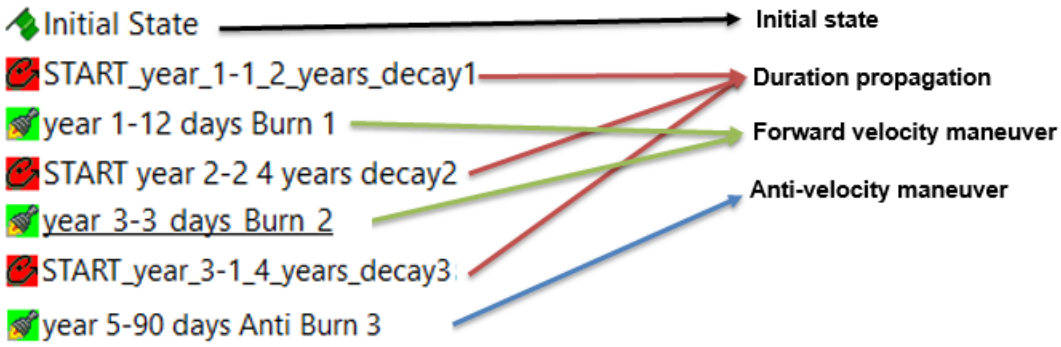

Figure 38: The five-year mission overview

- **Initial state**

The initial state of the satellite is presented in Figure 39, with reduced fuel from the phasing and a circular orbit. The satellite is assumed to be in a forward-flying position with a drag area of $0.01\ m^2$ and the recommended and confirmed drag coefficient of 2.2.

```
Spacecraft Configuration:
      Drag Area:  0.01 m^2
       SRP Area:  0.02 m^2
       Dry Mass:  3.9 kg
      Fuel Mass:  0.092 kg
     Total Mass:  3.992 kg
Area/Mass Ratio:  2.50501e-09 km^2/kg
  Tank Pressure:  0                          Pa
   Fuel Density:  0                          kg/m^3
             Cr:  1.000000
             Cd:  2.200000
 Rad Press Area:  0.02 m^2
Rad Press Coeff:  1.000000


User-selected results:
    Altitude Of Apoapsis =      404.9999999999972147 km
    Altitude Of Periapsis =      404.9999999999934630 km
```

Figure 39: The five-year mission initial state

- **Duration propagation (orbital decay)**

This segment represents the orbital decay over the duration of time. The duration was found by propagating for a period of time, until the perigee has dropped approximately 10 km below a benchmark altitude of 400 km. Then a thrust manoeuvre along the flight path will be initiated to raise the orbit again to close to that of the benchmark orbit. This benchmark altitude was chosen as the constellation will be deployed from the ISS, which also has a fluctuating altitude of between 400 km and 415 km, so the initial altitude will be different at the actual deployment. At the time of writing this thesis, the initial ISS orbit was at 405 km, so that was taken as the initial orbit for these simulations.

- **Forward velocity manoeuvre (orbit raising)**

This segment models an engine in the MCS. The Hypernova thruster defined in Figure 27 will still be used as the thruster of choice. For orbit rising manoeuvres, the thrust will be applied along the velocity vector for a period of time until the benchmark orbit of 400 km has been reached. When an altitude of 400 km is reached, the satellite will resume a normal decay again until a 10 km altitude drop has been reached. This cycle was repeated in the simulation for five years, segment by segment.

- **Anti-velocity manoeuvre (de-orbit)**

After the five years, there was sufficient fuel remaining to attempt to de-orbit.

- **The five-year mission results overview**

The MCS runs each segment of the mission until a stopping condition is met before moving on to the next segment. The overview of the mission in the MCS is presented in Figure 40.

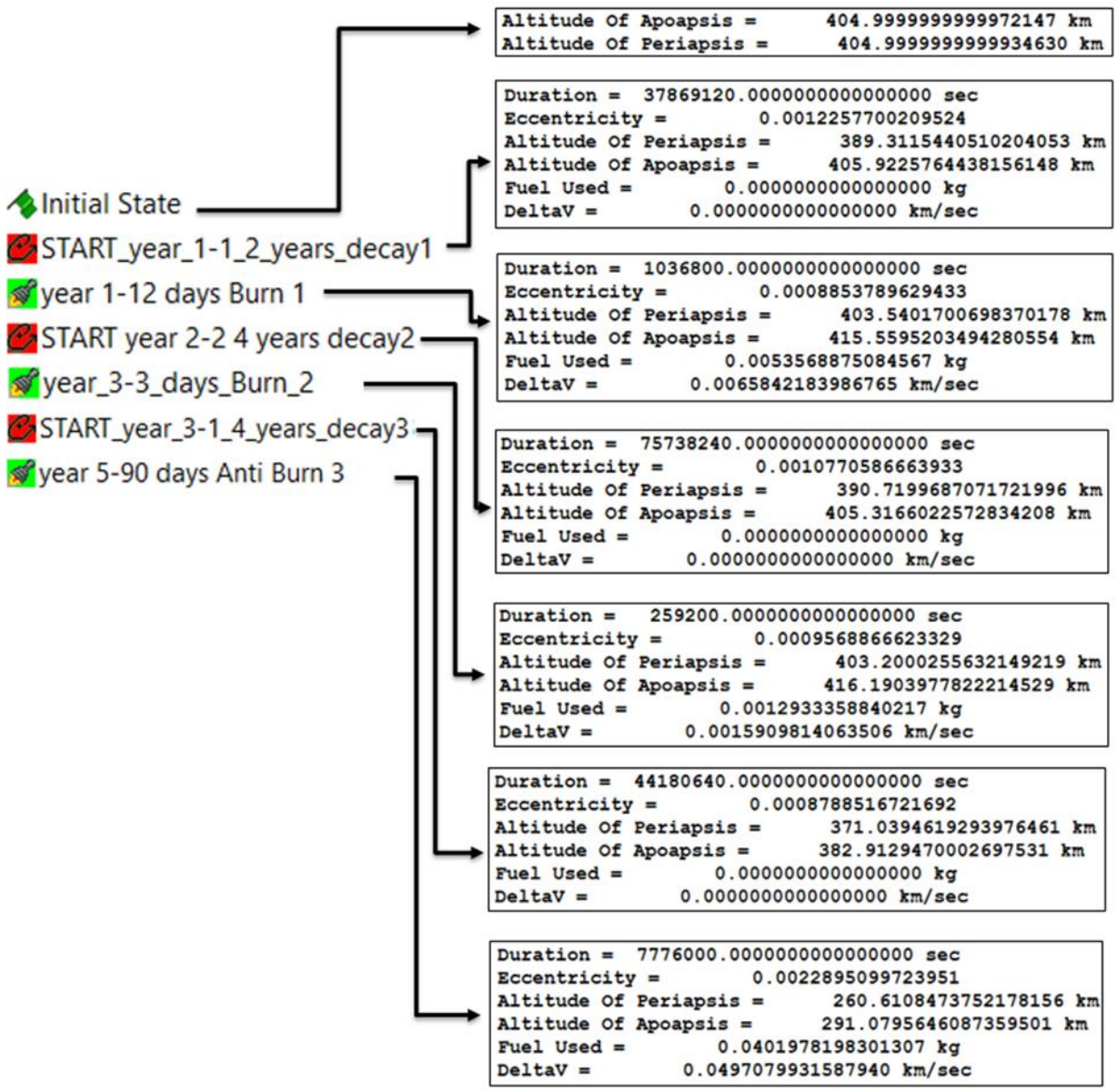

Figure 40: Five-year mission results overview

The mission overview in Figure 40 presents result of each stopping condition as each segment took place. In each case, the stopping condition was after a period of time.

- **A five-year mission results summary**

The mission sequence summary for the duration of five years is presented in Table 21.

Table 21: A five-year mission results summary

Year no.	Segment	Duration (Years)	Eccentricity	Altitude Of periapsis (km)	Altitude Of apoapsis (km)	Fuel used (g)	ΔV (m/s)
0	Initial state	0	0	405	405	0	0
1	START_year_1-1_2_years_decay1 (1.2 Years)	1.20066963	0.00122577	389.31	405.92	0	0
1	year 1-12 days Burn 1 (12 Days)	0.03287254	0.00088538	403.54	415.56	5.36	6.58
2	START year 2-2 4 years decay2 (2.4 Years)	2.40133925	0.00107706	390.72	405.32	0	0
3	year_3-3_days_Burn_2 (3 Days)	0.00821814	0.00095689	403.20	416.19	1.29	1.59
3	START year 3-1 4 years decay3 (1.4 Years)	1.40078123	0.00087885	371.04	382.91	0	0
5	year_5-90_days_Anti_Burn_3 (90 Days)	0.24654407	0.00228951	260.61	291.08	40.20	49.71

The mission was run with reduced fuel due to the orbit formation, and started with $92\ g/100\ g$ of the initial fuel. As a total, five segments were run throughout the five years, with the last segment, the sixth, being the de-orbit manoeuvre. The MCS ran the START orbital decay propagation segment in year 1 until a stopping condition of 1.2 years was met at a perigee altitude of 389 km. With the stopping condition met, a forward thrust manoeuvre segment was run for a period of 12 days to reach a perigee altitude of 403 km. This cost $5.4\ g$ of fuel and a ΔV of $6.58\ m/s$.

The next segment was updated with the new mass as there was less fuel remaining after the previous segment. The third orbital decay segment in year two was run until a stopping condition

of 2.4 years was met at a perigee altitude of 390 km. The second forward thrust manoeuvre segment in year 3 was run until a three-day duration stopping condition was met at a perigee altitude of 403 km, $1.3\ g$ of fuel used and a ΔV of $1.6\ m/s$. At this point, the total mission duration was approximately 3.6 years with 1.4 years of the mission remaining. The last orbital decay segment was run for the remaining 1.4 years and stopped at an perigee altitude of 371 km.

As the five-year mission duration was met with $92\ g - 5.4\ g - 1.3g = \ 85.4\ g$ of fuel left over, there was the possibility to de-orbit. The sixth segment in year 5 propagated an anti-velocity manoeuvre for 90 days and reached a perigee altitude of 260 km. This took $40.2\ g$ of fuel, which is less than half of the remaining fuel. This concludes that de-orbiting will be possible after five years with $44.64\ g$ of left-over fuel for any additional unforeseen manoeuvres that might be needed in the mission lifespan.

After the last segment at 260 km the atmospheric density will grow exponentially as altitude drops even more, increasing the drag force and making the de-orbiting even faster. With the use of the satellite lifetime tool in STK, the final deorbiting from 260 km using only atmospheric drag acting on the satellite was simulated and the results can be seen in Figure 41.

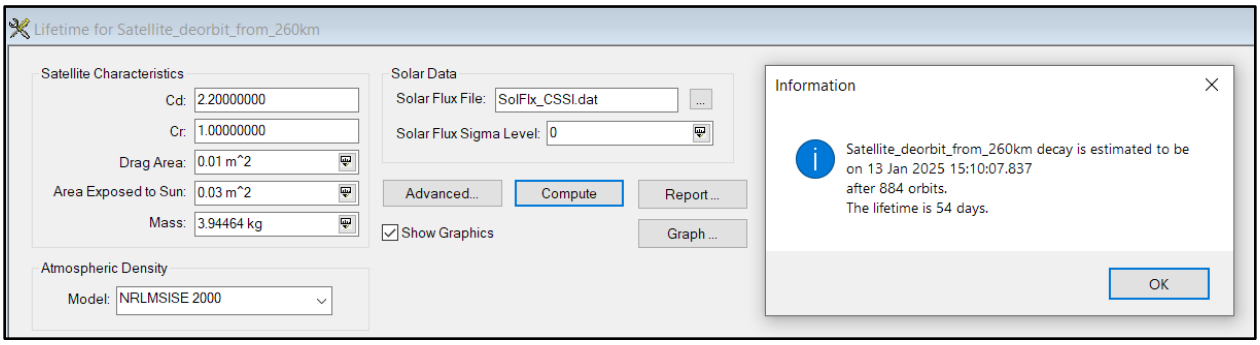

Figure 41: Lifetime for satellite deorbit from 260 km

From the final orbital elements at 260 km it will take approximately 54 days to completely deorbit the constellation. Figure 42 presents the graph of the five-year mission.

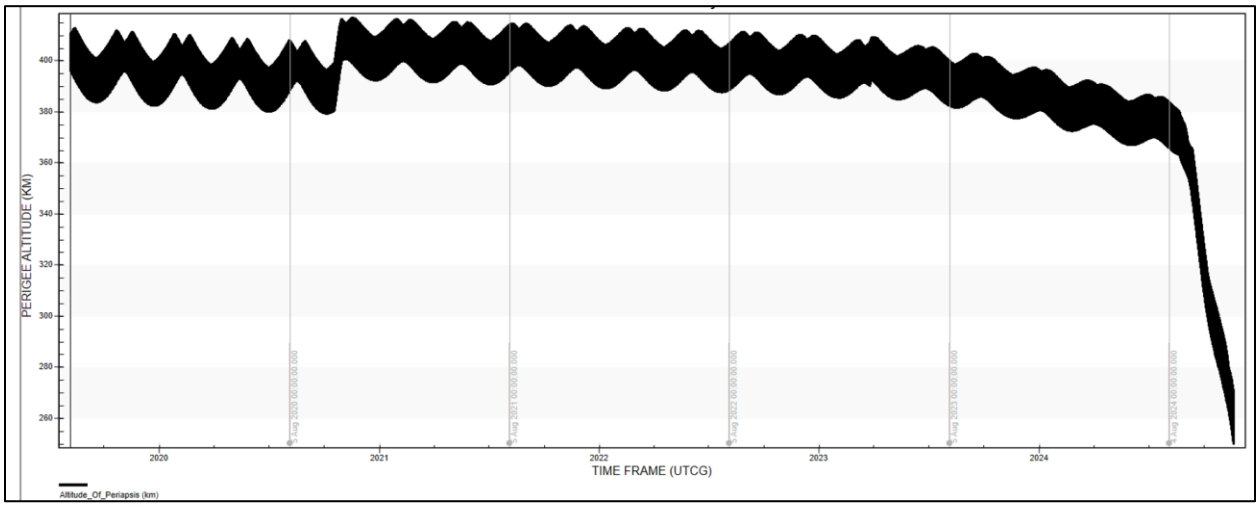

Figure 42: The five-year mission summary graph

3.5 SUMMARY

This chapter covered three main sections to determine whether orbital configuration and maintenance would be possible within the parameters of this research. The first part looked at the drag acting on the CubeSat, specifically the drag coefficient component, as this has a critical impact on the orbital lifetime of a satellite in LEO. The literature suggests that a drag coefficient of 2.2 is the norm for CubeSat-shaped satellites and through a case study using TLE data from a similar CubeSat mission, the estimated value of 2.2 was confirmed and used throughout all the calculations and simulations.

The second part focussed on the constellation itself in terms of what would be the optimal constellation for the best temporal performance for the South African EEZ and how it can be achieved. From a case study done by Mtshemla (2017), a Walker-delta 6x2 constellation configuration at an inclination of 39 degrees was the optimal choice with revisit times of approximate five minutes. With the mission requirements for this work stating that the constellation will be deployed from the ISS, a new case study was done to determine whether the same constellation configuration would yield similar results from the inclination of the ISS of 51.43 degrees. It was found that deploying 12 satellites in two planes from the ISS at a 400 km altitude, revisit times of approximate 8 minutes were achievable. Although this is slightly longer than the optimal configuration, it is still well within the 45 minutes specified within the mission requirements. It was also found that daily average access times of 13.6 hours were achievable compared to 16.4 hours from the optimal configuration.

The last section made use of STK Astrogator to simulate a five-year mission with the above orbital parameters when deployed from the ISS. The proper setup of Astrogator was necessary for the most accurate results. To refine the simulations, plane change was explored to establish whether it was possible to deploy all 12 satellites in one orbit from the ISS, as this would determine the number of planes that needed to be simulated. From section 3.3.4 it was found that plane change was not possible within the hardware capabilities due to the large ΔV costs that plane changing requires. The ΔV cost to plane-change the required 12.43 degrees was found to be $1659.62\ m/s$ while the Hypernova thruster can only achieve a maximum total ΔV of $124.184\ m/s$.This means two separate deployments will be necessary. With plane change not possible, it was only necessary to simulate one of the two planes. The simulations started with phasing six satellites from the same position into an evenly spread constellation to determine the amount of time it would take, as well as the amount of fuel it would use. With the $100\ g$ on-board propulsion only $8\ g$ was used in the worst case to form the constellation after 17.2 days.

Lastly, a five-year orbital maintenance simulation determined that it was only necessary to use the thruster twice in the five years, consuming a total of $6.7\ g$ of fuel and a total ΔV of $8.2\ m/s$ for the five years. This meant that there was $85.4\ g$ of fuel left over for de-orbiting of the satellite, which confirms that de-orbiting would be possible, as was asked in the research questions.

Having achieved the core of the research objectives, the next chapter will look at the link budget and link availability of the constellation to verify that the ISS orbital inclination still provides for a viable MDASat mission.

CHAPTER 4: LINK BUDGET CALCULATIONS AND SIMULATIONS

4.1 INTRODUCTION

This chapter covers the communication between the MDASat constellation orbiting over the South African EEZ and determines whether the constellation in Chapter 3 would be viable in terms of communication between the ground and the constellation. Four link budgets will be numerically calculated and simulated in STK for validation of the communications in the form of a link margin, namely:

- VHF AIS payload uplink from the ship beacon to the satellite;
- S-Band AIS beacon data downlink from the satellite to the ground station;
- UHF TLE downlink from the satellite to the ground station; and
- UHF uplink from the ground station to the satellite.

By implementing the basics of the communications design theory in conjunction with the communications hardware (see Appendix A), this section will calculate and determine whether the constellation will be able to establish a communications link between AIS ship beacons and the ground station. After a link has been confirmed, the performance of the link will be simulated in STK.

4.2 LINK BUDGET SETUP

For determining the link budget, the received signal power needs to be calculated in the worst-case scenario at an elevation angle of e_5 = 5° and an orbital height H = 400 km. For the purposes of the calculations, the performance specifications of the CPUT AIS, UHF- and S-band radios are assumed.

The following equations from Chapter 2 were used in calculating the link budgets (repeated here for ease of reference).

- Longest path distance (D_p)

$$D_p = R_e \left[\sqrt{\left(\frac{H+R_e}{R_e}\right)^2 - \cos^2(e_5)} - \sin(e_5) \right] \quad (2.19)$$

- Received signal power (P_r)

$$P_r = \frac{G_t G_r \lambda^2}{(4\pi D_p)^2} P_t \quad (2.18)$$

- Received noise power (N_{RX})

$$N_{RX} = kT_{sys} B\, G_{RX} \quad (2.12)$$

$$T_{RX} = (F-1)T_o \quad (2.13)$$

- Signal to noise ratio

$$\frac{S_o}{N_o} = \frac{S_i}{kT_{sys}B} \quad (2.20)$$

- Energy per bit-to-noise power spectral density ratio (E_b/N_o)

$$E_b/N_o = SNR/\eta \quad (2.24)$$

- Link margin

$$Link\ margin = \frac{E_b}{N_o}\ Calculated - \frac{E_b}{N_o} required \quad (2.25)$$

Where:

- D_p = Satellite path distance [m]
- R_e = Earth radius [m]
- H = Orbit height [m]
- e_5 = Elevation angle at 5°
- P_r = Received signal power
- P_t = Transmit power [dBm]
- λ = Electrical wavelength [m]
- D_p = Satellite path distance [m]
- G_r = Gain required by the receiving antenna [dBm]
- G_t = Gain required by the transmitting antenna [dBm]
- N_{RX} = Received noise power [dBm]
- T_{sys} = Overall system noise temperature [K]
- T_A = Receiver antenna noise temperature [K]
- T_{RX} = Transmitting temperature [K]
- B = Bandwidth [kHz]
- G_{RX} = Total receiver gain

- F = Noise figure [dB]
- T_o = Outside temperature [K]
- η_{BW} = Spectral efficiency [$bits/s/Hz$]

4.3 LINK BUDGET CALCULATIONS

The link validation for each link will be determined through a link margin to establish whether communication would be possible. It will be calculated numerically, followed by STK simulations.

A minimum bit-error-rate required by CPUT is a $BER = 10^{-6}$ and this will be used in the modulation schemes in Figure 16 and Figure 17 for calculating the link margin at a slant range angle of 5°. An antenna noise temperature of 1000 K at 5° will be assumed and used with an assumed outside ambient temperature of 17 °C for the system temperature calculations (this is a realistic temperature experienced with the ZACube-2 mssion). Each of the following link budgets will start with the hardware characteristics of the transmitter and receiver used in each scenario, followed by the calculated link budget results, and finally the STK simulations to compare the numerical results with the simulated results. The datasheets for the transmitters and receivers can be found in Appendix A. The ground station for the simulations is located at CPUT, Cape Town, and a ship transmitting AIS data in the EEZ just off the shore in Cape Town, South Africa, as seen in Figure 43.

Figure 43: Link budget transmission locations

4.3.1 VHF UPLINK TO SATELLITE

A ship will be transmitting AIS data over VHF to the VHF receiver of the satellite with the following hardware.

Table 22: VHF transmitter and receiver characteristics

AIS VHF beacon transmitter:	
Frequency	156.025 to 162.025 MHz in 25 kHz steps
Output power	2 W
Channel bandwidth	25 kHz
Channel step	25 kHz
Modulation modes	25 kHz GMSK (AIS transmit only)
Bit rate	9600 b/s (GMSK) and 1200 b/s (FSK)
Receiver sensitivity	< -107 dBm
VHF satellite receiver:	
DC power	< 220 mW
Frequency Sensitivity	140 – 150 MHz -117 dBm for 12 dB SINAD
Channel spacing	12.5 kHz
Noise figure	< 1.5 dB
Spurious responses	< -65 dB
Dynamic range	-117 dBm to -70 dBm
Frequency stability	± 2.5 ppm
Antenna gain	-10 dBi

4.3.1.1 VHF uplink budget numerical calculations

The VHF link uplink calculation results can be seen below in Table 23.

Table 23: VHF uplink results

VHF uplink budget results	**Output**	**Unit**
Received signal power:		
P_R	2,6924E-14	W
	-105,698631	dBm
Received noise power:		
N_{RX}	4,4479E-16	W
	-123,518495	dBm
Signal to noise ratio (SNR)		
SNR	17,8198638	dBm
Bit error to noise ratio		
E_b/N_0	21,9765515	dB
Link margin	10.0765515	dB

From Figure 17, using a GMSK and convolutional coded modulation scheme with a BER of 10^{-6}, the VHF uplink budget in Table 23 determined that a link margin of 10.1 dB is possible, which determines that acceptable communication will be possible between the satellite and the transmitter of the ship.

4.3.1.2 VHF uplink STK simulation

Figure 44 simulates the VHF uplink budget of two overpasses from the satellite where the results of interest for this link and all the links to follow lies on 5°.

Facility-Ship-Sensor-Sensor2-Transmitter-VHF_IAS_Transmitter_MEDIUM1-To-Satellite-CubeSat-Receiver-VHF_Receiver1

Elevation (deg)	Rcvd. Iso. Power (dBW)	Eb/No (dB)	Link Margin (dB)
5.000	-134.161	21.2029	12.7029
8.132	-132.929	22.3755	13.8755
10.490	-132.053	23.1888	14.6888
11.050	-131.865	23.3614	14.8614
9.505	-132.452	22.8205	14.3205
6.666	-133.563	21.7755	13.2755
5.000	-134.237	21.1287	12.6287

Elevation (deg)	Rcvd. Iso. Power (dBW)	Eb/No (dB)	Link Margin (dB)
5.000	-134.193	21.1718	12.6718
10.582	-132.039	23.2025	14.7025
18.833	-129.317	25.5758	17.0758
32.473	-126.011	27.8374	19.3374
47.032	-123.704	28.2489	19.7489
34.907	-125.582	28.0302	19.5302
20.434	-128.917	25.8970	17.3970
11.687	-131.720	23.4932	14.9932
5.853	-133.941	21.4138	12.9138
5.000	-134.285	21.0825	12.5825

Figure 44: Screen shot of link budget report for the VHF communications uplink

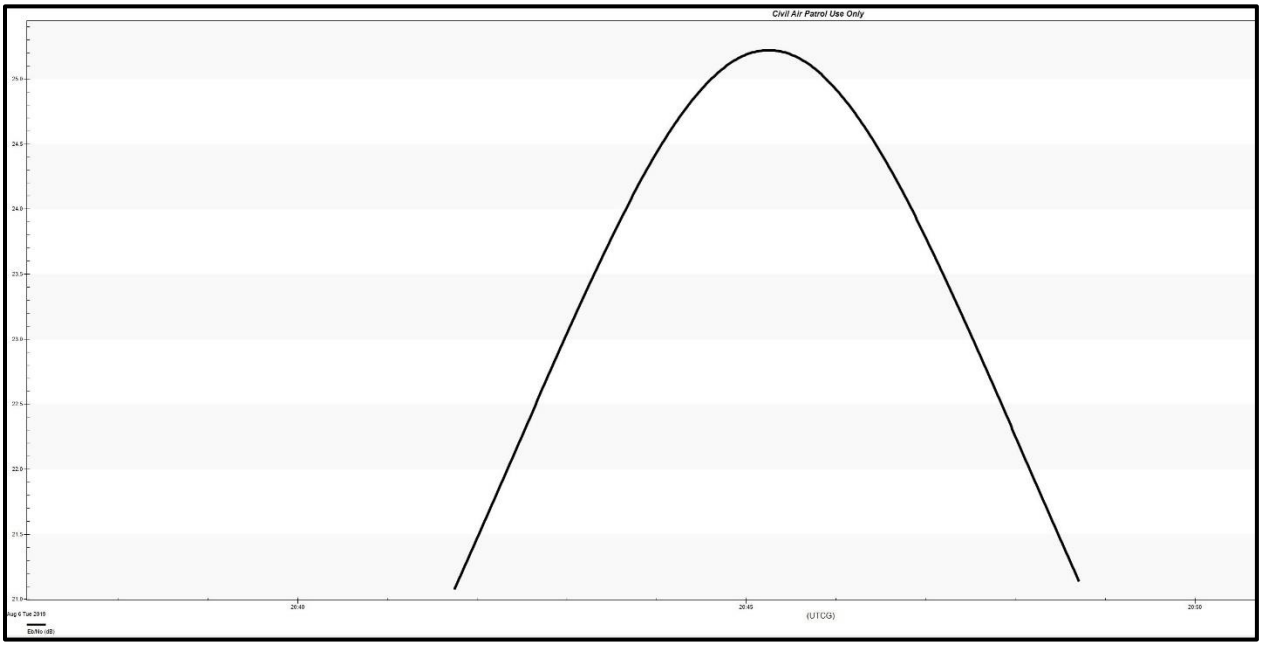

Figure 45: Simulated Eb/No for VHF 9600 bps AIS uplink for the satellite passing over the South African EEZ

With STK considering real-life conditions, such as location and atmospheric conditions and by using the same modulation scheme as the numerical calculations, a link margin of 12.7 dB was found at 5°. With comparison to the numerical link margin of 10.1 dB, the results are close enough to be acceptable and imply that communication will be possible for the VHF 9600 bps uplink. Figure 45 shows the expected graph plot of the overpass, showing the communications link getting stronger as the slant elevation angle approaches 90° where the path that the signal needs to travel, is the shortest.

4.3.2 S-BAND DOWNLINK FROM THE SATELLITE TO THE GROUND STATION

With a large amount of data that needs to be transmitted from the satellite to the ground station, the higher bitrate S-Band transmitter and receiver (at the ground station) will be used.

Table 24: S-Band transmitter and receiver characteristics

S-Band transmitter	
Frequency	2.2 GHz – 2.3 GHz (STXC) 2.4 GHz – 2.45 GHz (STX)
RF power	2 Watt (33 dBm)
Channel spacing	500 kHz
TX SNR	> 20 dB
Spurious response	< -60 dBc
*S*11:	< -15 dB
Antenna gain:	7 dBi
Beamwidth:	60°
Bit rate	2 Mbps
Ground S-Band receiver	
Receiver noise figure	0.9 dBi
Antenna gain	35.4dBi (RHCP or LHCP)
Downlink data	2 Mbps
Downlink modulation	Raised-Cosine BPSK, AFSK, FSK, GMSK, QPSK
Az/EL rotor accuracy	~ 0.1 deg

4.3.2.1 S-Band downlink budget numerical calculations

The S-Band downlink calculations can be seen below in Table 25.

Table 25: S-Band downlink budget results

S-Band downlink budget results	**Output**	**Unit**
Received signal power:		
P_R	1,0521E-12	W
	-89,7792564	dBm
Received noise power:		
N_{RX}	4,2081E-14	W
	-103,759104	dBm
Signal to noise ratio (SNR)		
SNR	13,9798478	dBm
Bit error to noise ratio		
E_b/N_0	15,5288674	
Link margin	4.72886739	dB

From Figure 16, using a QPSK modulation scheme with a BER of 10^{-6}, the S-Band link budget in Table 25 determined that a link margin of 4.7 dB is possible, which means that the satellite will be able to transmit data to the CPUT ground station over S-Band over a 2.4 GHz frequency.

4.3.2.2 S-Band downlink STK simulation

Figure 46 simulates the S-Band downlink budget of a single overpass from the satellite.

Facility-CPUT_Ground_Station-Sensor-SatelliteTracker-Receiver-SBAND_RECEIVERcomplex-To-Satellite-CubeSat-Transmitter-SBAND_transmitter1

Elevation (deg)	Rcvd. Iso. Power (dBm)	Eb/No (dB)	Link Margin (dB)
5.000	-89.163	15.7911	6.1911
8.659	-87.728	17.2260	7.6260
12.012	-86.505	18.4492	8.8492
13.651	-85.951	19.0031	9.4031
12.524	-86.358	18.5958	8.9958
9.410	-87.507	17.4476	7.8476
5.730	-88.953	16.0016	6.4016
5.000	-89.249	15.7051	6.1051

Figure 46: Screen shot of link budget report for the S-Band communications downlink

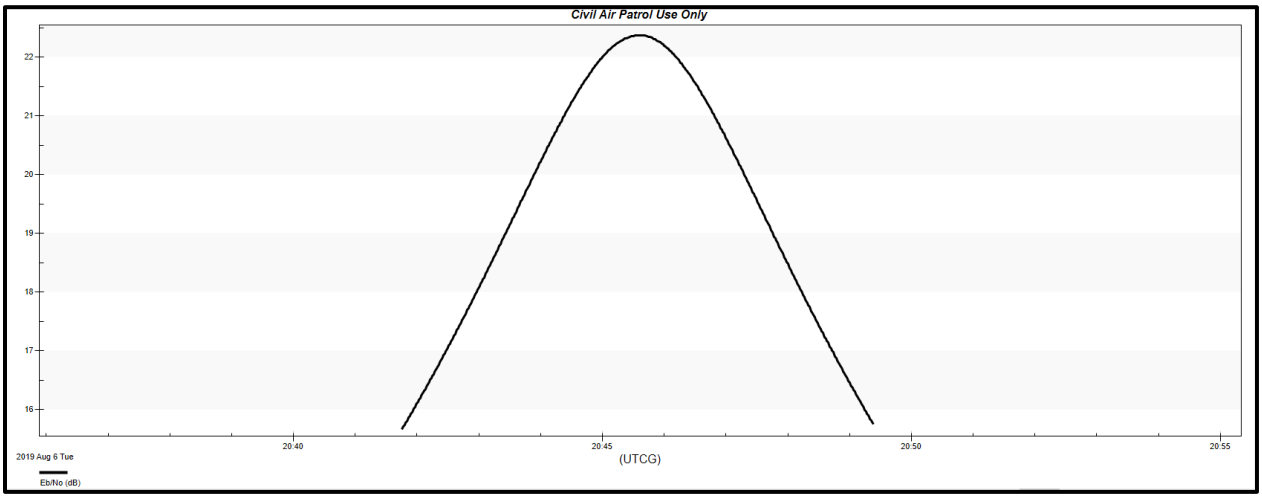

Figure 47: Simulated Eb/No for S-Band downlink for the satellite passing over the CPUT ground sensor located in South Africa

Due to STK implementing real-life conditions, the results are not expected to be exactly the same, and by comparison the numerical and simulated results are still close, and in the positive link margin range. This is acceptable and implies that communications will be reliable for the S-Band downlink.

4.3.3 UHF DOWNLINK FROM SATELLITE TO GROUND STATION

The satellite will transmit telemetry over UHF down to a ground station receiver located at CPUT in the Western Cape of South Africa, with the following hardware characteristics.

Table 26: UHF transmitter and receiver characteristics

Satellite UHF TLE transmitter	
DC power	1–2 W (30–33 dBm)
Frequency	400–420 MHz (CMCC) 430–440 MHz (CMC)
Sensitivity	Up to -121dBm
Channel spacing	25 kHz
Spurious response	< -65 dBc
Frequency deviation	3 kHz (FM)
Frequency stability	± 2.5 ppm
Ground UHF receiver:	
Receiver noise figure	2,0 dBi
Antenna gain	15.5 dBic gain, switchable RHCP-LHCP
Downlink data	1.2 - 9.6 kbps
Downlink modulation	Raised-Cosine BPSK, AFSK, FSK, GMSK, QPSK
Az/EL rotor accuracy	~ 0.1 deg

4.3.3.1 UHF downlink budget numerical calculations

The UHF downlink calculations can be seen below in Table 27.

Table 27: UHF downlink budget results

UHF downlink budget results	**Output**	**Unit**
Received signal power:		
P_R	6,8925E-14	W
	-101,616231	dBm
Received noise power:		
N_{RX}	4,8445E-16	W
	-123,147507	dBm
Signal to noise ratio (SNR)		
SNR	21,5312758	dBm
Bit error to noise ratio		
E_b/N_0	23,4694761	
Link margin	12.8694761	dB

From Figure 16, using a BPSK modulation scheme with a BER of 10^{-6}, the UHF link budget in Table 27 determined that a link margin of 12.9 dB is possible. This determines that the satellite will be able to transmit data to the CPUT ground station over UHF over a 400 MHz frequency.

4.3.3.2 UHF downlink STK simulation

Figure 48 simulates the UHF downlink budget of a single overpass from the satellite.

Facility-CPUT_Ground_Station-Sensor-SatelliteTracker-Receiver-UHF_RECEIVERcomplex-To-Satellite-CubeSat-Transmitter-UHF_transmitter

Elevation (deg)	Rcvd. Iso. Power (dBm)	Eb/No (dB)	Link Margin (dB)
5.000	-102.929	23.5116	13.9116
9.753	-101.079	25.3613	15.7613
15.467	-99.093	27.3473	17.7473
20.859	-97.483	28.9569	19.3569
21.826	-97.236	29.2041	19.6041
17.297	-98.566	27.8743	18.2743
11.482	-100.524	25.9163	16.3163
6.443	-102.445	23.9953	14.3953
5.000	-103.026	23.4137	13.8137

Figure 48: Screen shot of link budget report for the UHF communications downlink

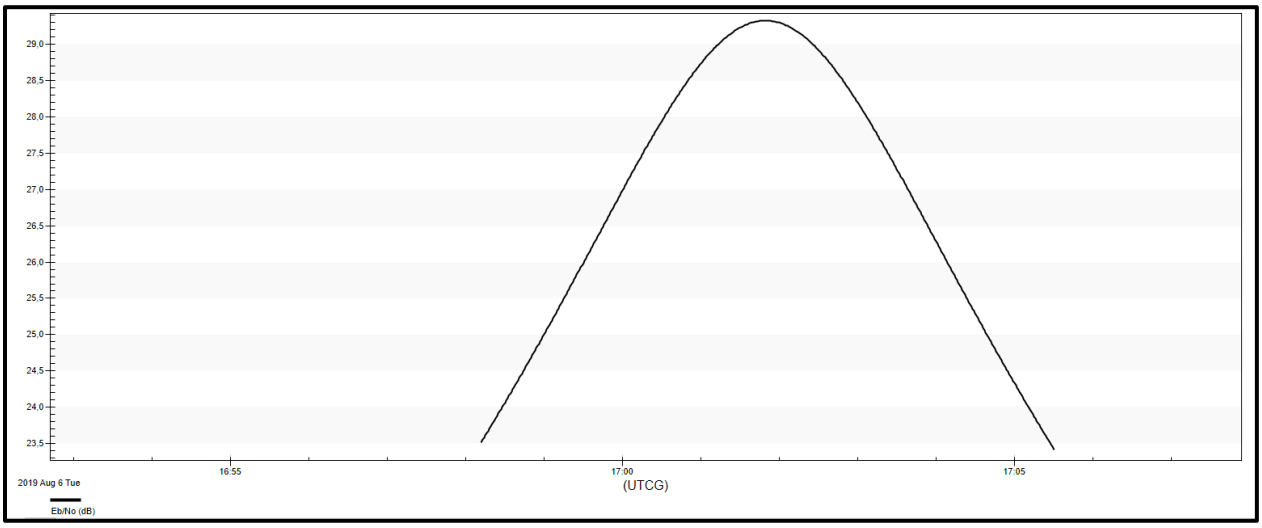

Figure 49: Simulated Eb/No for UHF 9600 bps downlink for the satellite passing over the CPUT ground station located in South Africa

The simulated UHF downlink results in Figure 48 estimates a link margin of 13.9 dB at an elevation angle of 5° which is 1 dB more than the numerical results. Therefore, communication between the satellite and the CPUT ground station for the UHF 9600 bps downlink will be possible.

4.3.4 UHF UPLINK FROM GROUNDSTATION TO SATELLITE

The CPUT ground station will transmit telecommands over UHF to the UHF receiver of the satellite.

Table 28: UHF ground station transmitter

Ground station UHF transmitter	
DC power	10 W (40 dBm)
Frequency	400–420 MHz (CMCC) 430–440 MHz (CMC)
RF power	27–33 dBm (3 dB steps)
Channel spacing	25 kHz
Spurious response	< -65 dBc
Frequency deviation	3 kHz (FM)
Frequency stability	± 2.5 ppm
Bit rate	1.2 - 9.6 kbps
Antenna gain	16 dBi
UHF satellite receiver:	
DC power	< 220 mW
Frequency Sensitivity	140–150 MHz -117 dBm for 12 dB SINAD
Channel spacing	12.5 kHz
Noise figure	< 1.5 dB
Spurious response	< -65 dB
Dynamic range	-117 dBm to -70 dBm
Frequency Stability	± 2.5 ppm
Antenna gain	-10dBi
Modulation scheme	GMSK

4.3.4.1 UHF uplink budget numerical calculations

The UHF uplink calculations can be seen below in Table 29.

Table 29: UHF uplink budget results

UHF uplink budget results	**Output**	**Unit**
Received signal power:		
P_R	7,2532E-13	W
	-91,3947006	dBm
Received noise power:		
N_{RX}	2,2146E-16	W
	-126,546988	dBm
Signal to noise ratio (SNR)		
SNR	35,1522872	dBm
Bit error to noise ratio		
E_b/N_0	36,7013068	
Link margin	26,2013068	dB

From Figure 17, using a GMSK and convolutional coded modulation scheme with a BER of 10^{-6}, the UHF uplink budget at a frequency of 430 MHz in Table 29 determined that a link margin of 26.2 dB is possible. This determines that communication will be possible between the CPUT ground station and a satellite passing over at 5°.

UHF uplink STK simulation

Figure 50 simulates the UHF uplink budget of a single overpass from the satellite.

Facility-CPUT-Sensor-Sensor1-Transmitter-UHF_transmittercomplex-To-Satellite-CubeSat-Receiver-UHF_RECEIVERcomplex1:

Elevation (deg)	Rcvd. Iso. Power (dBW)	Eb/No (dB)	Link Margin (dB)
5.000	-91.052	37.7535	27.2535
8.198	-89.274	39.5316	29.0316
10.768	-87.635	41.1708	30.6708
11.687	-86.668	42.1375	31.6375
10.429	-87.839	40.9664	30.4664
7.672	-89.525	39.2809	28.7809
5.000	-90.993	37.8131	27.3131

Figure 50: Screen shot of link budget report for the UHF communications uplink

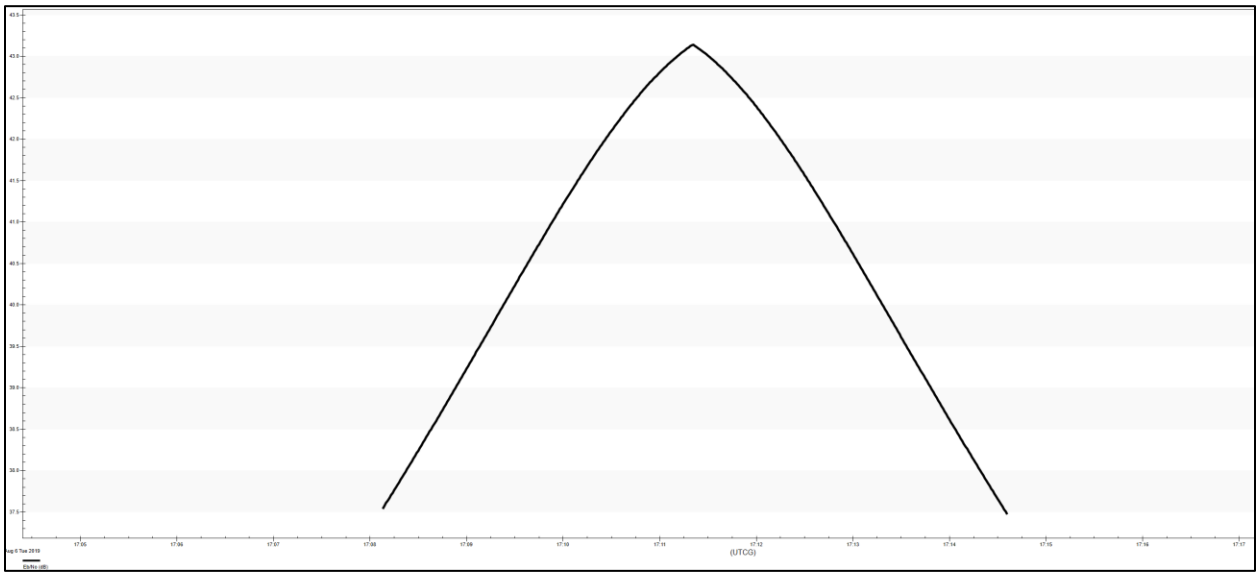

Figure 51: Simulated Eb/No for UHF 9600 bps uplink for the satellite passing over the CPUT ground station located in South Africa

With the ground station having much more power than a satellite, a strong link margin of 27.25 dB can be seen in the results in Figure 50.

With comparison to the numerical link margin of 26.2 dB, the simulated results are close again, determining that communications will be reliable for the UHF 9600 bps uplink from the CPUT ground station to an overpassing satellite, in the worst-case scenario of 5°.

4.4 LINK BUDGET COMPARISON OF RESULTS

The numerical and simulated results were expected to have small deviations from each other, due to the numerical calculations being basic, compared to the simulator having more input variables and conditions that were taken into account. The comparison of results on a 5° elevation angle can be found in Table 30.

Table 30: Link margin comparison of results

Link margin comparison of results			
Link	Numerical result (dB)	Simulated result (dB)	Difference (dB)
VHF uplink	10.1	12.7	2.6
S-Band downlink	4.8	6.2	1.4
UHF downlink	12.9	13.9	1
UHF uplink	26.2	27.3	1.1

By comparing the calculated and simulated results, it was expected to see small differences in values due to the simulations taking into account more real-world conditions, such as atmospheric conditions.

4.5 SUMMARY

This chapter determined whether the Walker-delta satellite constellation deployed from the ISS on an inclination of 51.43° would be able to communicate from and between a ship in the South African EEZ and a ground station located at CPUT in the Western Cape. Four link budgets, namely VHF uplink, S-Band downlink, UHF downlink and UHF uplink, were explored and determined.

The simulations only needed to simulate a single satellite as the ground station does not change location and the inclination for each satellite stays the same. The four link budgets were first numerically calculated and then simulated on STK to compare and determine link availability for each one of the budgets.

The numerical and simulated results of the link budgets determined that link availability was possible for each of the four links. This concluded that a Walker-delta satellite constellation deployed from the ISS will be able to communicate with the CPUT ground station and with the AIS beacon on a ship in the South African EEZ.

CHAPTER 5: CONCLUSIONS AND RECOMMENDATIONS

This chapter looks at conclusions, recommendations, future work and addresses the research questions.

5.1 INTRODUCTION

Electric propulsion revolutionised the small-satellite industry by providing on-board thrust capabilities to CubeSats, taking up as little as half a U of payload space.

Chapter 1 looked at the research overview with the research objectives to provide maritime domain awareness services for the South African EEZ through a nanosatellite constellation.

Chapter 2 looked at the literature of electric propulsion technology, different constellation configurations, orbital mechanics, space mission design software and communications systems.

Chapter 3 was the cornerstone of this work with two case studies and orbital simulations. The first section covered a case study on the drag coefficient used for small satellites with specific shapes. The case study looked at whether the industry-recommended drag coefficient of 2.2 would be viable for the mission specified in this work. The second case study was done on the orbital performance of the constellation to determine what configuration would be the most suitable for the South African EEZ, and whether the constellation would yield sufficient coverage. The final part of Chapter 3 was the simulations on the formation of the constellation from a single deployment of a cluster of CubeSats from the ISS, the maintenance of the constellation over a five-year mission and determining whether de-orbiting would be possible in terms of the remaining fuel after the five-year mission.

Chapter 4 covered the communication between the MDASat constellation orbiting over the EEZ in South Africa. Chapter 4 determined whether the constellation in Chapter 3 would be viable in terms of communication between the ground and the constellation, assuming commercially available communications systems. If communication would not be possible, the constellation would not be feasible for the mission. Four link budgets were numerically calculated and simulated in STK for validation of the communications. The four link budgets were done in the following sequence:

- VHF AIS payload uplink from the ship beacon to satellite;
- S-Band AIS beacon data downlink from satellite to ground station;
- UHF TLE downlink from satellite to ground station; and
- UHF uplink from ground station to satellite.

Each link budget was calculated and simulated for a worst-case scenario with an elevation angle of 5° from the satellite to ground with the satellite at an orbital height of 400 km.

Chapter 5 concludes with conclusions, recommendations and addressing the research questions.

5.2 ADDRESSING THE RESEARCH QUESTIONS

The research questions posed in Chapter 1 are addressed in the summary below.

- How long does it take to set up the constellation of satellites launched from the ISS?

For a single plane to phase out a cluster of six satellites evenly, Chapter 3, section 3.4.7 determined that it would take 17.208 days to separate and form the constellation through precise throttle and altitude control.

- Is propulsion needed or will altitude control using atmospheric drag be able to form and maintain the constellation?

Chapter 3, section 3.4.5.1 determined that differential drag would not be sufficient to form the constellation and that propulsion would be necessary. After 17.208 days the electric propulsion achieved the maximum phase angle of 180 degrees between two CubeSats while with the maximum drag possible only achieved 24 degrees during the same time. Additionally, from the data of the phasing with and without electric propulsion, the altitude difference was large enough that propulsion would be needed to correct for this altitude difference to lock the constellation in place.

- What is the ΔV budget for a five-year mission and is plane-change feasible within the capabilities of existing electrical propulsion systems?

From the results in Table 21 of Chapter 3 that covered all the manoeuvres from constellation configuration to maintaining a constellation for five years using electric propulsion, the ΔV budget

for the mission was found to be 9.97 m/s for the configuration of the constellation and 8.18 m/s for maintaining the constellation for five years. This is excluding de-orbiting that had a ΔV of 50 m/s in the opposite direction of flight.

From calculations at the beginning of Chapter 3 in section 3.4.4, it was found that plane change is currently not feasible within the capabilities of the hardware used in this work and that two deployments will be necessary to deploy the full 2-plane Walker-delta configuration. Future technologies could make plane change a possibility.

- What is the impact of lower orbits on constellation performance and can electric propulsion enable or improve utility of such lower orbits?

From Table 10 in Chapter 3 it can be seen that there is a 30 m/s velocity difference between a 398 km and a 388 km altitude, which implies that the revisit times would be slightly faster at the lower orbit. Chapter 3 also proved that the lower altitudes can be maintained and raised through electric propulsion with minimal fuel consumption with the thruster used in this work. A 5-year mission at a nominal orbital height of 400 km was deemed feasible.

- How long will it take for a satellite to de-orbit with and without propulsion?

The lifetime orbit tool of STK estimated a lifetime of 4.7 years before re-entry and in the simulations in Chapter 3 section 3.4.10, an anti-burn with the propulsion system lowered the altitude from 382 km to 260 km in three months. With the exponential increase in drag force as the altitude drops due to the atmospheric density that increases, STK lifetime orbit tool simulated a deorbit time from 260 km to final deorbit in 54 days without electric propulsion. The increase in atmospheric density due to altitude drop can be observed in Table 11 in Chapter 3.

- Does the constellation configuration support a feasible MDA case study in the South African EEZ?

Through STK simulations of the constellation over the area of interest, namely the EEZ of South Africa, it was found in Chapter 3 that a 6x2 Walker-delta constellation configuration deployed from the ISS would be feasible and should be explored as an option for the South African EEZ. Furthermore, Chapter 4 concluded that the constellation will be able to communicate between ships entering the South African EEZ and a ground station at CPUT in the Western Cape of South Africa over VHF, S-band and UHF frequencies.

5.3 CONCLUSIONS

This work presents the incorporation of electric propulsion into CubeSat missions to configure, form, maintain and de-orbit a 6x2 Walker-delta constellation of CubeSats. The design of the electric propulsion system was not covered. Rather, current electric propulsion technologies were implemented and the research and technologies available were stated and explained in the literature review in Chapter 2. FEEP electric propulsion was initially the thruster of choice, but as the work progressed a new type of plasma electric thruster came to light through local sources. This thesis is a continuation of the work done by Mtshemla (2017), where the optimal constellation configuration for the South African EEZ was investigated. To validate simulation parameters and results, a case study was done early in Chapter 3 to determine through an experimental approach whether the recommended drag coefficient of 2.2 for spacecraft was accurate. Through TLE data over a course of eleven months, it was determined that 2.2 was a good, estimated value to use.

In the next section of Chapter 3, a new case study was done to find the coverage and temporal performance of the constellation when deployed from the ISS. The results predicted that a 6x2 Walker-delta constellation in the ISS orbital plane would produce sufficient coverage and revisit times over the EEZ. With a confirmed constellation configuration, it was looked at how a cluster of CubeSats could be evenly spread out through one and two planes, using differential drag and electric propulsion. Using the STK Astrogator propagator, Chapter 3, section 3.4.7 showed that electric propulsion was needed to phase out the constellation in a single plane from a cluster of CubeSats. It was also determined that plane change with the current CubeSat technology was not possible and that two deployments in two planes were necessary.

The next phase was designing and simulating a five-year mission to determine whether the electric propulsion would be able to maintain a constellation for five years, as well as calculating whether there would be enough fuel on board to carry out the five-year mission after the initial formation using the thrusters. The five-year mission simulations started with a reduced amount of fuel due to the initial separation, and was successful with left-over fuel to de-orbit.

With the constellation being successful in terms of formation and maintenance, next a communication system was designed and simulated in Chapter 4 to determine whether a good and reliable communication link in the form of a link budget would be possible.

Four link budgets were numerically calculated, followed by simulations in determining whether communication was possible for the constellation. Chapter 4 found that a VHF AIS uplink from a ship in the South African EEZ to one of the satellites would have an expected link margin of 11.4 dB, an S-Band downlink from the satellite to the CPUT ground station in the Western Cape would have an expected link margin of 5.5 dB and the UHF downlink and UHF uplink expected a link margin of 13.4 dB and 26.75 dB, respectively.

From the work done in this thesis and the results of Chapter 3 and Chapter 4, it can be concluded that orbital configuration and maintenance of nanosatellite constellations through electric propulsion could be a possibility and a viable option for the South Africa EEZ for future CubeSat missions.

5.4 FUTURE WORK AND RECOMMENDATIONS

For future work, Chapter 3 section 3.4.9 simulated how electrical propulsion can be used to form a constellation of six satellites deployed together in a cluster from the ISS. With the electric propulsion technology used, a cluster of CubeSats can be evenly phased out in approximately 17.2 days, but the orbital elements for each CubeSat changed drastically; specifically the altitude and eccentricity of each CubeSat in relation to one another. Table 20 in Chapter 3 compared the perigee altitude and eccentricity of each CubeSat with another after phasing out evenly throughout the orbit, and altitude differences of almost 40 km between the highest and lowest altitudes were found. The orbit of each CubeSat also became more elliptical over time with a change in eccentricity between them. This means that the constellation is perfectly phased out at that instant in time, but will go out of phase again if the orbital elements of each CubeSat were not corrected to be the same for each one. Future work could focus on locking the constellation in place by using the orbital elements after the phasing of this work and use electric propulsion and other manoeuvres to level out the orbital elements to keep the formation.

It is recommended to explore more propulsion technologies as technology is improving and developing every day. In-house electric propulsion thruster design and development for mission-specific needs could also be a good option to pursue, as mission parameters can be designed with high precision using STK, specifically the Astrogator propagator. Having an in-house mission-specific thruster can have a wide range of benefits, compared to an off-the-shelf solution if enough

time and energy is put into it. Time and money can be saved by using locally sourced parts and components, while optimising the design for a specific mission and function. A specific mission could entail using electric propulsion purely for precise attitude control, making the thruster smaller and lighter with less fuel than a full thruster solution. This means the normal attitude control, e.g. momentum wheel, could be removed making the CubeSat lighter or having more room for additional payloads. On the other hand, a once-off burst electrical propulsion thruster can be developed for immediate collision avoidance as the conventional small satellite thrusters mostly focus on long, small thrust manoeuvres that cannot achieve immediate collision avoidance.

It is also recommended to look at additional deployment methods, such as precise orbital deployment and insertion of each satellite in the constellation, which would not only need extra fuel to form the constellation, but would also be able to deploy the constellation locked in place without the need to lock the constellation in place manually with propulsion and manoeuvres.

REFERENCES

AGI (Analytical Graphics Inc.). N.d. STK tutorials. Retrieved from https://help.agi.com/stk/11.0.1/Content/gator/astrogator.htm [Accessed 13 October 2018].

AGI (Analytical Graphics Inc.). 2020. Systems Tool Kit (STK). Retrieved from https://www.agi.com/products/stk> [Accessed 23 April 2020].

Águeda, A., Aivar, L., Tirado, J. and Dolado, J.C., 2013, August. In-orbit lifetime prediction for LEO and HEO based on orbit determination from TLE data. In Proceedings of the 6th European Conference on Space Debris (pp. 22-25).

An analysis of current propulsion systems. 2012. Retrieved from currentpropulsionsystems.weebly.com/electrothermal-propulsion-systems.html [Accessed day month year].

Anane, R., Raoof, K. & Bouallegue, R. 2015. On the evaluation of GMSK scheme with ECC techniques in wireless sensor network. International Journal of Wireless & Mobile Networks, 7(2):17–28.

Ashenberg, J. & Lorenzini, E. 1999. Active gravity-gradient stabilization of a satellite in elliptic orbits. Acta Astronautica, 45(10):619–627.

Baudet, L., Raurell, D.S. and Martinez, J.C., 2020. Simplifying The Design Of Smallsat Space Missions Using Innovative Tools And Platforms: beeKit and beeApp.

Bedingfield, K.L., 1996. Spacecraft system failures and anomalies attributed to the natural space environment (Vol. 1390). NASA.

Birkeland, R. & Skanke, P.E. 2018. CubeSat propulsion: Expanding the possibilities of the affordable space platform.

Birur, G.C. & Siebes, G. 2001. Encyclopedia of Physical Science and Technology. Third edition. Place: Publisher.

Bock, D. & Tajmar, M. 2018. Highly miniaturized FEEP propulsion system (NanoFEEP) for attitude and orbit control of CubeSats. Acta Astronautica, 144:422–428.

Botha, J.R. 2014. Design of an RF ion thruster. Electronic Engineering at Stellenbosch University.

Bradbury, L., Diaconu, D., Molgat Laurin, S., Beattie, A., Ma, C., Spydevold, I., Haugli, H., Zee, R., Harr, J. and Udnæs, F., 2019. NorSat-2: Enabling advanced maritime communication with VDES. Acta Astronautica, 156, pp.44-50.

Cakaj, Shkelzen, et al. 2011. The range and horizon plane simulation for ground stations of low earth orbiting (LEO) satellites. International Journal of Communications, Network and System Sciences, 4(9):585–589. doi: 10.4236/ijcns.2011.49070

Casalino, L. & Colasurdo, G. 2004. Optimization of variable-specific-impulse interplanetary trajectories. Journal of Guidance, Control, and Dynamics, 27(4):678–684.Combined Genetic Algorithm and Semianalytical Approach")

Clyde Space. 2017. Products. Retrieved from https://www.clyde.space/products/ [Accessed 22 July 2019].

Cowley, W.G. & Glover, D. 2008. Link budget study notes. Australia: University of South Australia.

CPUT (Cape Peninsula University of Technology). 2017. F'SATI. Retrieved from http://www.cput.ac.za/blogs/fsati/products/ [Accessed 22 July 2019].

CPUT (Cape Peninsula University of Technology). 2018. Leading the space race in Africa. Retrieved from https://www.cput.ac.za/newsroom/news/article/3979/leading-the-space-race-inafrica [Accessed 13 October 2019].

CubeSatShop. 2019. IFM Nano Thruster for CubeSats. Retrieved from www.cubesatshop.com/product/ifm-nano-thruster/

Curtis, H. 2013. Orbital mechanics for engineering students. Third edition. Place: Publisher.

Doshi, J. & Reneker, D.H. 1995. Electrospinning process and applications of electrospun fibers. edition_of_Interface_Document_for_NanoRacks_Smallsat_Customers.pdf

Enpulsion. 2019. IFM Nano Thruster. Retrieved from https://www.enpulsion.com/order/ifm-nano-thruster/ [Accessed 1 July 2019].

eoPortal. 2021. nSight-1. Retrieved from https://directory.eoportal.org/web/eoportal/satellite-missions/n/nsight-1#27bpP111fHerb [Accessed 29 May 2020].

Fernando, C. 1970. Nano satellite propulsion using FEEP thrusters. In initial surname (ed.). Title of book. Dordrecht: Springer, first–last page of chapter. Retrieved from link.springer.com/chapter/10.1007%2F978-94-017-3008-2_48

Fortescue, P., Stark, J. & Swinerd, G. 2011. Spacecraft systems engineering. Fourth edition. Place: Publisher.

Frisbee, R.H., 2003. Advanced space propulsion for the 21st century. Journal of propulsion and power, 19(6), pp.1129-1154.

Gagliano, J.R. 2018. Orbital constellation design and analysis using spherical trigonometry and genetic algorithms: 4

Gaposchkin, E.M. and Coster, A.J., 1988. Analysis of satellite drag. Lincoln Laboratory Journal, 1, pp.203-224.

Gaylor & David. 2000. Analysis of low thrust orbit transfers using the Lagrange planetary equations.

Goebel and Dan M., and Ira Katz. 2008. Fundamentals of electric propulsion: Ion and hall thrusters. Fundamentals of Electric Propulsion: Ion and Hall Thrusters: 1–2.

Hine, A.D. 2016. An exploration of CubeSat propulsion. Unpublished doctoral dissertation. City, abbreviated state name: Western Michigan University.

Hypernova Space Technologies. 2020. Next-generation small satellite propulsion. https://www.hypernovaspace.com/

Ioannides, P. & Balanis, C.A. 2005. Uniform circular arrays for smart antennas. IEEE Antennas and Propagation Magazine, 47(4):192–206.

Jahn, R.G. & Choueiri, E.Y. 2003. Electric propulsion

Jelem and David. 2018. Performance mapping and qualification of the IFM Nano Thruster FM for in orbit demonstration. 53rd AIAA/SAE/ASEE Joint Propulsion Conference. Place: Publisher, 1–10. doi: 10.2514/6.2017-4887

Johnson, N.L., 2001. Space debris modelling at NASA. EUROPEAN SPACE AGENCY-PUBLICATIONS-ESA SP, 473, pp.259-264.

Jordan, initial. 2000. Electric propulsion: Which one for my spacecraft? 11-14.

Kawnine, T. & Kawnine, M. 2015. Short review on electric propulsion system: Ion thruster. doi: 10.13140/2.1.2331.8406:2

Kramer, H. 2019. ZACUBE-2. eoPortal Directory, Retrieved from https://directory.eoportal.org/web/eoportal/satellite-missions/v-w-x-y-z/zacube-2 [Accessed 10 August 2019].

Larson, W.J. & Wertz, J.R. 2005. Space mission analysis and design. Torrance, CA: Microcosm.

Li, R. and Lei, J., 2021. The Determination of Satellite Orbital Decay From POD Data During Geomagnetic Storms. Space Weather, 19(4), p.e2020SW002664.

Mance, S.R. 2010. AN INVESTIGATION INTO SATELLITE DRAG MODELING PERFORMANCE:

Marinan, A. 2013. From CubeSats to constellations: Systems design and performance analysis. Unpublished MSc thesis. Cambridge, MA: Massachusetts Institute of Technology.

McCune, E. 2017. Signal design and figure of merit for green communication links. In 2017 IEEE Radio and Wireless Symposium. Place: IEEE, 22–25.

Mitterauer, J. 1987. Field emission electric propulsion: Emission site distribution of slit emitters. IEEE Transactions on Plasma Science, 15(5):593–598.

Moe, K., Moe, M.M. & Wallace, S. 1998. Improved satellite drag coefficient calculations from orbital measurements of energy accommodation.

Mostaza Prieto, D., Graziano, B.P. & Roberts, P.C.E. 2014. Spacecraft drag modelling. Progress in Aerospace Sciences, 64:56–65. doi: 10.1016/j.paerosci.2013.09.001

Mtshemla, K. 2017. Mission design of a CubeSat constellation for in-situ monitoring applications. Unpublished MA thesis. Place: Cape Peninsula University of Technology.

Myers, R.M. 1993. Electromagnetic propulsion for spacecraft. 1993 Aerospace Design Conference.

NanoRacks. 2013. NanoRacks CubeSat Deployer (NRCSD) interface control document.

Oleson S.R. 1993. An analytical optimization of electric propulsion orbit transfer vehicles.

Oltrogge, D. & Leveque, K. 2011. SSC11-VII-2: An evaluation of CubeSat orbital decay.

Omar, S.R. & Bevilacqua, R. 2017. Spacecraft de-orbit point targeting using aerodynamic drag.

Operation Phakisa. 2019. Title of webpage. www.operationphakisa.gov.za/Pages/Home.aspx page 13, December 2013. URL http://nanoracks.com/wp-content/uploads/Current_

Papanikolaou, T. & Tsoulis, D. 2018. Assessment of earth gravity field models in the medium to high frequency spectrum based on GRACE and GOCE dynamic orbit analysis.

Pilinski, M. & Palo, S.E. 2009. An innovative method for measuring drag on small satellites.

Pisacane, V. 2005. Fundamentals of space systems. Oxford: Oxford University Press.

Pozar, D.M., 2012. Microwave Engineering.Fourth Editions, University of Massachusetts at Amherst, John Wiley & Sons.

Propulsion, S. and OpenCourseWare, M. 2019. Space Propulsion. Aeronautics and Astronautics. MIT OpenCourseWare. Retrieved from https://ocw.aprende.org/courses/aeronautics-and-astronautics/16-522-space-propulsion-spring-2015/index.htm [Accessed 2 June 2019].

Rawashdeh, initial & Samir, A. 2015. CubeSat aerodynamic stability at ISS altitude and inclination.

Reissner, A. 2016. The IFM 350 Nano Thruster: Introducing very high Δv capabilities for nanosats and CubeSats. 52nd AIAA/SAE/ASEE Joint Propulsion Conference. Place: Publisher, 3. doi: 10.2514/6.2016-5044

Reissner, A., Buldrini, N., Seifert, B., Hörbe, T., Plesescu, F., Del Amo, J.G. & Massotti, L. 2016. 10 000h lifetime testing of the mN-FEEP thruster. 52nd AIAA/SAE/ASEE Joint Propulsion Conference.

Robert, J. & Edgar, C. 2003. Electric propulsion. 10.1016/B0-12-227410-5/00201-5 SATELLITE OPERATIONS :4

Savitri, T., Kim, Y., Jo, S. and Bang, H., 2017. Satellite constellation orbit design optimization with combined genetic algorithm and semianalytical approach. International Journal of Aerospace Engineering, 2017.

Scharlemann, C., Tajmar, M., Vasiljevich, I., Buldrini, N., Krejci, D. & Seifert, B. 2011. Propulsion for nanosatellites. In 32nd International Electric Propulsion Conference. Volume 171. Wiesbaden: IEPC.

Satsearch.co. 2021. NanoThruster A - XS | satsearch. [online] Available at: <https://satsearch.co/products/hypernova-nano-thruster-a-xs> [Accessed 21 November 2021].

Sin, E., Arcak, M. & Packard, A. 2017. Small satellite constellation separation using linear programming based differential drag commands.

Skanke, P.E. & Birkeland, R. 2018. CubeSat propulsion: Expanding the possibilities of the affordable space platform.

Sklar, B. 2001. Digital communications: Fundamentals and applications. Second edition. Upper Saddle River, NY: Prentice Hall.

Smith, S. 2017. CubeSat de-orbit point targeting using drag modulations. Unpublished doctoral dissertation. San José, CA: San José State University.

Space-Track. 2020. SSA sharing and orbital data requests.. org.

Storch, J.A. 2002. Aerodynamic disturbances on spacecraft in free-molecular flow:

Sturdivant, R. & Chong, E. 2016. Systems engineering of a terabit elliptic orbit satellite and phased array ground station for IoT connectivity and consumer internet access. Place: IEEE.

Sudhir Babu, A. & Sambasiva Rao, K. 2011. Evaluation of BER for AWGN, Rayleigh and Rician fading channels under various modulation schemes. International Journal of Computer Applications, 26(9):23–28.

Taylor, A., McDowell, J.C. and Elvis, M., 2018. A Delta-V map of the known Main Belt Asteroids. Acta Astronautica, 146, pp.73-82.

Tiwari, A. 2019. Specific impulse: Definition, formula and units. Science ABC. Retrieved from https://www.scienceabc.com/pure-sciences/specific-impulse-definition-formula-and-units.html [Accessed 9 June 2019].

Vallado, D.A. 2013. Fundamentals of astrodynamics and applications. Fourth edition. El Segundo, CA: Microcosm.

Vallado, D.A. & Cefola, P.J. 2012. Two-line element sets – practice and use.

Vallado, D.A. & Finkleman, D. 2014. A critical assessment of satellite drag and atmospheric density modeling. Acta Astronautica, 95:141–165.

Vallado, D., 2005. Using EOP and space weather data for satellite operations.

Vanderwyst and Anton Sivaram. 2006. Field emission electric propulsion thruster modeling and simulation.

Wertz, J. 2005. Space mission analysis and design. El Segundo, CA: Microcosm.

Yuen, J.H. (Ed.). 2013. Deep space telecommunications systems engineering. Place: Springer Science & Business Media.

APPENDICES

Appendix A:

Communication systems datasheets:

CubeSat UHF Antenna System

- Frequency range: 400 MHz to 500 MHz
- Max RF Power: 10 W
- Return Loss (400–500 MHz): > 14 dB
- Noise Figure (Nadir Pointing): 360 K
- Temperature Range – –40 °C +85 °C
- Mass (typical):
  - 1x1U: 33 g
  - 1x2U: 50 g
  - 2x2U: 65 g
- Peak Gain (typical):
  - 1x1U: 1.37 dB
  - 1x2U: 2.86 dB
  - 2x2U: 2 ... 3 dB
- Dimensions:
  - 1x1U: 99.6 x 99.6 x 7.7 mm
  - 1x2U: : 222 x 96 x 7.7 mm
  - 2x2U: 224 x 222 x 7.7 mm

Reverence: https://nanoavionics.com/cubesat-components/cubesat-uhf-antenna/

Endurosat UHF Transceiver II

FEATURES	
Frequency Range (Tx/Rx)	400 to 403 MHz or 430 to 440 MHz
Default Modulation	2GFSK
Additional Supported Modulations	OOK, GMSK, 2FSK, 4FSK, 4GFSK
Mass	94 g
Telemetry Beacon	configurable AX.25
Typical Tx Power	1 W (up to 2 W upon request)
Firmware Updates	Local and remote (in-flight) secured application update
Power Amplifier Efficiency	> 70%
Frequency Stability	+/- 2.5 ppm
Configurable Data Rate	up to 19.2 kbps
Sensitivity	up to -121 dBm
Interfaces	RS485 / UART / I2C / USB-C

Reverence:https://www.endurosat.com/cubesat-store/cubesat-communication-modules/uhf-transceiver-ii/

Nanoavionics CubeSat AIS Receiver

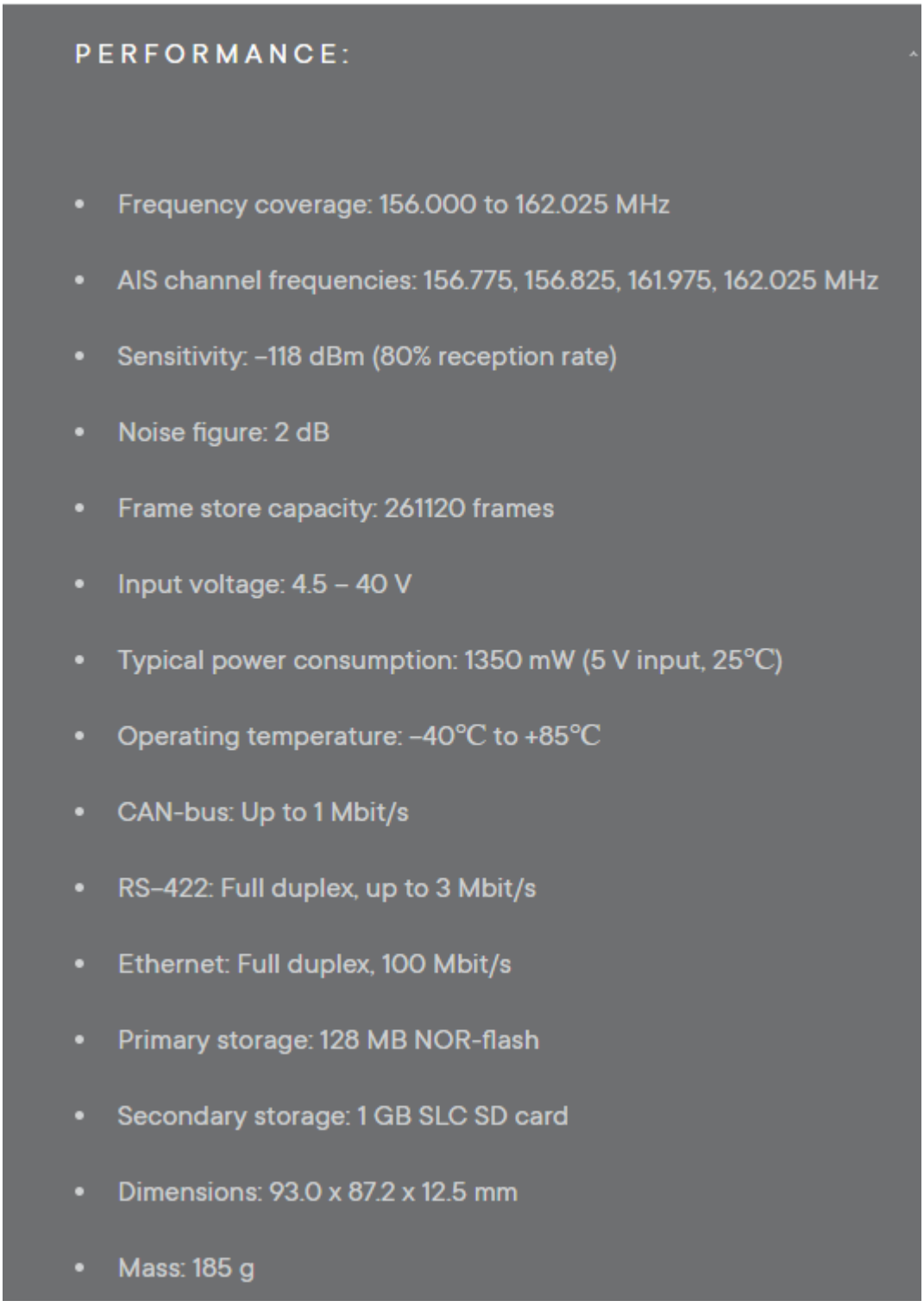

Reverence: https://nanoavionics.com/cubesat-components/cubesat-ais-receiver/

R4 AIS Class B Transponder

Physical

Dimensions: 213 x 128 x 54 mm (L x W x H)

Weight: 650g

Power

DC (10.8 - 15.6V)

Average power consumption 4W, peak current 2A

GPS Receiver (AIS Internal)

EC 61108-1 compliant

Electrical Interfaces

RS232 38.4kBaud bi-directional

RS422 NMEA 38.4kBaud bi-directional

Connectors

VHF antenna connector (BNC-F)

GPS antenna connector (TNC-F)

Serial Data RS232/RS422 (DB9-F)

Power/Tx off switch (ConXall Mini-ConX)

VHF Transceiver

Transmitter x 1

Receiver x 2 (One receiver time shared between AIS and DSC)

Frequency: 156.025 to 162.025 MHz in 25 kHz steps

Output Power: 33dBm ± 1.5 dB

Modulation:

25kHz GMSK (AIS, TX and RX), 25kHz AFSK (DSC,RX only)

Bit rate: 9600 b/s ± 50 ppm (GMSK), 1200 b/s ± 30 ppm (FSK)

Environmental

IEC 60945 (protected equipment)

Operating temperature: -25ºC to +55ºC

Reverence: https://www.saab.com/globalassets/r4-ais-product-sheet-110511.pdf

ISIS VHF/UHF/S-Band Ground Station Kit

Radio Characteristics

VHF – UHF Transceiver		
Frequency Ranges	RX	Amateur: 144 – 146 MHz and 435 – 438 MHz Commercial: 400.15 – 402 MHz
	TX	Amateur: 145.8 – 146 MHz and 435 – 438 MHz Commercial: 148 – 149.9 MHz
Frequency Stability		±2 ppm at 25°C
Modulation Schemes & Data rates	RX	AFSK @ 1.2 kbps BPSK(-G3RUH) @ 1.2, 2.4, 4.8, and 9.6 kbps FSK @ 1.2, 2.4, and 4.8 kbps FSK-G3RUH @ 2.4, 4.8, and 9.6 kbps
	TX	AFSK @ 1.2 kbps FSK-G3RUH @ 2.4, 4.8, 9.6 kbps
Output Power		Switchable 40 dBm and 50dBm
Reference Input		External 10 MHz input
Data link layer protocol		AX.25
Data Interfaces		IQ data output, Raw bytes output, KISS input & output, Binary input & output
Low Rate S-Band Receiver		
Frequency Ranges	RX	Amateur: 2400 – 2450 MHz Commercial: 2200 – 2290 MHz
Frequency Stability		±2 ppm at 25°C
Modulation Schemes	RX	BPSK, BPSK-G3RUH, AFSK, FSK, FSK-G3RUH
Data rates	RX	9.6, 14.4, 28.8, 57.6, 115.2 kbps
Data link layer protocol		AX.25
Data Interfaces		IQ data output, Raw bytes output, KISS output, Binary output
High Rate S-Band Receiver		
Frequency Ranges	RX	Amateur: 2400 – 2450 MHz Commercial: 2200 – 2290 MHz
Frequency Stability		±0.01 ppm at 25°C
Modulation Schemes	RX	BPSK, OQPSK
Data rates	RX	625 – 5000 ksymbols/s
Data link layer protocol		CCSDS
Data Interfaces		Binary output

Reverence: https://www.isispace.nl/wp-content/uploads/2016/02/ISIS.GSKit_.DS_.301_v1.1-VHFUHFS-Band-Ground-Station-DataSheet-for-website.pdf

Antenna Characteristics

Description		Amateur	Commercial
Gain	VHF	12.3 dBic	11.5 dBic
	UHF	15.5 dBic	15.0 dBic
	S-Band (Ø1.9 m)	31.4 dBic	
Front-to-Back Ratio	VHF	20 dB	
	UHF	18 dB	20 dB
Beamwidth	VHF	52°	53°
	UHF	30°	35°
	S-Band (Ø1.9 m)	5.1°	
Polarization	VHF	Switchable LHCP and RHCP	
	UHF	Switchable LHCP and RHCP	
	S-Band	Either LHCP or RHCP	
Overall System Noise Figure (typical)*	VHF	2.2 dB	-
	UHF	2.6 dB	3.3 dB

Reverence: https://www.isispace.nl/wp-content/uploads/2016/02/ISIS.GSKit_.DS_.301_v1.1-VHFUHFS-Band-Ground-Station-DataSheet-for-website.pdf